

AD-A150 107

THEORETICAL STUDY OF COLLECTIVE ION ACCELERATION IN THE

1/2

LUCE DIODE(U) MISSION RESEARCH CORP ALBUQUERQUE NM

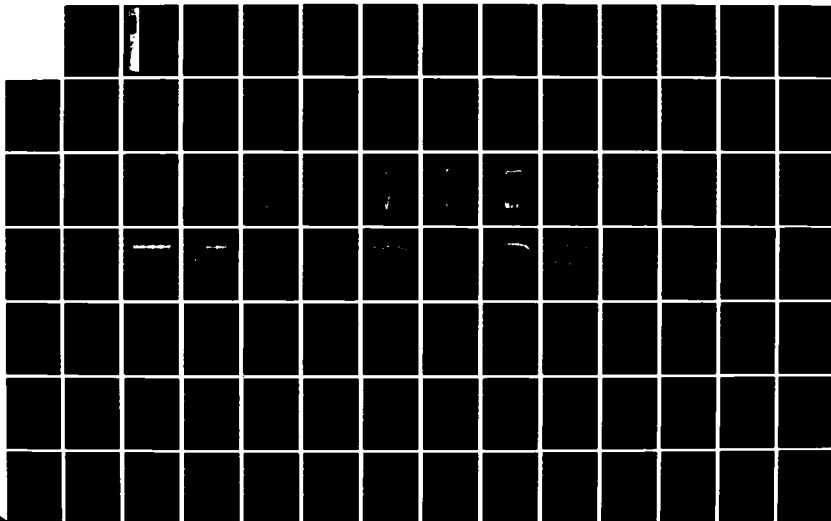
D J SULLIVAN ET AL. NOV 84 AMRC-R-663 AFOSR-TR-84-1224

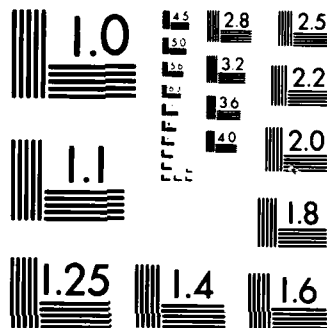
UNCLASSIFIED

F49620-82-C-0087

F/G 20/9

NL





MICROCOPY RESOLUTION TEST CHART
NATIONAL BUREAU OF STANDARDS-1963-A

AFOSR-TR-84-1224

(11)

AD-A150 107

AMRC-R-663
Copy 15FINAL REPORTTHEORETICAL STUDY OF COLLECTIVE ION ACCELERATION
IN THE LUCE DIODEDonald J. Sullivan (MRC)
Rickey J. Faeh (LANL)

November 1984

Prepared for: Air Force Office of Scientific Research
Physics Directorate
Bolling Air Force Base
Washington, DC 20332

Under Contract: F49620-82-C-0087

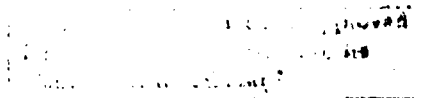
Prepared by: MISSION RESEARCH CORPORATION
1720 Randolph Road, S.E.
Albuquerque, New Mexico 87106DTIC
ELECTE
FEB 05 1985
E

Research sponsored by the Air Force Office of Scientific Research (AFSC), under contract #49620-82-C-0087. The United States Government is authorized to reproduce and distribute reprints for governmental purposes notwithstanding any copyright notation herein.

This manuscript is submitted for publication with the understanding that the United States Government is authorized to reproduce and distribute reprints for governmental purposes.

DTIC FILE COPY

85 01 25 071



AA

UNCLASSIFIED

SECURITY CLASSIFICATION OF THIS PAGE (When Data Entered)

REPORT DOCUMENTATION PAGE		READ INSTRUCTIONS BEFORE COMPLETING FORM	
1. REPORT NUMBER AFOSR TR. 1224	2. GOVT ACCESSION NO. -11-A150 107	3. RECIPIENT'S CATALOG NUMBER	
4. TITLE (and Subtitle) THEORETICAL STUDY OF COLLECTIVE ION ACCELERATION IN THE LUCE DIODE		5. TYPE OF REPORT & PERIOD COVERED Final Report Jul 1982-Jul 1983	
7. AUTHOR(s) D. J. Sullivan R. J. Faehl (LANL)		6. PERFORMING ORG. REPORT NUMBER AMRC-R-663	
9. PERFORMING ORGANIZATION NAME AND ADDRESS MISSION RESEARCH CORPORATION 1720 Randolph Road, S.E. Albuquerque, NM 87106		8. CONTRACT OR GRANT NUMBER(s) F49620-82-C-0087	
11. CONTROLLING OFFICE NAME AND ADDRESS Air Force Office of Scientific Research Building 410, Physics Directorate Bolling Air Force Base, DC 20332		10. PROGRAM ELEMENT, PROJECT, TASK AREA & WORK UNIT NUMBERS 61102F 2301/A7	
14. MONITORING AGENCY NAME & ADDRESS (if different from Controlling Office)		12. REPORT DATE November 1984	
		13. NUMBER OF PAGES	
		15. SECURITY CLASS. (of this report) Unclassified	
		15a. DECLASSIFICATION DOWNGRADING SCHEDULE	
16. DISTRIBUTION STATEMENT (of this Report) Approved for Public Release; Distribution Unlimited			
17. DISTRIBUTION STATEMENT (of the abstract entered in Block 20, if different from Report)			
18. SUPPLEMENTARY NOTES			
19. KEY WORDS (Continue on reverse side if necessary and identify by block number) Collective Ion Acceleration, Computer Simulation Luce Diode Electron-ion Streaming Instability, Ion Acoustic Instability,			
20. ABSTRACT (Continue on reverse side if necessary and identify by block number) The most successful collective ion acceleration to date has been observed when a relativistic electron beam has been discharged in the Luce diode (dielectric anode) geometry. In these experiments the ratio of peak proton energy to beam kinetic energy has been as high as 30. The ion source is a plasma formed on the anode surface by electron impact ionization of the dielectric material. The diode physics, which couples the electron beam generation to the number of ions extracted from the plasma, — (Continued)			

is an essential feature of the acceleration mechanism in the Luce configuration. Simulations where the electron beam is injected through a preformed dense plasma are significantly different from those where the electron beam self-consistently determines the ion plasma density and dynamics in the diode. The main difference is in unstable wave growth. In the Luce diode the instability is predominant. In other localized plasma source collective ion accelerators the main acceleration takes place due to a hydrodynamic plasma free expansion. However, both Luce diodes and other plasma source accelerators can display both mechanisms to some extent.

Two-dimensional electromagnetic particle-in-cell simulations which are based on the Cornell University Luce diode experiments have been carried out. The simulations include an exact model of the electron beam generator's diode and the drift space where the collective ion acceleration takes place. Ions with peak energies eight times the electron beam kinetic energy are observed. Ion acceleration is clearly due to trapping in a train of traveling waves. The source of the waves is two-fold. First occurring spatially, as well as, temporally is an ion-electron two-stream instability. This is not a classical Buneman instability because of the high temperature of the electron beam. The relativistic warm beam instability results in a significantly lower wave phase velocity. This is important for two reasons. It allows for the trapping of low velocity ions exiting the diode. It also results in a significantly longer growth distance before trapping of electrons in the instability generated plasma wave leads to nonlinear saturation. The second wave growth mechanism is a result of the saturation of the first. As the electron beam continues to heat due to electron trapping, the electron and ion distributions become unstable to an ion-acoustic instability leading to large amplitude wave generation and further ion acceleration. The presence of two electrostatic waves of different frequencies allows for microwave production through an inverse parametric instability. The instability growth rates, saturation length and microwave production are consistent with experimental results.

A-1

A-1

ABSTRACT

The most successful collective ion acceleration to date has been observed when a relativistic electron beam has been discharged in the Luce diode (dielectric anode) geometry. In these experiments, the ratio of peak proton energy to beam kinetic energy has been as high as 30. The ion source is a plasma formed on the anode surface by electron impact ionization of the dielectric material. The diode physics, which couples the electron beam generation to the number of ions extracted from the plasma, is an essential feature of the acceleration mechanism in the Luce configuration. Simulations where the electron beam is injected through a preformed dense plasma are significantly different from those where the electron beam self-consistently determines the ion plasma density and dynamics in the diode. The main difference is in unstable wave growth. In the Luce diode the instability is predominant. In other localized plasma source collective ion accelerators the main acceleration takes place due to a hydrodynamic plasma free expansion. However, both Luce diodes and other plasma source accelerators can display both mechanisms to some extent.

Two-dimensional electromagnetic particle-in-cell simulations which are based on the Cornell University Luce diode experiments have been carried out. The simulations include an exact model of the electron beam generator's diode and the drift space where the collective ion acceleration takes place. Ions with peak energies eight times the electron beam kinetic energy are observed. Ion acceleration is clearly due to trapping in a train of traveling waves. The source of the waves is two-fold. First occurring spatially, as well as, temporally is an ion-electron two-stream instability. This is not a classical Buneman instability because of the high temperature of the electron beam. The relativistic warm beam instability results in a significantly lower wave phase velocity. This is important for two reasons. It allows for the trapping of low velocity

ions exiting the diode. It also results in a significantly longer growth distance before trapping of electrons in the instability generated plasma wave leads to nonlinear saturation. The second wave growth mechanism is a result of the saturation of the first. As the electron beam continues to heat due to electron trapping, the electron and ion distributions become unstable to an ion acoustic instability leading to large amplitude wave generation and further ion acceleration. The presence of two electrostatic waves of different frequencies allows for microwave production through an inverse parametric instability. The instability growth rates, saturation length and microwave production are consistent with experimental results.

CONTENTS

<u>SECTION</u>	<u>Page</u>
ABSTRACT	i
I INTRODUCTION	5
II REVIEW OF LUCE DIODE EXPERIMENTS	7
III CODE DESCRIPTION AND MODIFICATIONS	12
IV SIMULATION OF COLLECTIVE ION ACCELERATION FROM A PREFORMED PLASMA	17
V SIMULATION OF COLLECTIVE ION ACCELERATION IN THE LUCE DIODE	25
VI THEORY OF ION ACCELERATION AND COMPARISON TO EXPERIMENT AND SIMULATION	58
VII TECHNICAL REQUIREMENTS AND TASKS	71
REFERENCES	76
APPENDIX A - REPRINTS OF PUBLICATIONS	A-1
APPENDIX B - SPACE-CHARGE DRIVEN COLLECTIVE ION ACCELERATION	B-1
APPENDIX C - LOCALIZED PLASMA SOURCE COLLECTIVE ACCELERATOR, <u>Physics and Applications</u> , AMRC-N-164, February, 1981	C-1
APPENDIX D - NUMERICAL SIMULATION AND COMPARISON BETWEEN TWO KNOWN MODES OF COLLECTIVE ION ACCELERATION	D-1

LIST OF ILLUSTRATIONS

<u>Figure</u>		<u>Page</u>
1	Idealized configuration for a Luce diode. The half angles θ are equal. d is the A-K gap spacing. L_a is the saturation acceleration length. The region enclosed by the solid line contains a large fraction of the beam. The electrons eventually fill the entire drift region. Dashed lines are typical high energy ion trajectories.	8
2	Electrostatic potential on axis at time $\tau = 1000 \omega_p^{-1}$. $(\gamma_0 - 1) = 4$ for the electron beam.	19
3	Time history of the minimum potential in the cylinder. $(\gamma_0 - 1) = 4$ for the electron beam.	19
4	Scaled electron and ion number as a function of axial length at time $\tau = 1000 \omega_p^{-1}$.	21
5	Electron and ion momentum phase space versus axial length at time $\tau = 1000 \omega_p^{-1}$.	22
6	Momentum distribution functions for electrons and ions. The hot propagating electron beam results in a peak ion energy of 2.5 times the beam kinetic energy at $\tau = 1000 \omega_p^{-1}$.	
7	Electron momentum space and real space at 3.3 nanoseconds.	26
8	Ion momentum space and real space at 3.3 nanoseconds. m_i/m_e is 459.	28
9	Electron momentum space and real space at 11.0 nanoseconds.	29
10	Ion momentum space and real space at 11.0 nanoseconds. m_i/m_e is 459.	30
11	Movie frames of a) the ion real (R-Z) space, b) ion axial momentum and c) electron axial momentum phase spaces at $t = 6.7$ ns. The units of Z and R are cm, PZ is $\beta_z \gamma$, and $m_i/m_e = 1836$.	33

LIST OF ILLUSTRATIONS (Continued)

Figure		Page
12	Movie frames of a) the ion real (R-Z) space, b) ion axial momentum and c) electron axial momentum phase spaces at $t = 13.3$ ns. The units of Z and R are cm, PZ is $\beta_Z \gamma$, and $m_i/m_e = 1836$.	34
13	Movie frames of a) the ion real (R-Z) space, b) ion axial momentum and c) electron axial momentum phase spaces at $t = 28$ ns. The units of Z and R are cm, PZ is $\beta_Z \gamma$, and $m_i/m_e = 1836$.	35
14	Probe history of the axial electric field at $r = 0$ cm; $Z = 0$ cm from 24 ns to 35 ns and its Fourier transform. Largest amplitude frequency $f = 39$ GHz.	38
15	Probe history of the axial electric field at $r = 0$ cm; $Z = 4.0$ cm from 0 ns to 12 ns and its Fourier transform. Largest amplitude low frequency $f = 40$ GHz.	39
16	Probe history of the axial electric field at $r = 0$ cm; $Z = 5.0$ cm from 24 ns to 35 ns and its Fourier transform. Largest amplitude frequency $f = 3.3$ GHz.	40
17	Probe history of the axial electric field at $r = 0$ cm; $Z = 10$ cm from 24 ns to 35 ns and its Fourier transform. Largest amplitude frequency $f = 1.4$ GHz.	41
18	Probe history of the axial electric field at $r = 0$ cm; $Z = 20$ cm from 24 ns to 35 ns and its Fourier transform. Largest amplitude frequency $f = 250$ MHz.	42
19	Probe history of the axial electric field at $r = 0.6$ cm; $Z = 20$ cm from 0 ns to 12 ns and its Fourier transform.	44
20	Probe history of the axial electric field at $r = 0.6$ cm; $Z = 20$ cm from 12 ns to 24 ns and its Fourier transform. Largest amplitude frequency $f = 250$ MHz.	45
21	Probe history of the axial electric field at $r = 0.6$ cm; $Z = 20$ cm from 24 ns to 35 ns and its Fourier transform. Largest amplitude frequency $f = 250$ MHz.	46
22	Axial slices at different radii of a) axial current density and b) charge density as a function of Z at $t = 12.0$ ns. The large amplitude slice is at $r = 0$ indicating the beam pinch point is near 2.5 cm.	47

LIST OF ILLUSTRATIONS (Concluded)

<u>Figure</u>		<u>Page</u>
23	Axial slices at different radii of a) axial current density and b) charge density as a function of Z at $t = 23.3$ ns. The large amplitude slice is at $r = 0$ indicating the beam pinch point is near 2.5 cm.	48
24	Axial slices at different radii of a) axial current density and b) charge density as a function of Z at $t = 34.7$ ns. The large amplitude slice is at $r = 0$ indicating the beam pinch point is near 2.5 cm.	49
25	Plots of the radial integrals of a) the radial current density and b) the charge density as a function of Z at $t = 34.7$ ns.	50
26	Histograms of the electron beam distribution functions for a) axial momentum, b) radial momentum and c) kinetic energy at $t = 12$ ns.	52
27	Histograms of the electron beam distribution functions for a) axial momentum, b) radial momentum and c) kinetic energy at $t = 23.3$ ns.	53
28	Histograms of the electron beam distribution functions for a) axial momentum, b) radial momentum and c) kinetic energy at $t = 34.7$ ns.	54
29	Histograms of the ion beam distribution functions for a) axial momentum, b) radial momentum and c) kinetic energy at $t = 12$ ns.	55
30	Histograms of the ion beam distribution functions for a) axial momentum, b) radial momentum and c) kinetic energy at $t = 23.3$ ns.	56
31	Histograms of the ion beam distribution functions for a) axial momentum, b) radial momentum and c) kinetic energy at $t = 34.7$ ns.	57
32	Plot of critical drift velocity as a function of T_e/T_i for the onset of electrostatic instability in an electron-ion plasma.	62
33	Scattering (temperature) reduces phase velocity of the most unstable mode. This example is for 500 keV electron and ion beams, and quarter mass protons.	64
34	The plasma wave scatters off of the ion acoustic wave to create the electromagnetic wave.	69

SECTION I

INTRODUCTION

Collective ion acceleration is a speculative but potentially very significant application of intense relativistic electron beams. One seeks to harness the megavolt-per-centimeter electric fields of such beams to produce compact and economical accelerators with substantial currents of light or heavy ions and energies up to several hundred MeV per nucleon. Collectively accelerated high-current ion beams have application in the field of neutron production for simulation and have numerous civilian uses as well. Interest in collective acceleration is indicated by a large list of experimental and theoretical studies (Ref. 1).

The most successful collective ion acceleration to date has been observed when a relativistic electron beam has been discharged in the Luce diode (dielectric anode) geometry (Ref. 2). In these experiments, the ratio of peak proton energy to beam kinetic energy has been as high as 30 (Ref. 3). The ion source is a plasma formed on the anode surface by electron impact ionization of the dielectric material (Refs. 4-11). The diode physics, which couples the electron beam generation to the number of ions extracted from the plasma, is an essential feature of the acceleration mechanism in the Luce configuration. Simulations where the electron beam is injected through a preformed dense plasma are significantly different from those where the electron beam self-consistently determines the ion plasma density and dynamics in the diode. The main difference is in unstable wave growth. In the Luce diode the instability is predominant. In other localized plasma source collective ion accelerators the main acceleration takes place due to a hydrodynamic plasma free expansion. However, both Luce diodes and other plasma source accelerators can display both mechanisms to some extent.

The authors have been conducting a joint computational research program on the physics of the Luce diode over the last several years (Refs. 12-18). This work has culminated in a two-dimensional electromagnetic model for the dielectric anode configuration, which includes self-consistently the diode physics of the problem. Our results tend to verify conclusions of the experiments performed at Cornell University (Refs. 5-7). Based on our latest simulations our understanding of the theory of the Luce diode has been modified to some extent from an earlier hypothesis (Ref. 14).

This report is organized as follows. In Section II Luce diode experiments in general and the results of the Cornell University program in particular are reviewed. Because so much of the current effort is based on simulation results, Section III is a review of the code CCUBE. This section also deals with several modifications to the code which were critical to successful completion of this research effort. Section IV outlines the results of earlier simulations of collective ion acceleration from preformed plasma. These results and the explanation for this mode of acceleration contrast sharply with the Luce diode simulations reported in Section V. The theory of acceleration in the Luce diode, and comparison of it to experimental and simulation results is made in Section VI. Finally, Section VII reviews the Technical Requirements and Tasks.

Appendix A contains reprints of Luce diode results reported under this contract. Appendix B is a copy of an American Physical Society talk given to explain collective ion acceleration due to the hydrodynamic expansion of a plasma. A report on Luce diode experimental results, design optimization considerations, and applications is reproduced in Appendix C. Finally, a reprint of the 1984 American Physical Society presentation, which shows the contrast in the different mechanisms (preformed plasma vs. Luce diode type) of collective ion acceleration, is given in Appendix D.

SECTION II

REVIEW OF LUCE DIODE EXPERIMENTS

Although experiments and theory have been carried out over the last ten years to explain collective ion acceleration in the Luce diode, it remains both the most successful and least understood of all collective ion acceleration schemes. In its simplest form the Luce diode consists of a tapered cathode and a dielectric anode. This is depicted in Figure 1. The center of the anode has a hole concentric with and of a size approximately equal to the cathode shank diameter. The electron beam is generated by explosive field emission. The electrons are emitted from the tapered section of the cathode, which experiences the highest electric fields and is not magnetically insulated as is the cathode shank.

Since the dielectric anode acts initially as an insulator, the potential difference the electrons experience is due to the voltage rise between the cathode and outer conducting wall of the drift tube or a conducting anode holder. Thus, in the absence of a strong, externally imposed, axial magnetic field, the electrons move radially outward from the cathode tip. These electrons bombard the dielectric. After a sufficient amount of energy is deposited, a plasma is formed on the anode surface, which acts to ground the anode to the drift tube wall. This process is accomplished in the first several nanoseconds of the beam pulse. Ions from the anode plasma are drawn toward the cathode to establish a bipolar flow across the anode-cathode (A-K) gap. Once a sufficient number of ions are present to provide neutralization, the electron and ion plasma begins to propagate into the drift tube region where collective ion acceleration takes place.

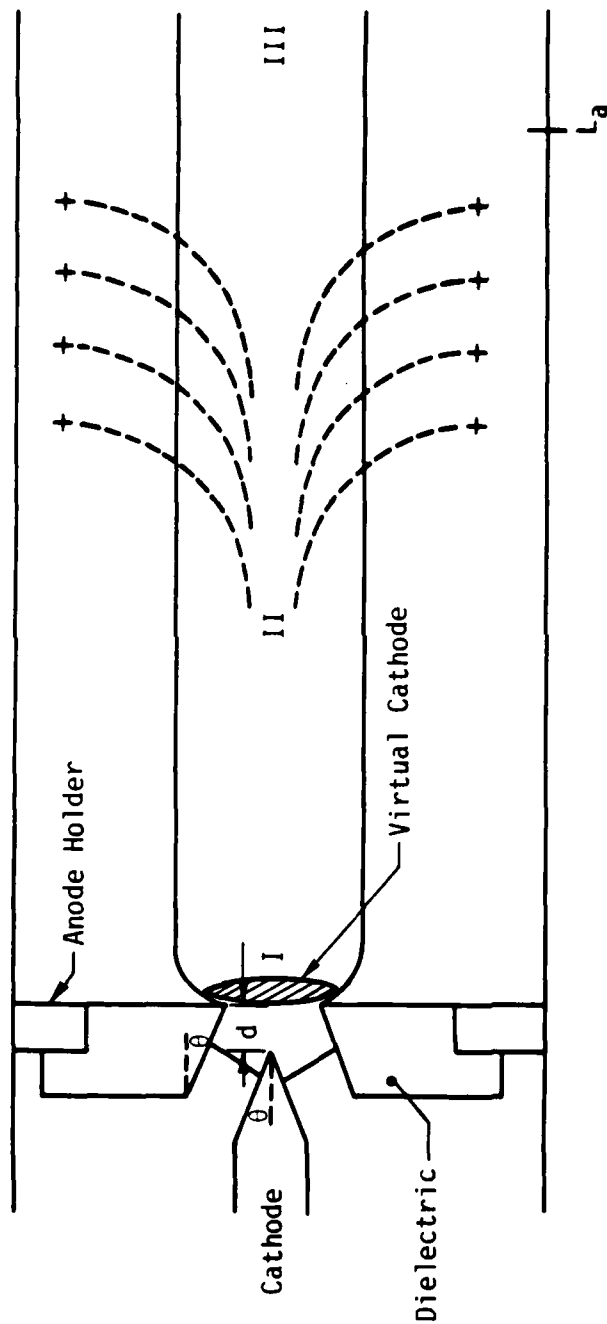


Figure 1. Idealized configuration for a Luce diode. The half angles θ are equal. d is the A-K gap spacing. L_a is the saturation acceleration length. The region enclosed by the solid line contains a large fraction of the beam. The electrons eventually fill the entire drift region. Dashed lines are typical high energy ion trajectories.

Many variations on the Luce diode have been tried experimentally with different degrees of success. These include dielectric channels (Refs. 19, 20), reflex tetrodes (Ref. 21), and addition of "lenses" (Ref. 3) or a helical slow wave structure (Ref. 10) to the basic dielectric anode design. There exist almost as many theories to explain the collective acceleration as there are experiments. They range from vortex filaments (Ref. 3) to cavity resonators (Ref. 9) to a deep stationary well/moving potential well (Refs. 4, 10, 11, 19-21). Until recently, this latter explanation has been used most frequently to describe the acceleration process. It is based on the same theory used to depict collective ion acceleration in a low density gas (Refs. 22-25).

Recent experiments (Refs. 6, 7) on the Luce diode at Cornell University, however, shed doubt on these schemes. We have chosen to model these studies in our work, because they contain the most detailed diagnostics available. Also, the experiments were conducted on the fundamental dielectric anode design, so that the results are not ambiguously tied to elaborate configurations. A short summary of the Cornell results is appropriate.

Polyethelene or another insulator (Lexan or Teflon) coated with diffusion pump oil was found to be the best ion (proton) source. By replacing various surfaces of the dielectric with conductors, the ions were found to originate at the inside taper of the anode. The electrons were emitted from the tapered section of the cathode (see Figure 1). Provided the A-K gap spacing and, therefore, impedance were in a certain range, bipolar flow in the diode and beam propagation into the drift space were established in 6-10 nanoseconds. The flow, however, was not space-charge limited as evidenced by the fact that the diode perveance ($I/V^{3/2}$) was proportional to $d^{-1/2}$ instead of d^{-2} where d is the A-K gap spacing. When d was related to diode impedance, good collective acceleration was found only over a narrow range ($Z = 8.5 \Omega - 11.5 \Omega$). This indicates that the acceleration mechanism is strongly tied to the diode physics.

The most crucial results of the experiments were the following:

(1) The maximum ratio of ion energy to beam kinetic energy was 22.0. This is the highest acceleration factor witnessed in a basic Luce diode.

(2) The highest energy ions did not occur until late in the beam pulse ($t > 55$ nanoseconds) and were correlated in time with moderate frequency microwaves (1.7 GHz - 2.8 GHz).

(3) The highest energy ions appeared in bunches corresponding to a frequency of 200 - 300 MHz.

(4) The propagating beam front had a measured velocity of from 0.04 to 0.05 c, corresponding to an ion energy approximately twice the electron beam kinetic energy.

(5) No electrons with an energy greater than 1.2 times the electron beam energy were observed early in the pulse.

(6) The net beam current increased monotonically in time and axial length over the beam pulse. The maximum was approximately equal to the Alfven current of the beam.

(7) The maximum ion energies were measured within 13 cm of the anode back plane indicating a short saturation length for the acceleration mechanism.

The deep stationary potential well/moving potential well has grave difficulty in explaining items 2 through 5. Indeed, in light of these results any beam front mechanism is called into question. The

Cornell researchers have speculated, based on the the microwave frequency observed, that electrostatic waves generated by an ion-electron two-stream instability are responsible for the highest energy ions. The linear theory of the instability is in fair agreement with the experimental results. The possibility that this instability is responsible for the ion acceleration was first proposed by Godfrey and Thode (Ref. 26). A more encompassing hypothesis has been drawn up to explain other details of the observed acceleration (Ref. 14). This theory has been significantly modified. The acceleration is viewed as occurring in three stages corresponding to regions I, II, and III of Figure 1. The theory utilizes the latest non-linear results pertaining to the ion acoustic (Ref. 27) and ion-electron two-stream (Refs. 28, 29) instabilities. The theory is consistent with both experimental and simulation results on instability frequencies, wave phase velocities, microwave production and saturation mechanism and length.

SECTION III

CODE DESCRIPTION AND MODIFICATIONS

Because this effort relied so heavily on simulation, it is appropriate to give a brief outline of the code and how it was utilized.

The numerical calculations were performed principally with the powerful, state-of-the-art computer code, CCUBE (Version Two). This is a relativistic, electromagnetic, particle-in-cell plasma simulation code designed specifically for electron and ion beam studies. It exists in two- and three-dimensional forms. Both versions treat self-consistently the time-dependent trajectories of tens of thousands of individual plasma particles over thousands of plasma periods. At each time step current associated with the electrons and ions are interpolated onto a two-dimensional spatial mesh. The three-dimensional code, IVORY, further decomposes the currents into Fourier modes in the third coordinate direction, assumed periodic. These quantities in turn serve as source terms in Maxwell's equations for determining the electromagnetic fields on the mesh. Finally, the fields are interpolated back to the particle positions (including Fourier recomposition, if appropriate) and the particle momenta and positions advanced. This leap-frog procedure is repeated many thousands of times and forms the heart of the code.

Fourier representation of field variation in the third dimension was chosen for economy. This special approach requires significantly less computer memory and running time than a spatial approach when a half-dozen or less azimuthal modes must be represented accurately. Generally, this is true of relativistic beam problems. When many more modes are required, a finite difference representation is superior. Very few three-dimensional PIC codes of any sort exist. We chose CCUBE as the most suitable for the research performed here.

Dimensionality aside, CCUBE differs from other plasma simulation codes in three important respects. First, it employs a Galerkin finite-difference algorithm for advancing particle quantities. This has the effect of creating a Lagrangian interface between particles and fields, thereby eliminating the virulent numerical Cherenkov instability and ameliorating other troublesome numerical problems. Second, the algorithm for advancing the electromagnetic fields incorporates backward biasing to damp unwanted high frequency field fluctuations and to further suppress possible numerical instabilities. The MRC-developed time-biased field solver has the additional valuable attribute of significantly relaxing the Courant time-step constraint, reducing computing time. Third, the code is written for arbitrary orthogonal coordinates. Thus, one can convert, say cylindrical to parabolic coordinates merely by redefining arrays of metric elements. Nonuniform zoning of the spatial mesh is accomplished with equal ease. Computations for the Luce diode research effort employed only cylindrical (r - z) geometry in two dimensions.

A number of other features deserve mention. For compatibility with nonuniform zoning, variable particle weighting within particle type, with several particle species permitted, is implemented. The code supports periodic, wave transmitting, and inhomogeneous Dirichlet-Neumann field boundary conditions. Particles can be absorbed, reflected, or injected from surfaces not necessarily coinciding with edges of the mesh. Magnetic fields, which are based on a separate code used to design field coils, can be programmed into CCUBE. The physics for wave launching and Luce particle field emission from surfaces, which was necessary for the self-consistent diode simulations, is incorporated. CCUBE is tightly optimized for efficient operation.

Diagnostics include microfiche plots of various slices through particle phase space, particle distribution functions, contour plots and one-dimensional cuts of fields and currents, and histories of particle and

field energies and other selected quantities. Color movies of particle and field data can be generated concurrently. In addition to the more traditional simulation diagnostics just mentioned, CCUBE contains numerical equivalents of such experimental diagnostics as Faraday cups, calorimeters, compensated diamagnetic loops, Rogowski coils, and local probes for field and current measurements. Each diagnostic is time dependent and can be Fourier analyzed. CCUBE has been utilized to study the fundamental properties of nonneutral beams, in slow wave structure research, in beam-plasma interaction studies, diode and transmission line design, free electron laser investigations, and microwave generation.

In the course of the Luce diode research, MRC has developed a new Poisson solver (POIS) for correcting RHOBG, the electrostatic error in $\nabla \cdot E = \rho$, or initializing electric fields. It is available as a 3-D version in IVORY and as 2-D Historian updates for CCUBE on the CRAY computer.

The solver itself is a modified successive over-relaxation (SOR) method called the "Chebyshev" method because of the polynomial coefficients used to enhance convergence. An iterative solution for the electrostatic potential " ϕ " is found at each grid mesh-point using an odd/even "checker-board" sweep across the mesh. The number of iterations (KSWP) required for convergence is in the range $N/4$ to N , where N is the maximum number of grid points in either direction along the 2-D mesh (the actual value varies with complexity of boundary conditions, geometry, and the accuracy of an initial guess for ϕ). Problems may be solved in any orthogonal coordinate system where the metric is a function of the mesh variables $X1$ and $X2$ such that $h_{ij} = f_i(X1) \cdot f_j(X2)$. For initializing the potential from a charge distribution, a recommended value for KSWP is N , or even $2N$. For correcting RHOBG errors in problems with non-laminar charge flow it is best to call POIS every time step. Further information on solution techniques can be found in "Methods in Computational Physics", Vol. 9 (1970), Academic Press.

This solver can treat internal boundaries on the 2-D mesh. A large conductor (e.g., cathode) exposed to a time varying E-field is treated as though grounded. A free-floating conductor cannot be treated readily by POIS except in the steady-state limit. However, since RHOBG must be zero inside the conductor, the standard grounded boundary conditions of the conductor surface may be used for POIS to correct satisfactorily the electric field errors elsewhere on the grid.

Boundary conditions must also be set on the E-field that are consistent with those on the potential. As a general rule, all E-field components which lie physically on or within the boundary where ϕ is set to zero (or a constant) must also be set to zero.

Tests have shown that the Poisson correction usually drops the RHOBG error by 2-4 orders of magnitude, but at an increased running cost of typically 30%. This correction, however, lowers electrostatic noise growth to an extent that a very large number of iterations are possible before cumulative errors begin to disrupt the problem physics, many times the number of cycles without POIS. This was of crucial concern for the simulations described in Section V where the number of time steps required to model 35 nanoseconds of real time was 42,000.

In addition to the Poisson corrector a spacial spectral analyzer was included for the axial electric field and charge density diagnostics. This enables one to immediately observe the wave number spectrum of the electrostatic wave, as well as, the charge bunching taking place in the plasma. It relies on performing a Fast Fourier Transform on these two quantities as a function of x whenever a "snapshot" of the spatial diagnostics is taken at a prescribed time. In conjunction with the frequency spectrum derived from the time histories of different field probes at various locations, we have a good picture of the evolution of both ω and k .

As noted above, simulations were carried out using CCUBE. The code can solve self-consistently for the time dependent trajectories of

tens of thousand of plasma particles over thousands of plasma periods. All variables are expressed in dimensionless terms. Therefore, length is in units of c/ω_p ; time is measured in units of ω_p^{-1} ; and particle momentum is given by $v_i = \beta_i \gamma$ ($i = 1, 2, 3$), where ω_p is the initial electron plasma frequency. Some simulations have ω_p set equal to a constant ω_0 . The value of ω_0 was chosen to be 3×10^{10} so that $c/\omega_0 = 1$ cm and $\omega_0 = 33$ picoseconds.

SECTION IV

SIMULATION OF COLLECTIVE ION ACCELERATION FROM A PREFORMED PLASMA

Computer simulations using the two-dimensional electromagnetic particle-in-cell plasma simulation code CCUBE have been conducted over the last few years in an attempt to understand the acceleration method in the Luce diode. These simulations fall into two categories. The first class of simulations involved injecting an electron beam with a current above the space-charge limit through a dense preformed plasma. Typical parameters for the electron beam were 2.0 MeV and 76.5 kA. This yields a $v/\gamma = .9$ where v is current normalized to mc^3/e (17 kA) and γ is the beam relativistic factor. Here, m is electron mass, e is electronic charge and c is the speed of light. The beam kinetic energy can be represented as $(\gamma_0 - 1)mc^2$ where $\gamma_0 = 5$. The cylindrical drift space was $200 c/\omega_p$ long and $50 c/\omega_p$ in radius. The ratio of plasma density to beam density, n_p/n_b , was 35. The plasma filled the drift tube radially and extended out from the injection boundary for $10 c/\omega_p$. In order to give some physical interpretation to these dimensions, assume the beam density was 10^{12} cm^{-3} . Then the plasma density would be $3.5 \times 10^{13} \text{ cm}^{-3}$, c/ω_p would equal 0.9 millimeters, and the box length would be 18 centimeters. Also, the code unit for time is ω_p^{-1} so that assuming this density implies $\omega_p^{-1} = 3$ picoseconds. Because the beam radius was half the drift tube radius, the beam current exceeded the space-charge limiting current by a factor of 3.5 for a 2.0 MeV beam. No axial magnetic field was imposed.

The salient features and conclusions of these runs are presented in Appendix B. A brief review is worthwhile here.

(1) At no time during the simulation does the virtual cathode detach from the vacuum/plasma interface and start to move. Rather, the downstream side of the potential well propagates along with the electron beam. The potential well on the cylinder axis late in time is given in Figure 2.

(2) At no time does the virtual cathode produce a "deep" potential well equivalent to twice or three times the beam kinetic energy. Figure 3 presents a time history of the absolute value of the minimum potential in the cylinder. Even with an unrealistic beam rise time of $15 \omega_p^{-1}$ the potential exceeds $(\gamma_0 - 1)mc^2/e$ by only 30% for a transient period. This same result is also true in the absence of ions (Ref. 30).

(3) The position of the beam front is defined by the leading edge of the ions (see Figure 4). The ions provide partial charge neutralization to the beam, which in conjunction with the beam's self-magnetic field permits propagation without an external axial magnetic field. The beam front velocity from Figure 4 is 0.15 c for this reduced mass ratio, or a velocity of 0.04 c for protons with the same momentum profile.

(4) The propagating electron beam is hot with a temperature of several hundred keV, while the ions tend to be relatively cold. This can be seen in the particle plots of Figure 5 and the electron and ion distribution functions shown in Figure 6. The electron temperature from Figure 6 is 470 keV. This heating is due to electron reflexing in the preformed plasma and virtual cathode oscillation. The production of hot electrons is even more pronounced in simulations where n_p/n_b is greater and there is a larger beam-plasma interaction region (see Appendix B).

(5) The ion distribution in Figure 6 clearly shows collective ion acceleration without the presence of a deep potential/moving potential well. In this case where $m_i/m_e = 500$ the ratio of peak ion energy to beam kinetic energy is 2.5. In cases where the axial extent of the plasma is large and heating is more pronounced, factors of 4 - 5 are observed.

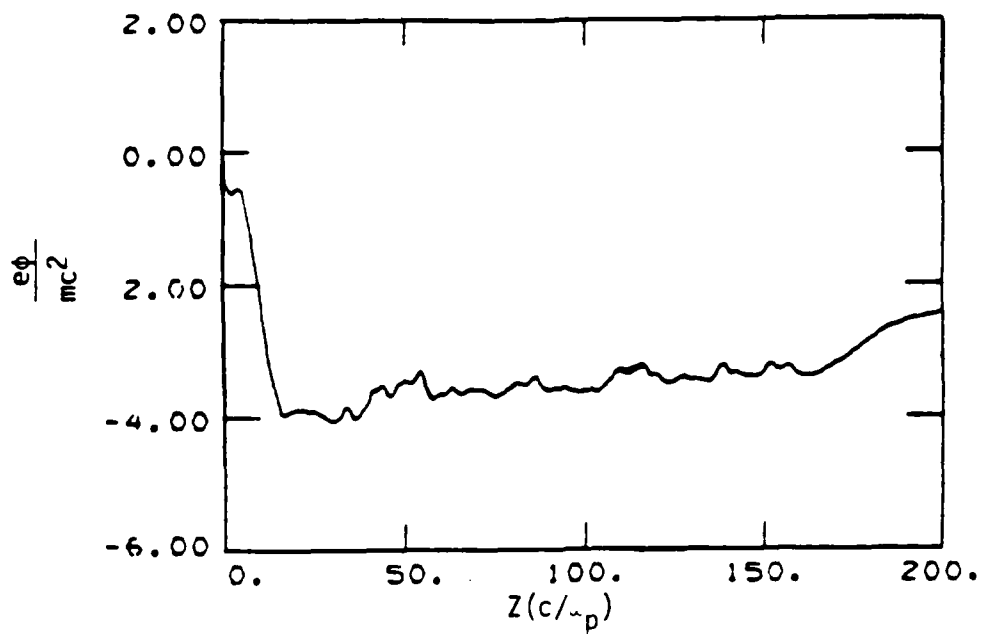


Figure 2. Electrostatic potential on axis at time $\tau = 1000 \omega_p^{-1}$.
 $(\gamma_0 - 1) = 4$ for the electron beam.

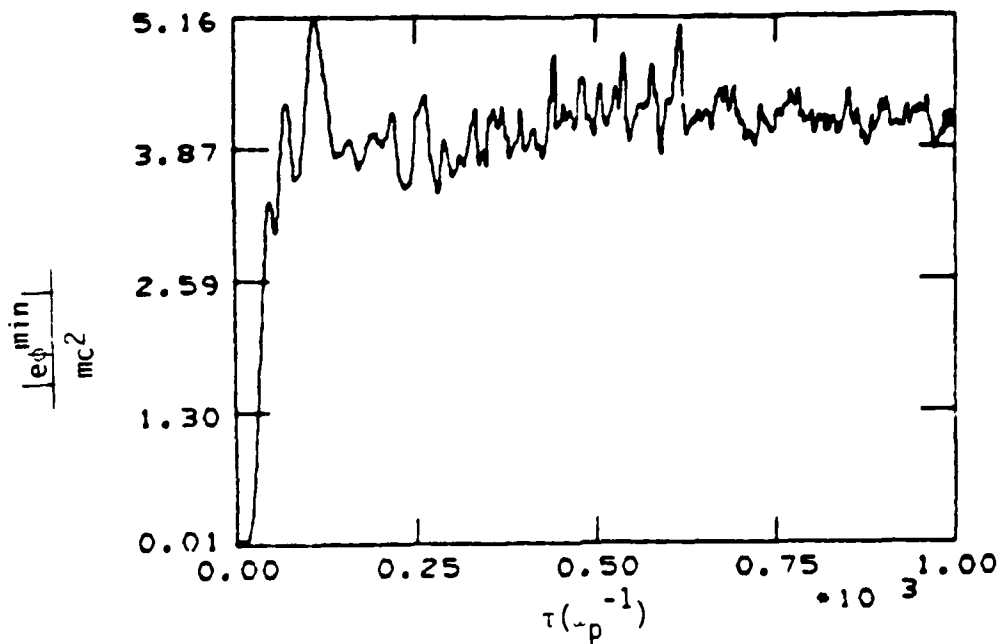


Figure 3. Time history of the minimum potential in the cylinder.
 $(\gamma_0 - 1) = 4$ for the electron beam.

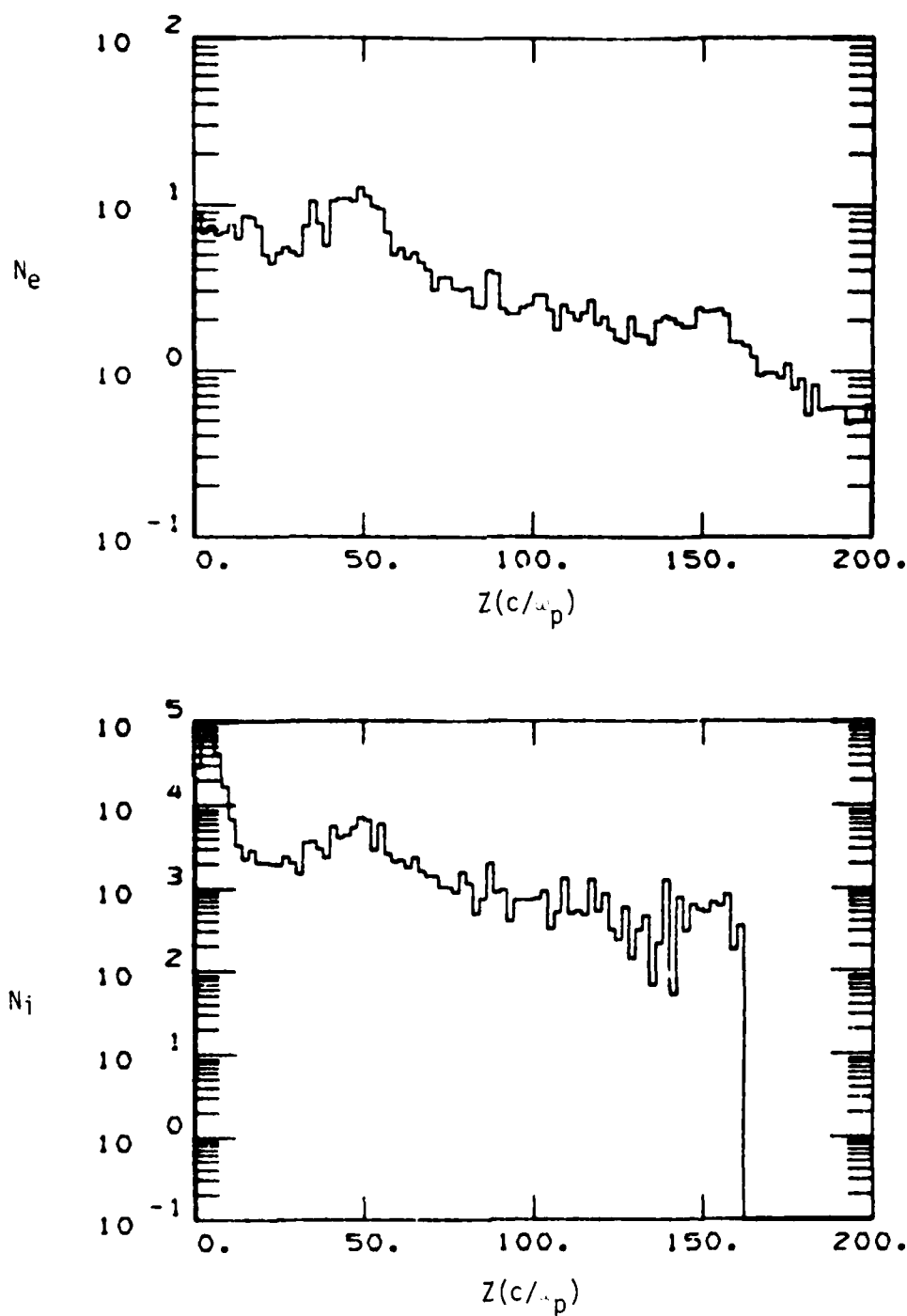


Figure 4. Scaled electron and ion number as a function of axial length at time $\tau = 1000 \omega_p^{-1}$. $N_j = \bar{n}_j \int_0^R \frac{m_j}{e} n dr$, $m_i/m_e = 500$. The two species plasma approximates quasineutrality.

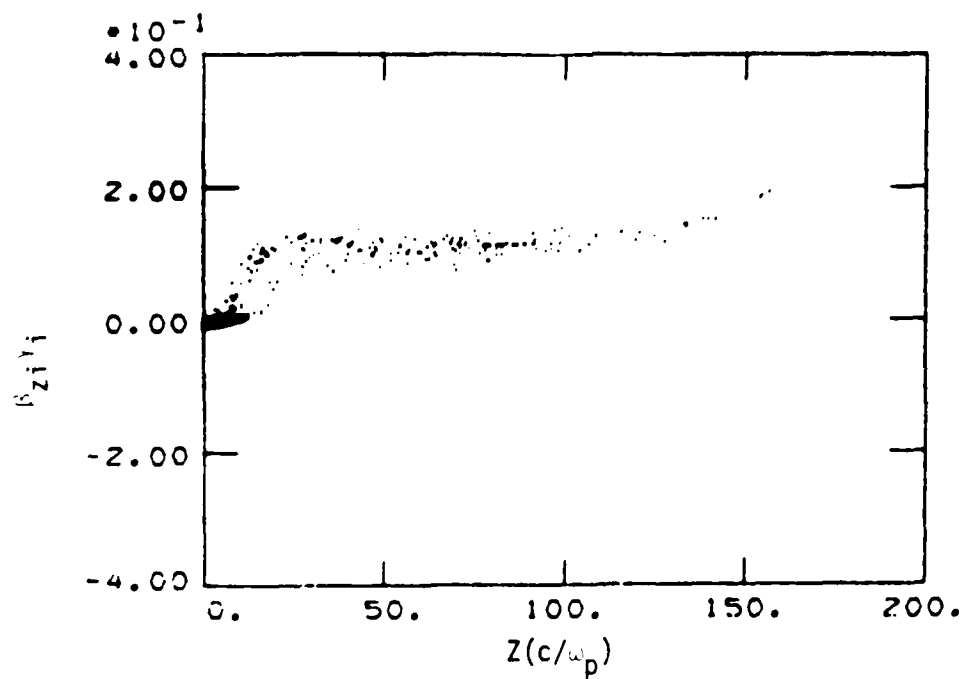
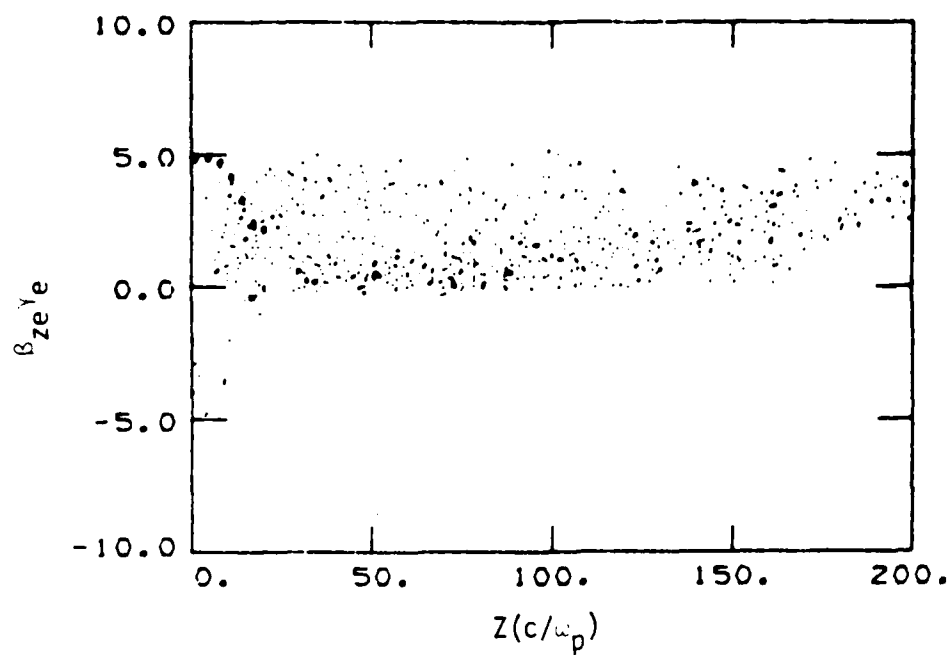


Figure 5. Electron and ion momentum phase space versus axial length at time $\tau = 1000 \omega_p^{-1}$.

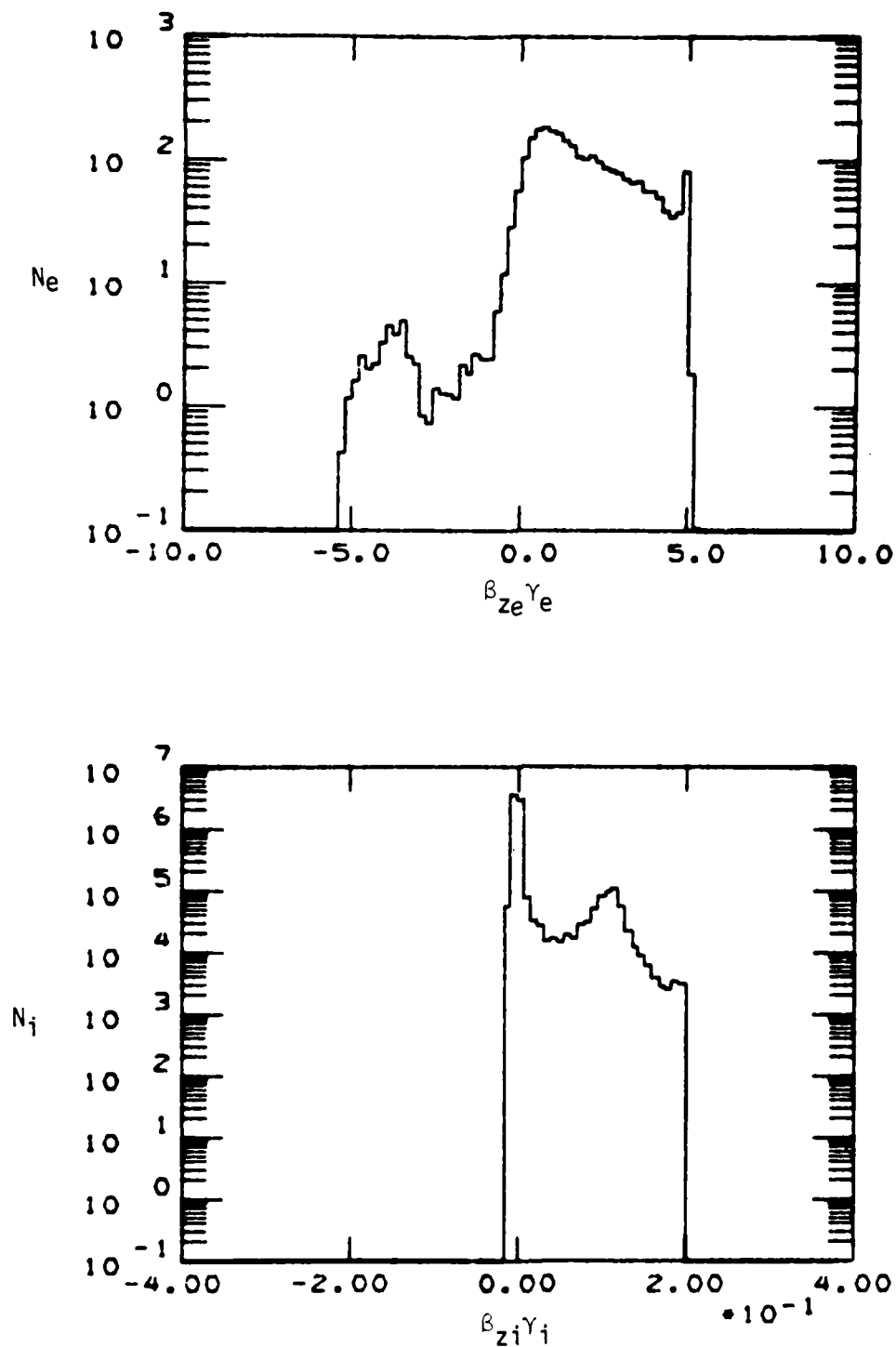


Figure 6. Momentum distribution functions for electrons and ions. The hot propagating electron beam results in a peak ion energy of 2.5 times the beam kinetic energy at $k = 1000 \text{ } \mu\text{p}^{-1}$.

No diode physics is included in these simulations. Because diode physics apparently plays a strong role in collective ion acceleration in the Luce geometry, these simulations do not address the appropriate problem. Indeed, they appear to be more analogous to other collective ion acceleration experiments involving neutral gas puffs (Refs. 31-33). Although the gas is localized near the anode, it provides an extended source relative to the surface plasma available from dielectric anodes, reflex tetrodes, and dielectric channels. In addition to the difference in spatial extent, the plasma formation process is different. Electron and ion avalanching in the gas decouple the beam from self-consistently determining the plasma density and number of ions drawn out of the diode into the acceleration region. In this case n_p may be greater than n_b as in the simulations.

It is interesting to note the results of experiments conducted at the University of California at Irvine on collective acceleration from neutral gas puffs (Ref. 31). Only a narrow range in time delay between gas injection and beam firing resulted in ion acceleration comparable to the Luce diode. However, acceleration factors of 4 - 6 times the beam energy were observed over a wide range in delay times. This would seem to indicate that the spatial extent and n_p value of the plasma are critical, if one is trying to emulate the Luce diode with a gas puff. Also noteworthy is the fact that peak ion acceleration correlates with a strong microwave signal. Finally, increasing the axial magnetic field beyond a critical value decreases the ion acceleration. These last two observations are in agreement with the dielectric anode experiments at Cornell (Refs. 6, 7).

If one considers collective acceleration in a dense plasma as different from acceleration in a Luce diode, both experiments and simulations are explained well by the theory of Ryutov and Stupakov (Ref. 34,

35). They studied electron cloud formation and dynamics produced by beam electrons reflexing through an anode foil. Based on a one-dimensional electrostatic analysis, which in part is equivalent to imposing an infinite axial magnetic field, they concluded that the cloud density could greatly exceed the beam density. Heating of the electron cloud by the beam led to a hydrodynamic plasma expansion, which transferred energy to the ions. By assuming quasineutrality they derived equations which showed maximum ion energies of 2 - 5 times the beam kinetic energy depending on the initial γ of the beam. In particular the energy of the ions saturates such that

$$\epsilon_{ion} = 2(\gamma_0 - 1) mc^2 \quad \gamma_0 \geq 1 \quad (1a)$$

$$\epsilon_{ion} = 5(\gamma_0 - 1) mc^2 \quad \gamma_0 \gg 1 \quad (1b)$$

Note also from the ion plot of Figure 5 that this is predominantly a beam front mechanism. This feature has been reported as one of the main characteristics of gas puff experiments (Refs. 32, 33). These analytical results qualitatively agree in all respects with our simulations of collective ion acceleration in a preformed dense plasma.

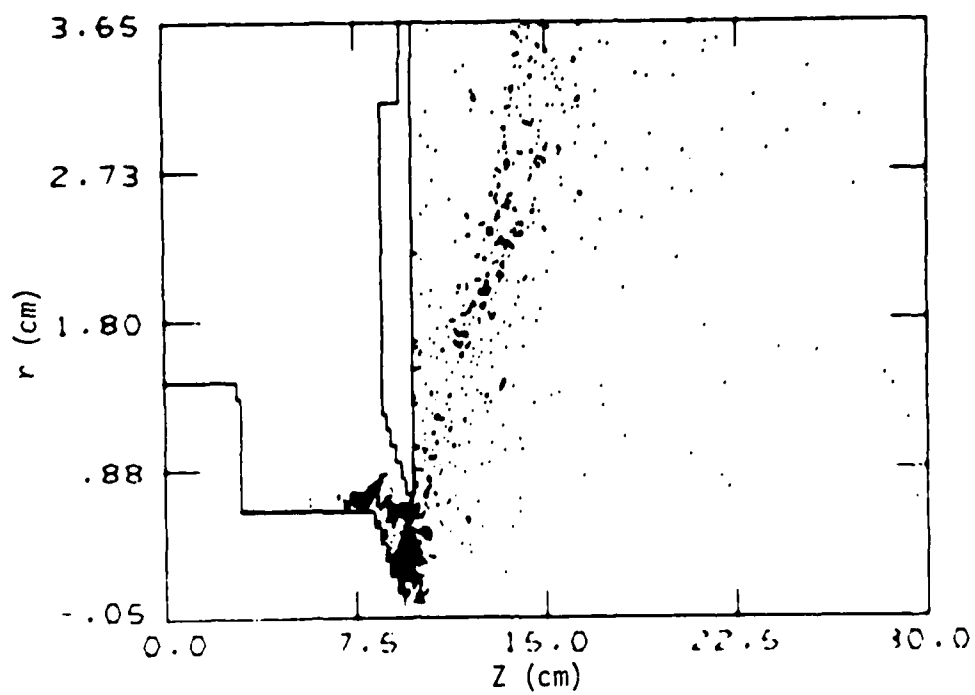
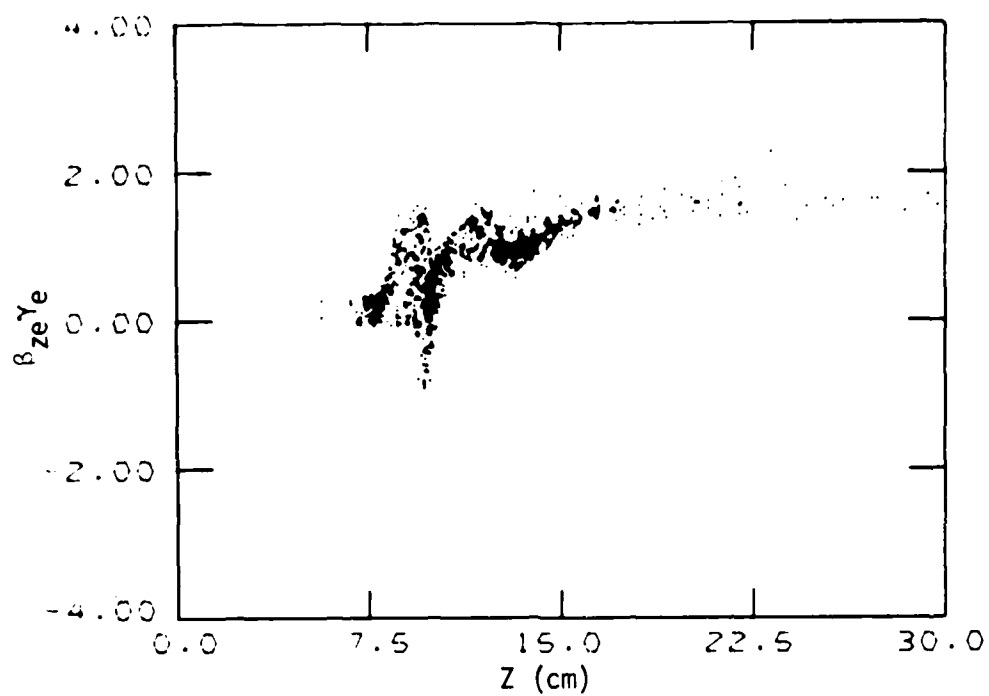
SECTION V

SIMULATION OF COLLECTIVE ION ACCELERATION IN THE LUCE DIODE

Because of the code results simulating collective acceleration in a preformed plasma and the Cornell experiments, it has become clear that accurate inclusion of the diode physics or its consequences is an important aspect of studying the Luce diode. As noted earlier the Cornell experiments were chosen as the simulation model, because of the extensive diagnostic information and its simple design. Extensive modification of CCUBE was necessary. Many numerical problems in the ion emission algorithm were encountered. Finally, a simulation was produced which included an exact replica of the Cornell diode and was sufficiently numerically stable to accurately depict the problem physics. The results of this run are in striking contrast to the earlier simulations.

In the simulation a TEM wave is launched down the coaxial transmission line and onto the cathode. When the electric field on a cathode cell exceeds a threshold value, electrons are emitted from the cell. Electrons bombarding the anode trigger ion emission from anode cells in the tapered section of the dielectric. Ion emission takes place on an ion time scale and electron emission occurs every time step. The value of ω_p in these simulations is taken to be $3 \times 10^{10} \text{ sec}^{-1}$ so that $c/\omega_p = 1.0 \text{ cm}$ and $\omega_p^{-1} = 0.033 \text{ nanoseconds}$.

Compare the schematic of Figure 1 to the structure in Figure 7. Figure 7 represents the electron beam momentum space and real space early in the beam pulse. A hot-emitted electron beam and virtual cathode are evident in the top particle plot. The electron beam downstream of the virtual cathode is relatively cold at this time in contrast to the earlier simulations modeling injection through a dense plasma. The equivalent ion



TIME = 100.0000

Figure 7. Electron momentum space and real space at 3.3 nanoseconds.

diagrams are given in Figure 8. Note that in this simulation a very short pulse risetime and a mass ratio of $m_i/m_e = 459$ are used to save computer time.

The cold electron and ion beams propagating in the drift tube clearly suggest the possibility of an ion-electron two-stream instability. At this early stage, however, the plasma is not spatially long enough for real wave growth.

As the ions propagate they neutralize the electron space-charge. This allows several things to occur. First, a larger net current can propagate downstream. The net current profile is a strong indication of plasma propagation. In the Cornell experiments (Refs. 6,7) it took some 40-50 ns to establish a relatively constant net current out to 20 cm from the anode. This is an important consideration, because of the spatial growth lengths for the streaming instabilities.

Second, more electrons exit the pinched beam diode. Initially, the virtual cathode acts as a filter to transmit only those electrons which have the highest axial momentum. This results in a cold beam. The "hot" electrons with large transverse and small axial momenta are reflected back into the diode. The space-charge neutralization caused by the ions allows a larger portion of the electron beam, and therefore hotter electrons to cross the virtual cathode. The resultant beam which is "warm" as it exits the virtual cathode can be seen in Figure 9. Note, however, that the virtual cathode continues to function as a limiter to maintain quasi-neutrality in the drift tube.

The co-streaming of the warm electron beam and relatively cold ion beam is susceptible to a relativistic, warm electron-ion streaming instability. This instability is the source of the wave acceleration of ions seen in Figure 10. The peak ion energy is six times the beam kinetic

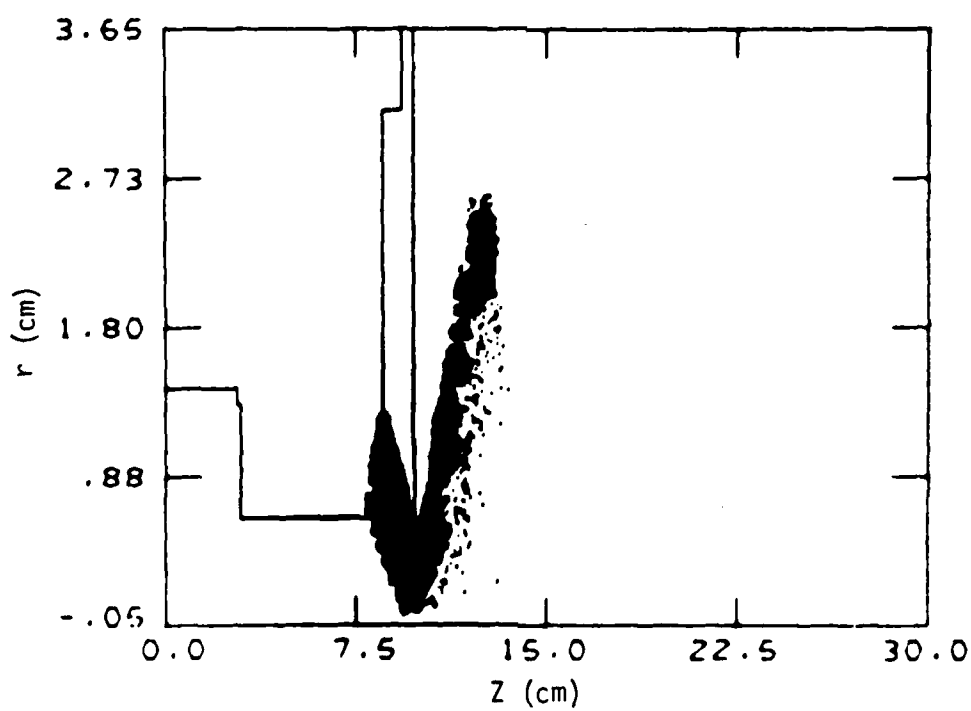
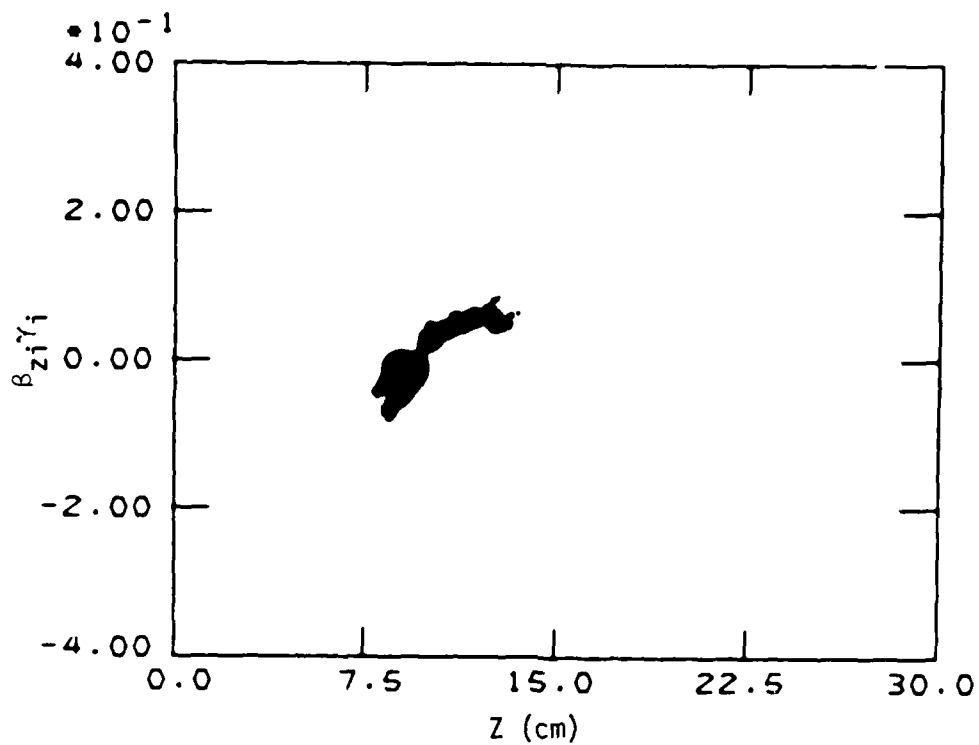


Figure 8. Ion momentum space and real space at 3.3 nanoseconds.
 m_i/m_e is 459.

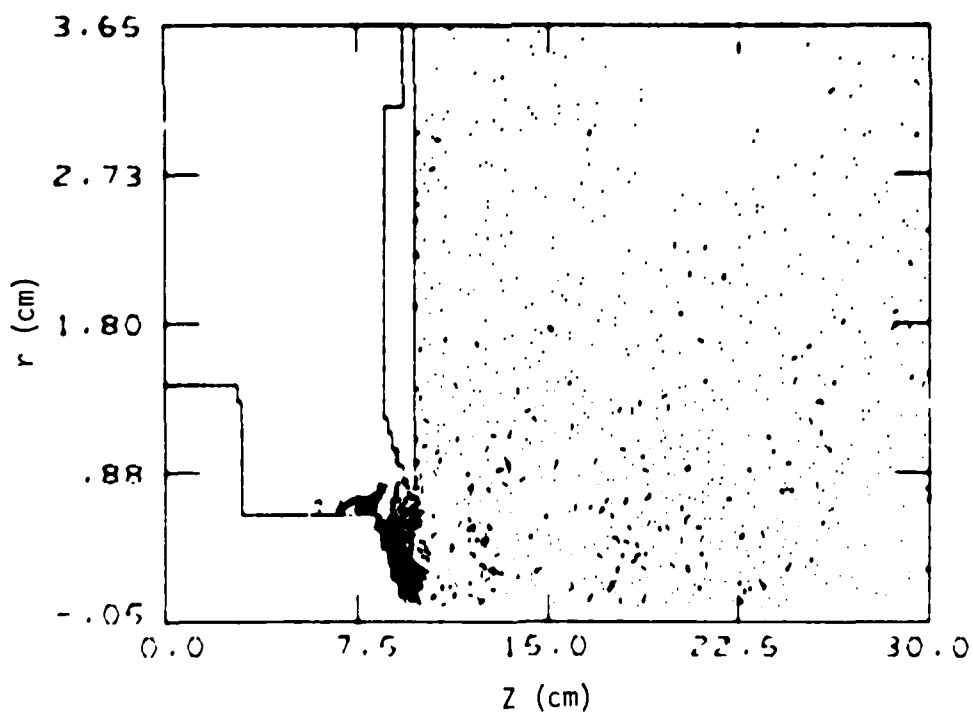
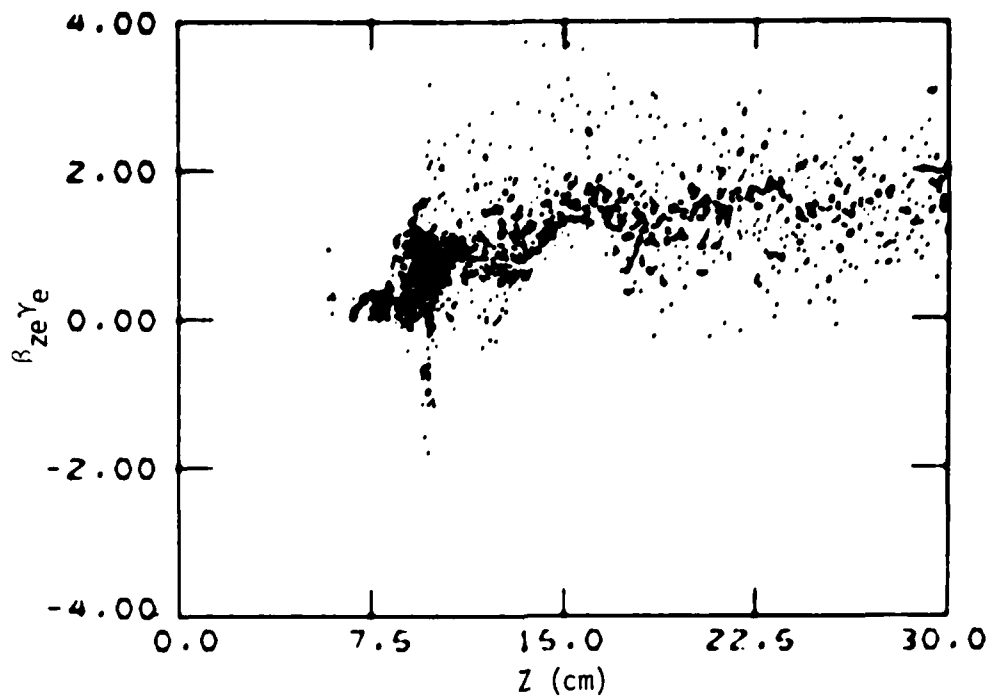


Figure 9. Electron momentum space and real space at 11.0 nanoseconds.

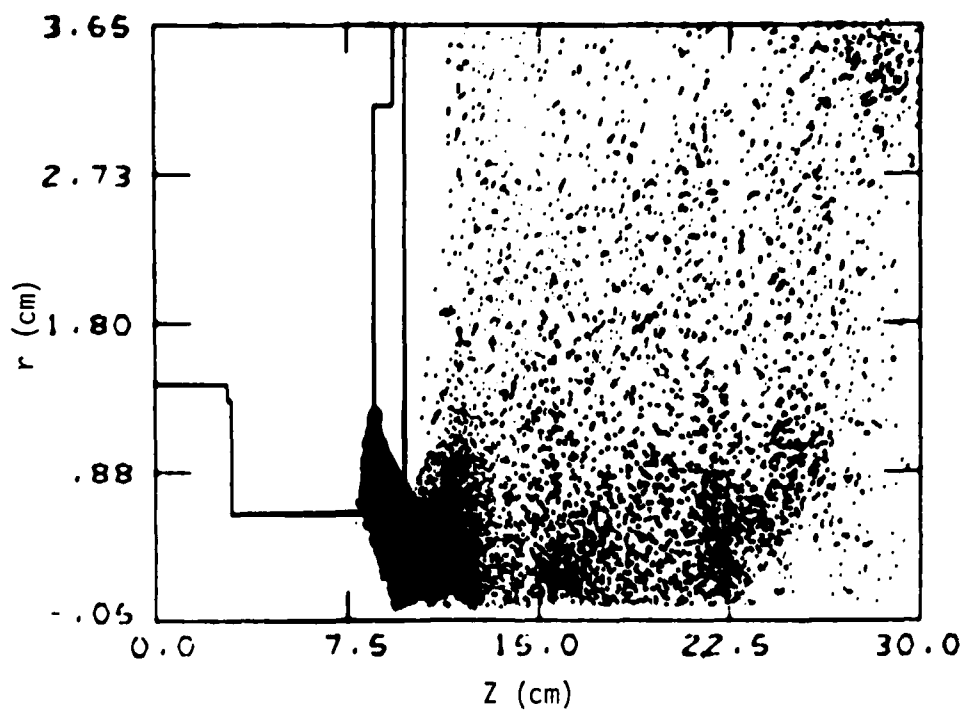
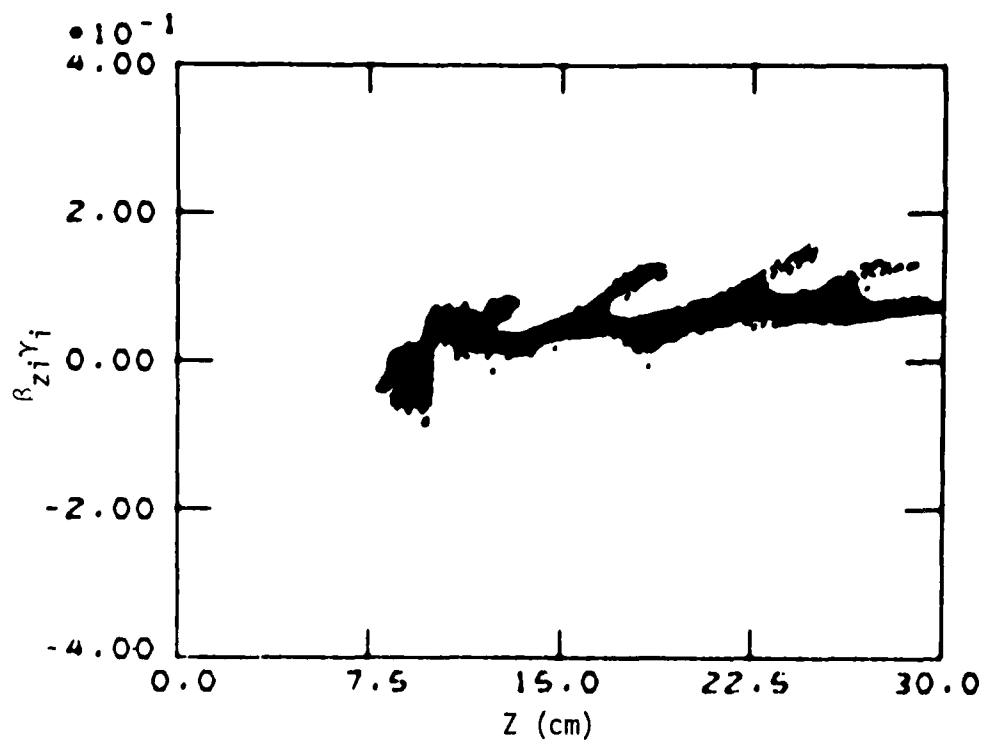


Figure 10. Ion momentum space and real space at 11.0 nanoseconds.
 m_i/m_e is 459.

energy. The streamers accelerating out of the main ion beam phase space coincide with high density ion bunches. The wave producing the ion acceleration must have a slow phase velocity and sufficiently large amplitude to trap ions and carry them along. These requirements are met based on the dispersion relation for plasma waves on a warm electron beam.

The low wave phase velocity has the two desired effects. Namely, it allows for trapping of low velocity ions, and it retards instability saturation by making it harder for the electrons to be trapped and deplete the wave energy. The latter results in larger saturated wave amplitudes. The wave cannot propagate with the electrons indefinitely with no dissipation. Figure 9 shows the electron beam becoming turbulent at approximately 12 centimeters from the anode back plane. The cause of the turbulence is due to electrons performing trapping oscillations in the waves. This is the natural saturation mechanism for a two-stream instability. The trapping results in electron beam heating which saturates the waves.

In order to compare the experimental and computer results, two adjustments to the simulation are required. First, the fast beam risetime and ion production lead to propagation out of the diode in less than 2 nanoseconds. The experimentally observed time is 6-10 nanoseconds. Second, the instability growth rate depends on the square root of the ion-to-electron mass ratio. Here, that ratio is only one-quarter of the actual proton-to-electron value. Therefore, the 11 nanoseconds of simulation time correspond to from 26-30 nanoseconds of the experiment. This indicates that the simulation has not progressed far enough to obtain the maximum ion acceleration witnessed in the experiments. More importantly, for whatever reason these simulations do not reproduce the low frequency ion bunching associated with the highest energy ions or its microwave signature. Expressing this another way, we have not witnessed in these simulations the expected ion acoustic instability.

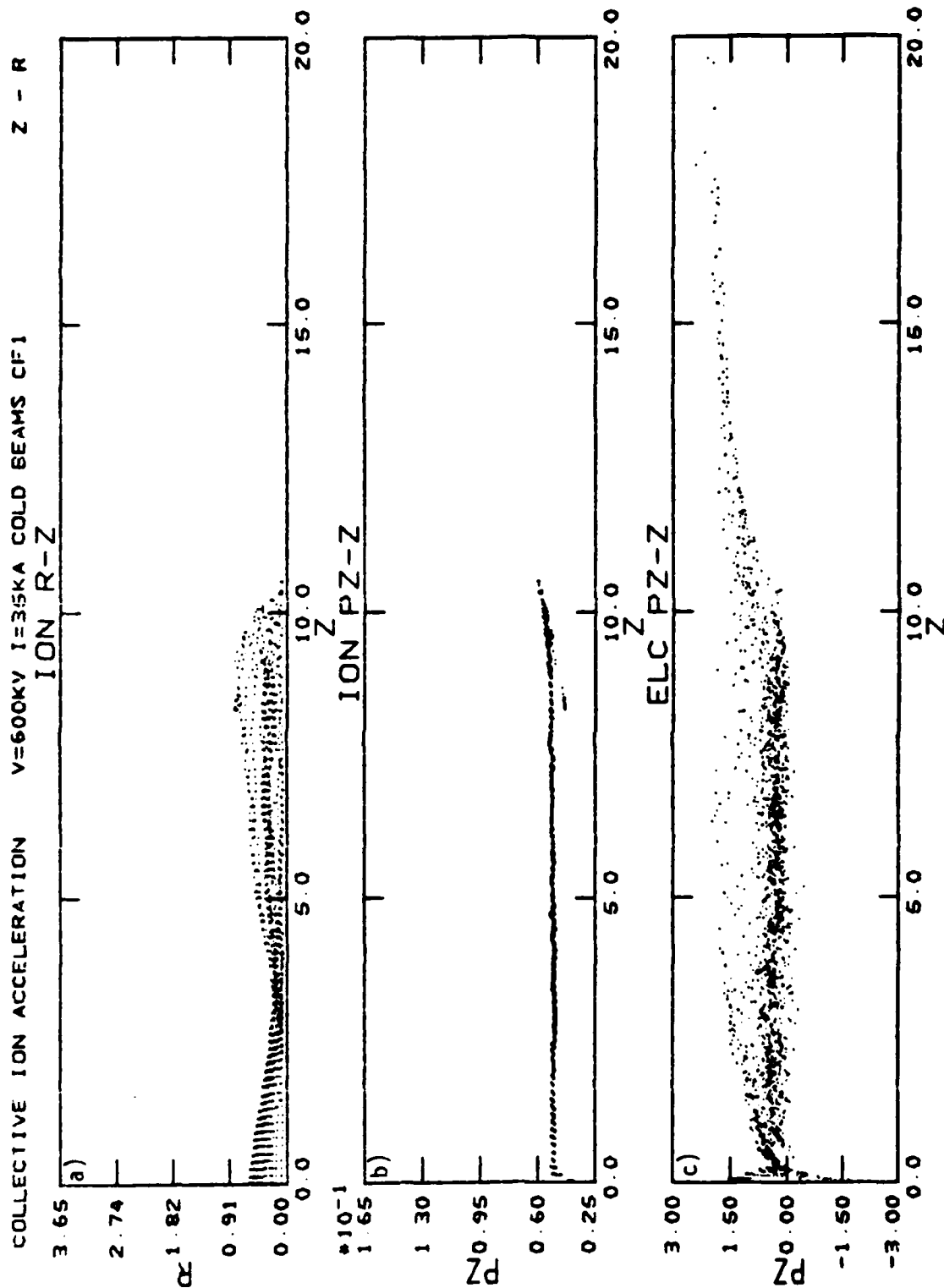
One of the major drawbacks of running the Luce diode simulations was our inability to produce an impedance low enough to match the experimental range of 8.5Ω - 11.5Ω . We also experienced numerical instability

problems when attempting to run the simulation for the large number of time steps required. By this point, however, it was obvious that the main distinction between the simulations using a preformed plasma and those modeling the self-consistent diode physics was the diode/virtual cathode properties of producing and maintaining a quasi-neutral plasma in the drift region for an unlimited time. In preformed plasma simulations the ions could be depleted after a short period.

In order to run the simulations for long periods, we injected two equal density, $n_i = n_e$, equal energy (600 kV) beams modeling the left hand boundary as a ground plane. The drift tube radius was kept at 3.65 cm and the beam radii were set to 6 mm - the same size as the hole in the dielectric anode. In an attempt to directly compare the simulation results with experiment, we chose the ratio of ion mass m_0 to electron mass m_e to be 1836 - the proton/electron mass ratio. The injected electron beam current was 35 kA, which is equal to the Alfvén current for a 600 keV beam. The initial temperature for both ions and electrons was zero. The simulation was run for the equivalent of 35 nanoseconds. The usual 6-10 nanoseconds for ion propagation to start in the diode would have to be added to the simulation time for comparison with experiment.

The results of this particular simulation are extraordinary. The ratio of maximum ion to electron beam energy reached a factor of eight or 4.8 MeV. Moreover, the peak energy ions are produced periodically at a frequency of 250 MHz. The main acceleration took place after the electron beam pinch point and was related to instability-driven plasma waves whose frequency, wavelength, phase velocity, and amplitude were 3.3 GHz, 0.4 cm, 0.044 c, and 2 MV/cm, respectively. These frequency numbers are in excellent agreement with the Cornell experiment.

The results of this simulation will now be discussed in detail. Figures 11, 12, and 13 are frames from a movie showing the real ion (r-z)



TIME = 200.0000

Figure 11. Movie frames of a) the ion real (R-Z) space b) ion axial momentum and c) electron axial momentum phase spaces at $t = 6.7$ ns. The units of Z and R are cm, PZ is $\beta_Z \gamma$, and $m_i/m_e = 1836$.

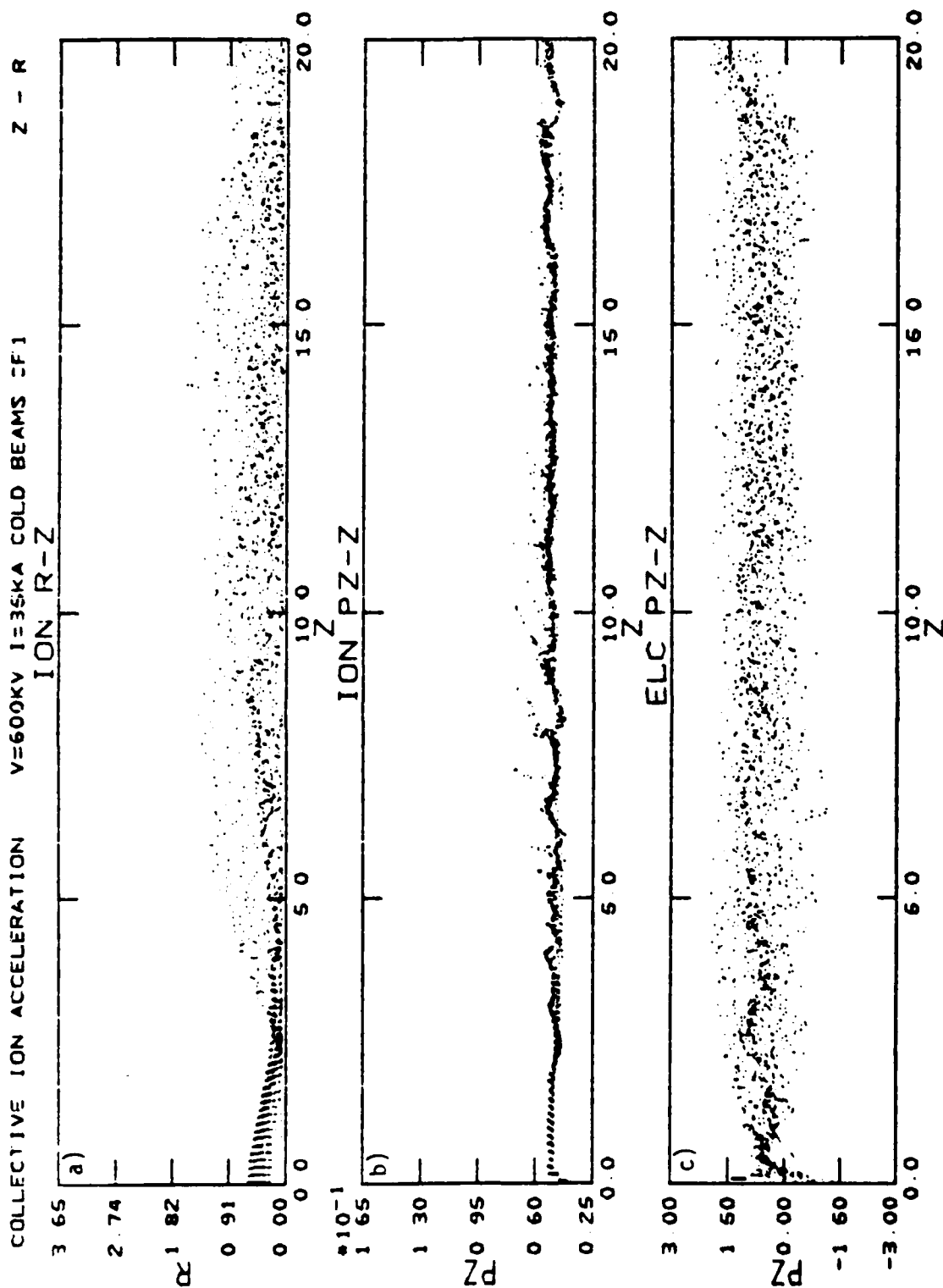
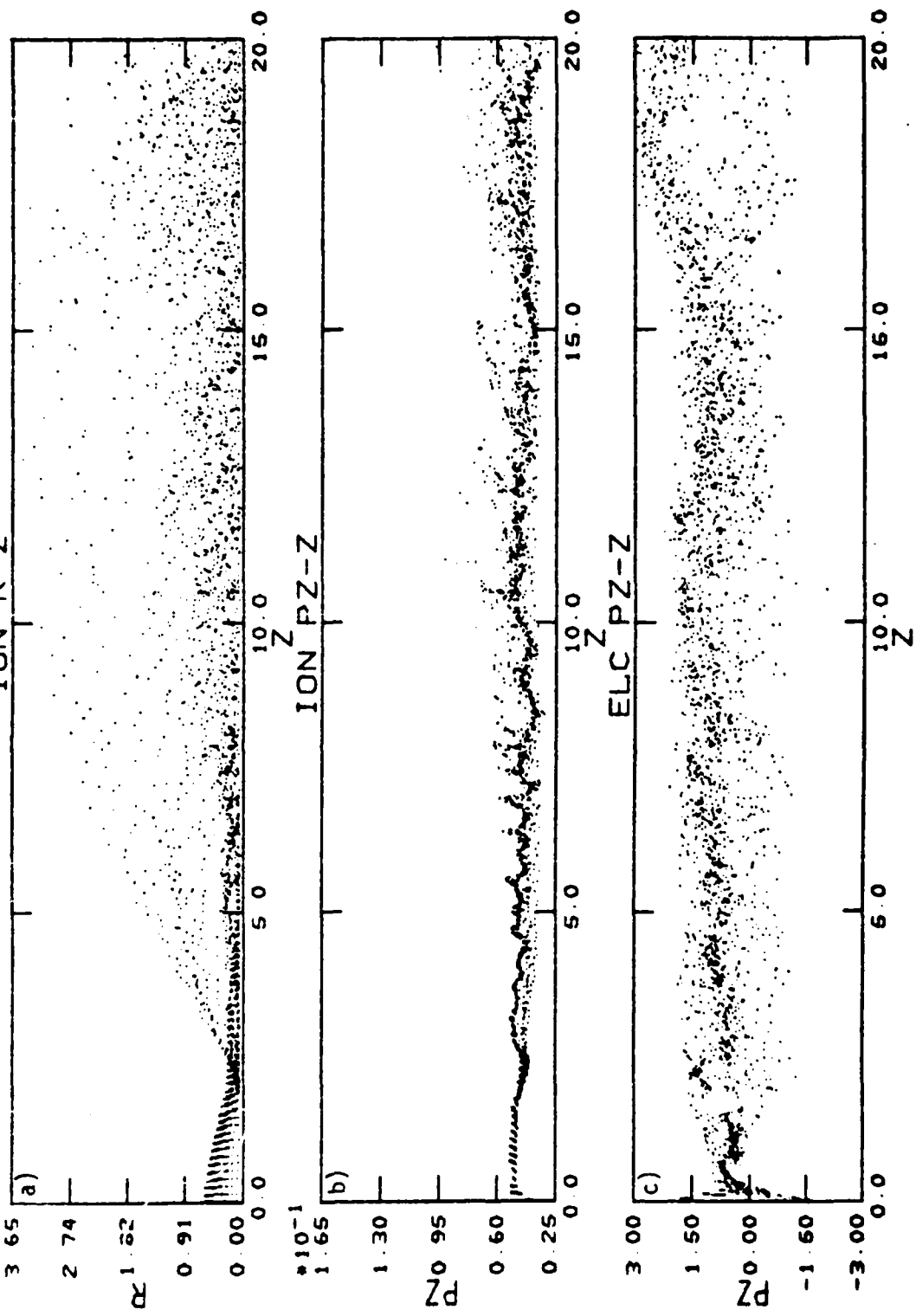


Figure 12. Movie frames of a) the ion real (R-Z) space, b) ion axial momentum and c) electron axial momentum phase spaces at $t = 13.3$ ns. The units of Z and R are cm, PZ is $\beta_2 \gamma$, and $m_i/m_e = 1836$.

COLLECTIVE ION ACCELERATION V=600KV I=35KA COLD BEAMS CF1 Z - R
ION R-Z



TIME = 840.0000

Figure 13. Movie frames of a) the ion real (R-Z) space b) ion axial momentum and c) electron axial momentum phase spaces at $t = 28$ ns. The units of Z and R are cm, PZ is $\beta_Z \gamma$, and $m_i/m_e = 1836$.

space and the axial momentum (phase) of both ions and electrons as a function of z at 200 (3.67 ns), 400 (13.33 ns), and 840 (28.0 ns) ω_0^{-1} . Recall that $\omega_0 = 3 \times 10^{10} \text{ sec}^{-1}$. The ion phase space in Figure 11 clearly shows the hydrodynamic driven acceleration at the head of the beam discussed in the previous section. The beam front is propagating at a velocity of 0.053 c, while the majority of ions behind the front have a velocity of roughly 0.03 c. there is no evidence of wave growth at $\omega_0 \tau = 200$. The ion real space clearly shows a strong pinch at $z = 2.5 \text{ cm}$ and the virtual cathode is well established. The net current downstream is being limited by it to approximately 15 kA, and it clearly has affected the electron beam temperature severely. Note that the ion pinch is formed electrostatically in response to a strong electron beam magnetostatic pinch at the same longitudinal location.

In Figure 12 at $\omega_0 \tau = 400$ a short wavelength instability is starting to accelerate ions. Note that this only occurs on the downstream side of the pinch where extremely high charge densities are present. This will have a large effect on the growth rate and frequency of the instability. The electron beam appears measurably hotter downstream, after saturation of the instability due to electron trapping.

Finally, inspection of Figure 13 clearly shows a continued short wavelength instability past the pinch point in the ion phase space. However, this is followed by a the 250 MHz, approximately 8 cm wavelength instability noted earlier. This yields a phase velocity of about 0.07 c. Ions, which have been accelerated by the first instability before it is saturated, are further accelerated by the second instability in a two-stage process. The strength of the latter is evident in its affect on the electron beam phase space.

An examination of the time histories and Fourier transforms of longitudinal electric field probes is educational, because it shows the

growth rates of the instabilities and amplitudes of the accelerating fields. The first probe (Fig. 14) is located on axis near the injection plane ($r = 0, z = 0$). The very high frequency oscillation is due to the motion of the virtual cathode. It is oscillating at a frequency of 39 GHz with an amplitude of 1.5 MV/cm superimposed on a static 4.5 MV/cm field normal to the injection boundary. Even though this is a large field, its frequency is much too high for the ions to respond.

The growth of the short wavelength instability is shown in Figure 15. This probe is located at $r = 0, z = 4$ cm - just past the pinch point. The wave has saturated at 0.6 MV/cm by $\omega_0 \tau = 300$ (10 ns) into the simulation. Its frequency is 4.0 GHz. It appears to have grown from noise in roughly 4 ns. The probe in Figure 16 is located at $r = 0, z = 5$ cm. The probe shows the E-field signal late in time (24-35 ns). It has clearly saturated at an amplitude approaching 2 MV/cm. Its frequency, which is extremely monochromatic is 3.3 GHz. Finally, the probe at $r = 0, z = 10$ cm is depicted in Figure 17. It is less monochromatic, has a lower frequency (1.4 GHz), and a lower amplitude (1 MV/cm) than the previous one. The following points should be noted with regard to Figures 15-17. First, the frequency of the stability decreases steadily away from the pinch point. This is the natural result of beam expansion decreasing the plasma frequency, which results in a decrease in the frequency of the most unstable mode. Second, the amplitude of the wave saturates at 2 MV/cm by approximately 2.5 cm or 6 wavelengths after the pinch point. It stays relatively constant in amplitude for 3.5 cm before being damped drastically by nonlinear trapping of electrons.

The nature of the long wavelength instability is also readily described by longitudinal electric field probes. Figure 18 is a probe located at $r = 0, z = 20$ cm. The higher frequency wave is barely visible in the Fourier transform. However, a 1.25 MV/cm, 250 MHz wave is evident.

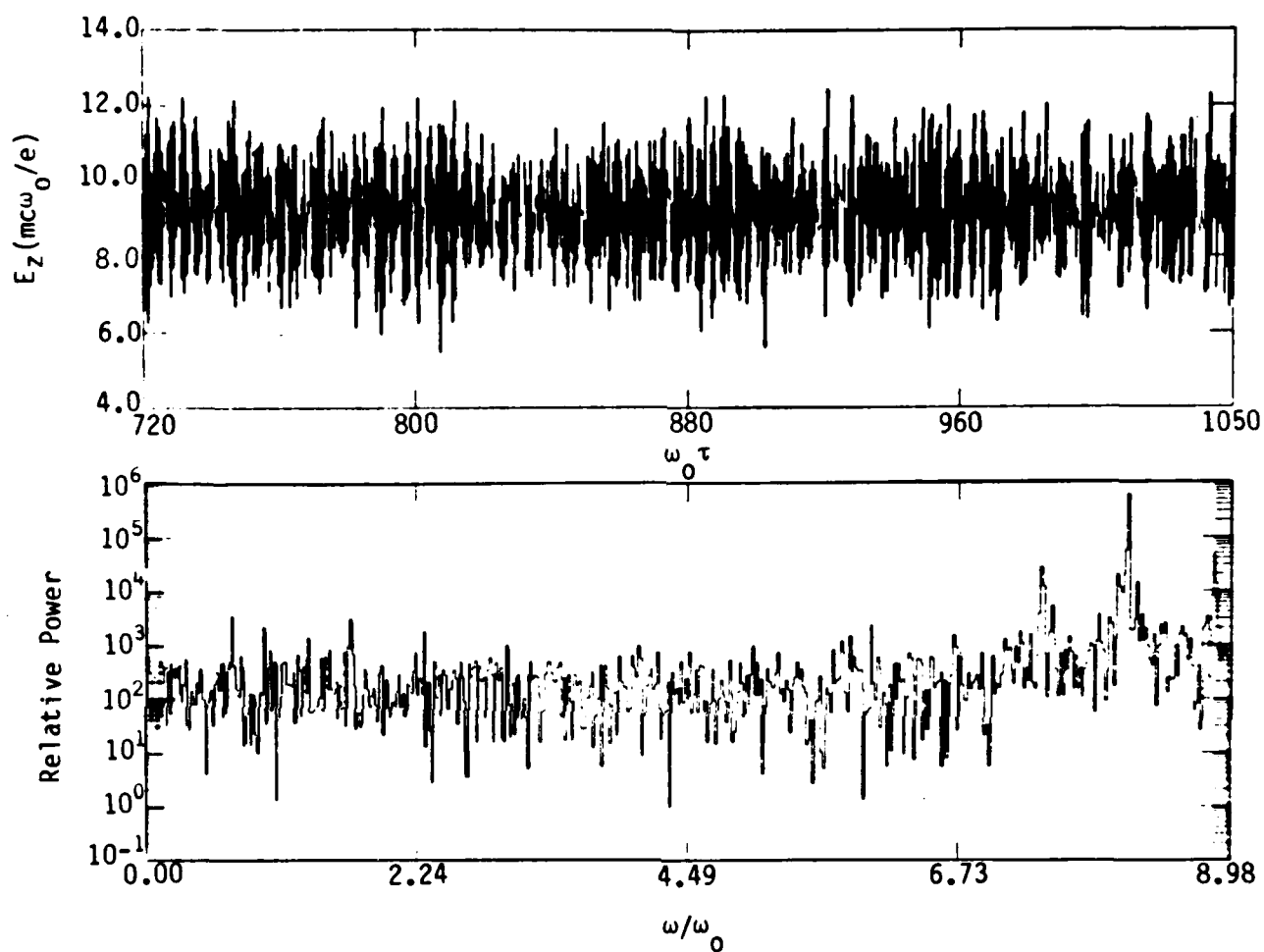


Figure 14. Probe history of the axial electric field at $r = 0$ cm; $Z = 0$ cm from 24 ns to 35 ns and its Fourier transform. Largest amplitude frequency $f = 39$ GHz.

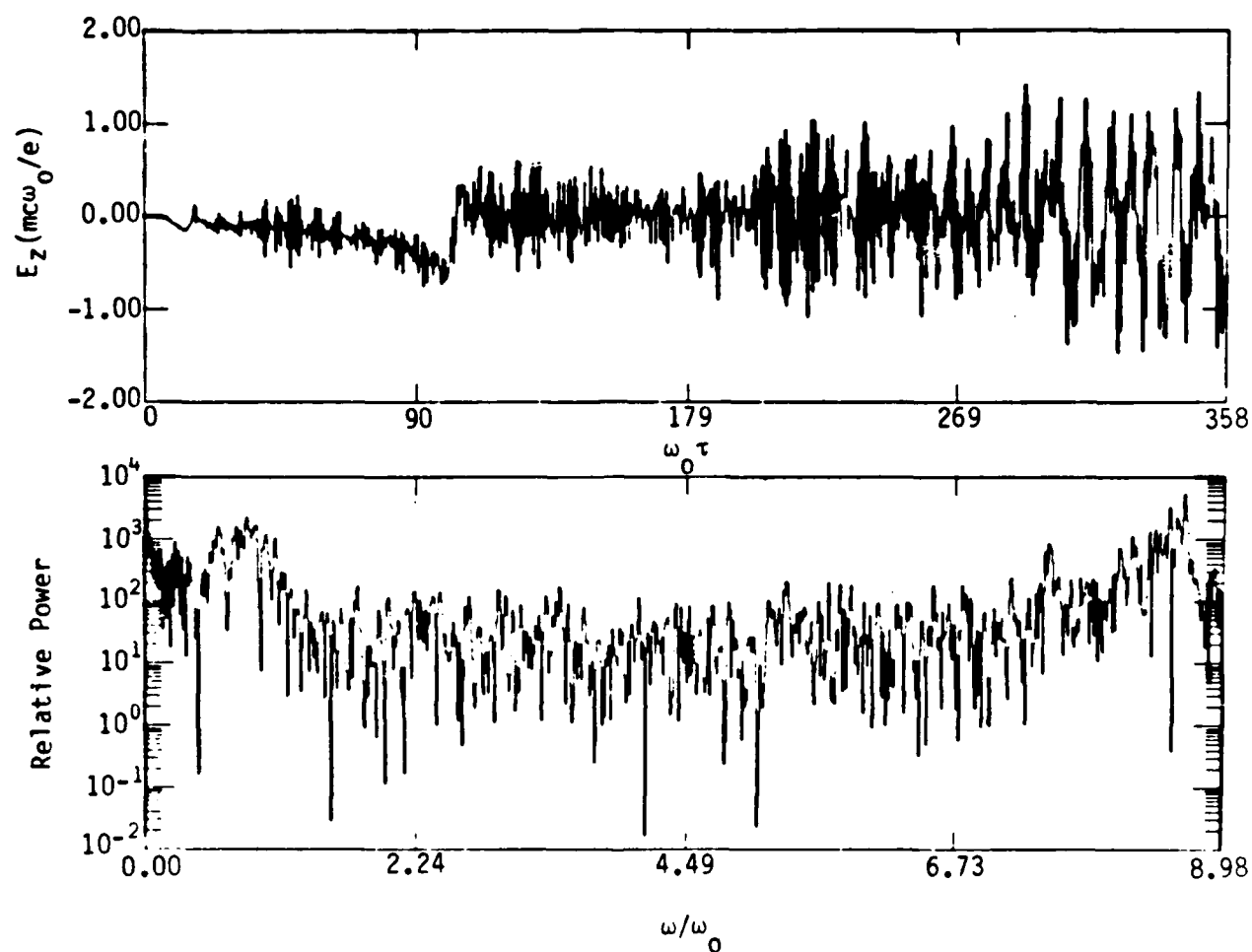


Figure 15. Probe history of the axial electric field at $r = 0$ cm; $Z = 4.0$ cm from 0 ns to 12 ns and its Fourier transform. Largest amplitude low frequency $f = 4.0$ GHz.

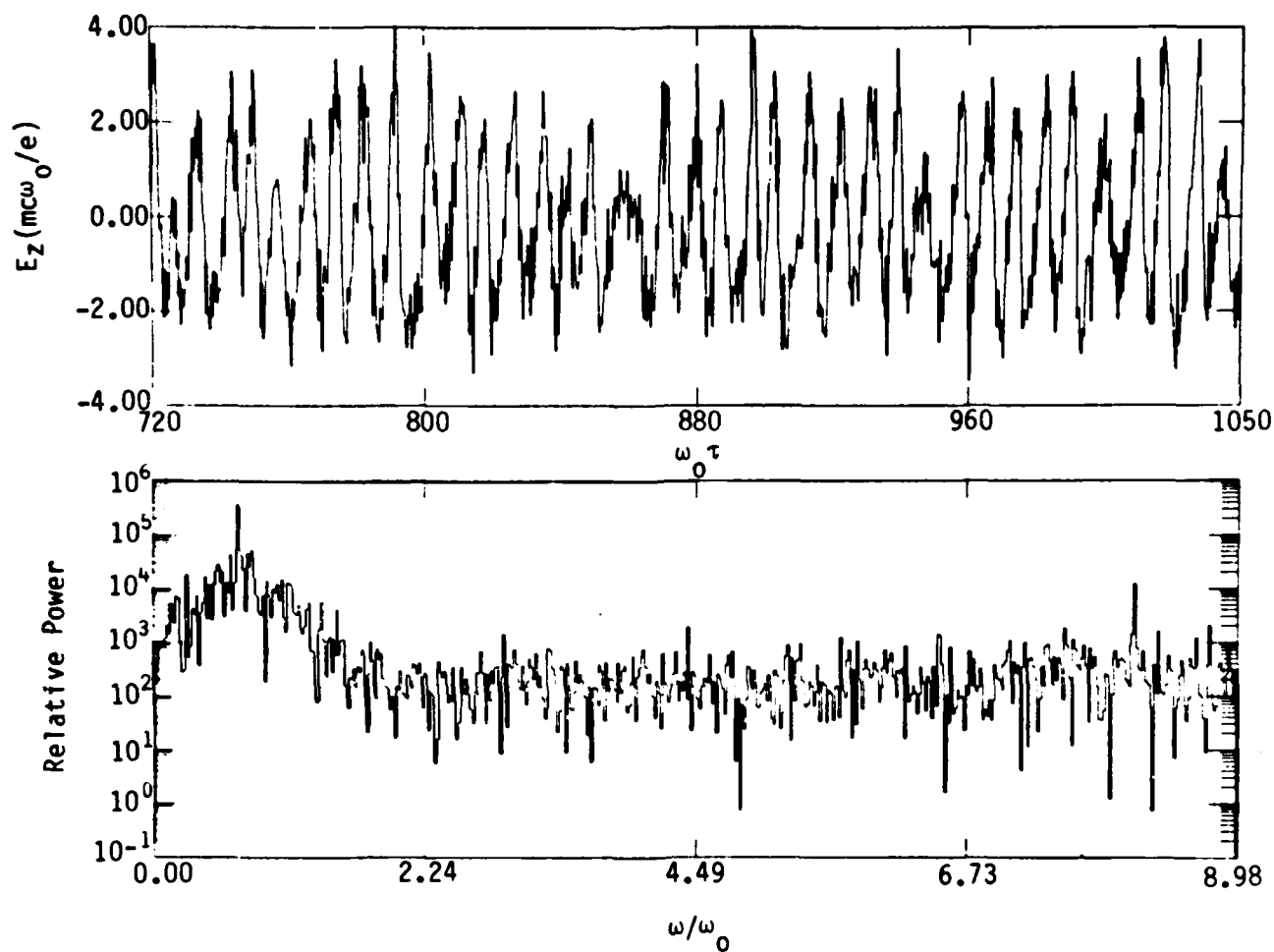


Figure 16. Probe history of the axial electric field at $r = 0$ cm; $Z = 5.0$ cm from 24 ns to 35 ns and its Fourier transform. Largest amplitude frequency $f = 3.3$ GHz.

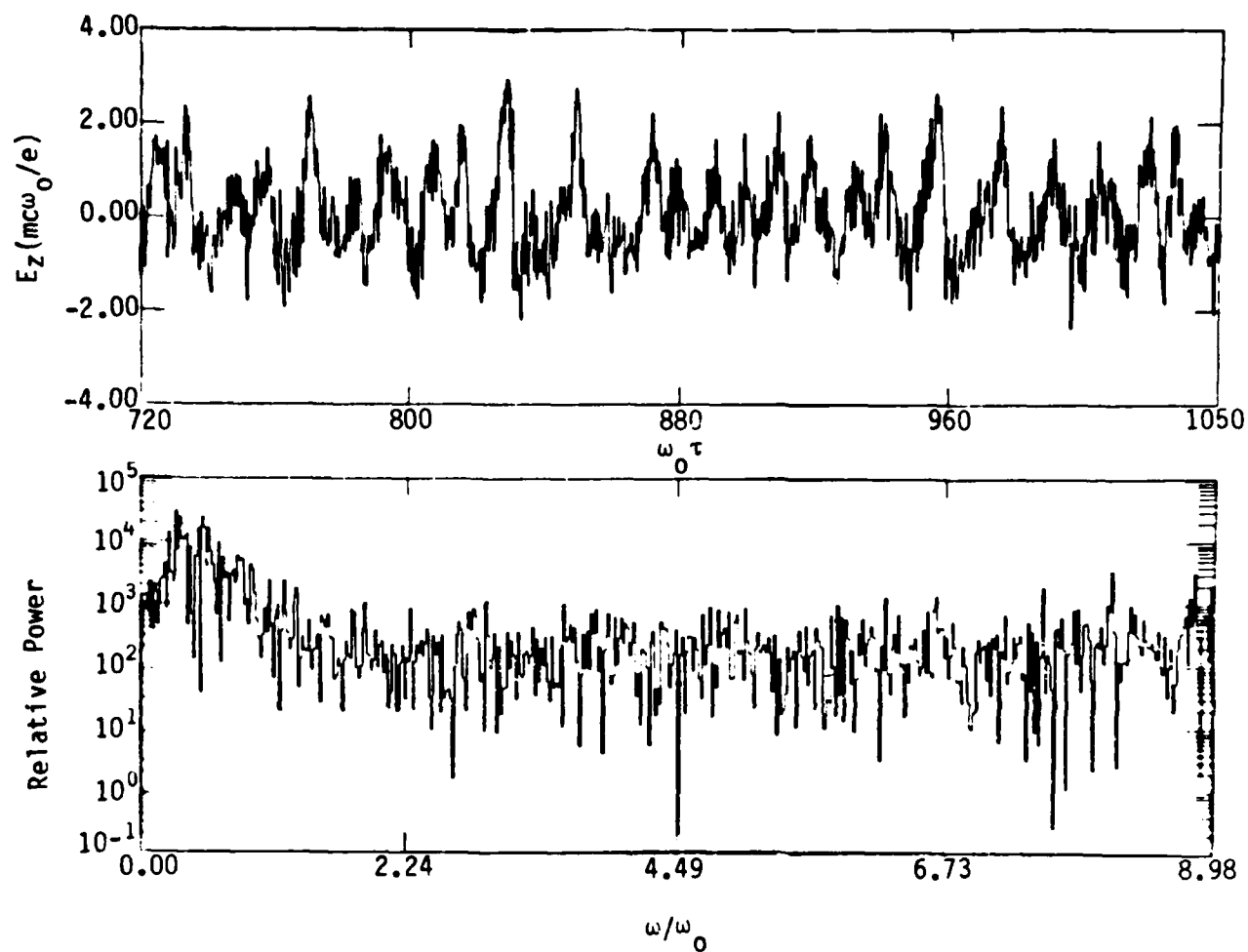


Figure 17. Probe history of the axial electric field at $r = 0$ cm; $Z = 10$ cm from 24 ns to 35 ns and its Fourier transform. Largest amplitude frequency $f = 1.4$ GHz.

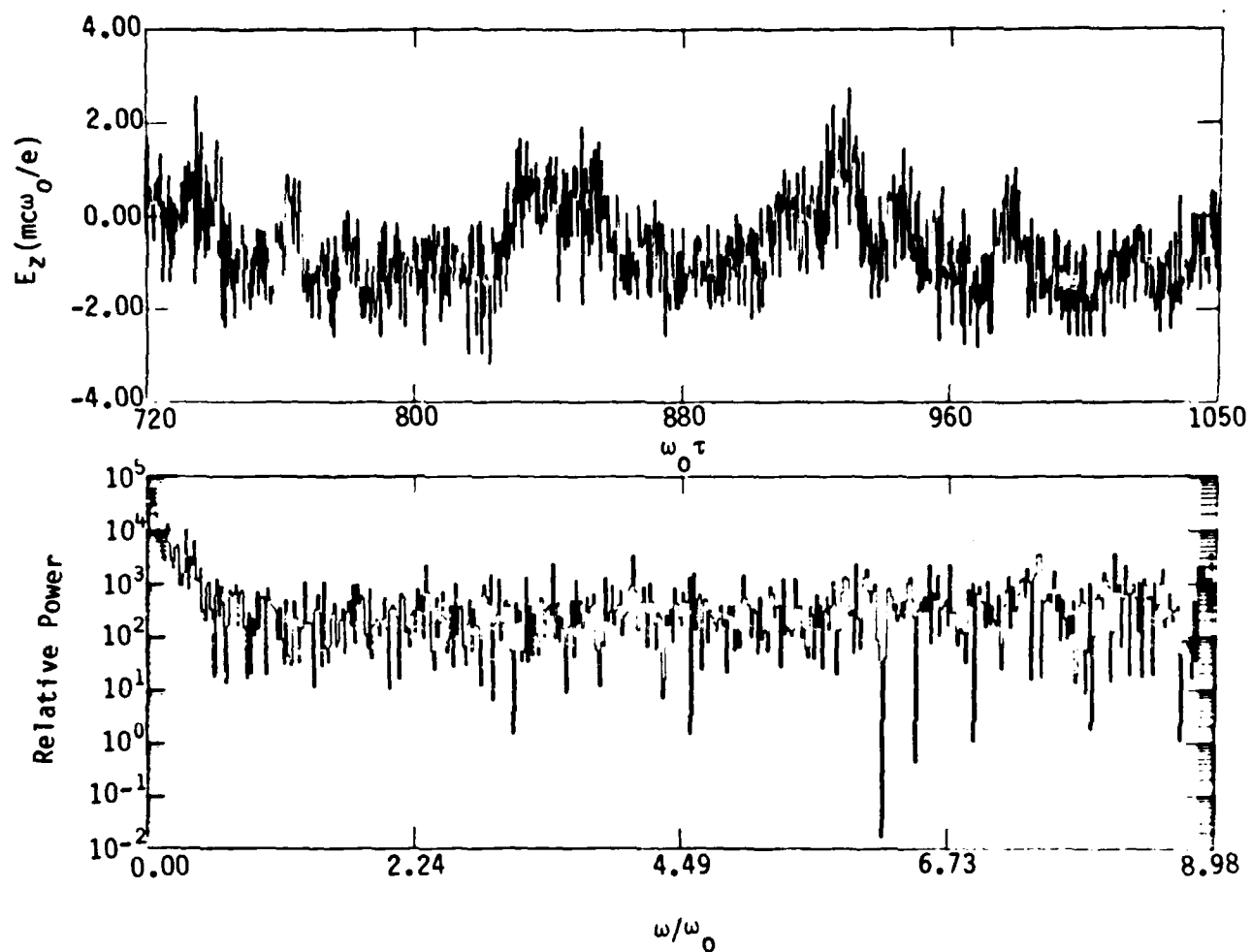


Figure 18. Probe history of the axial electric field at $r = 0$ cm; $Z = 20$ cm from 24 ns to 35 ns and its Fourier transform. Largest amplitude frequency $f = 250$ MHz.

The slow growth rate of the instability is shown in Figure 19. The probe is located at $r = 0.6$ cm, $z = 20$ cm for $t = 0-12$ ns. This is the radial location of the initially injected beams' outer edge. Probes at the same location but later in time ($t = 12-35$ ns) are shown in Figures 20 and 21. The clean 250 MHz signature is also present here and is in phase with the wave on axis showing its radial extent. However, the amplitude at this radius saturates at 0.5 MV/cm or more than a factor of two lower than on axis.

The growth of charge and current density on axis is shown in Figures 22-24. Each plot has several axial slices at different radial locations. Disregard all but the high amplitude one, which is the cut across z at $r = 0$. These diagnostics were taken at approximately $t = 12$, 23.3, and 34.7 ns. The first large amplitude, positive charge density spike denotes the location of the pinch point. It remains fairly stationary at 2.5 cm. The wavelength of the higher frequency instability is clear in all of the charge density graphs. For all practical purposes it has disappeared by $z = 10$ cm. The current density downstream of the pinch grows as a function of time, just as observed experimentally.

A noteworthy feature in Figure 24 is the presence of a large current density wave. This moves and corresponds exactly in space and time with the long wavelength instability mode. Its presence is also obvious in Figure 25, which is the charge and current density as a function of z integrated radially at $t = 34.7$ ns. Particularly interesting is the large negative radial current density associated with electrons being swept out radially to the wall. This lack of radial confinement is probably also responsible for the large loss of high energy ions at this location witnessed experimentally (Refs. 5,6, and see Appendix C).

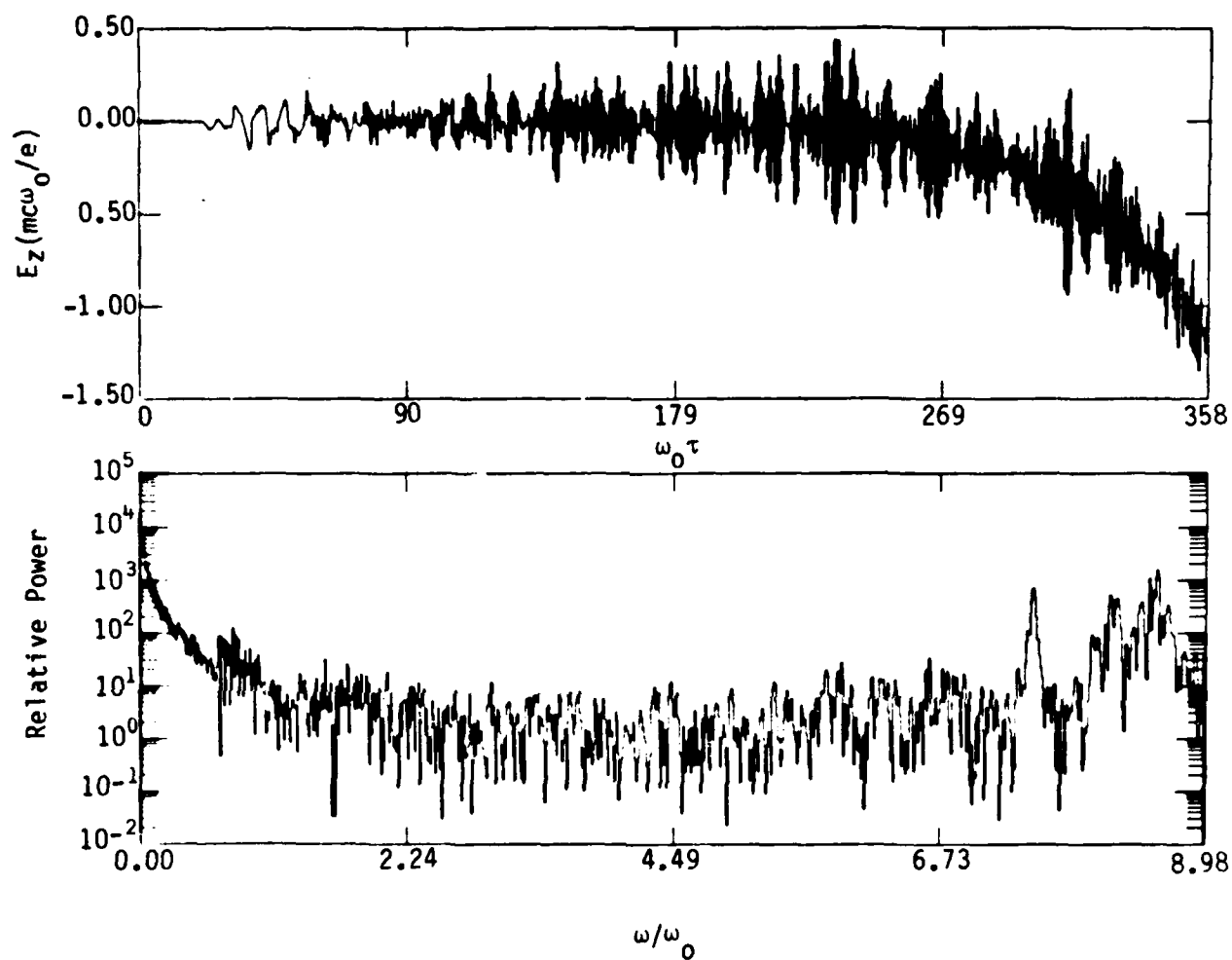


Figure 19. Probe history of the axial electric field at $r = 0.6$ cm; $Z = 20$ cm from 0 ns to 12 ns and its Fourier transform.

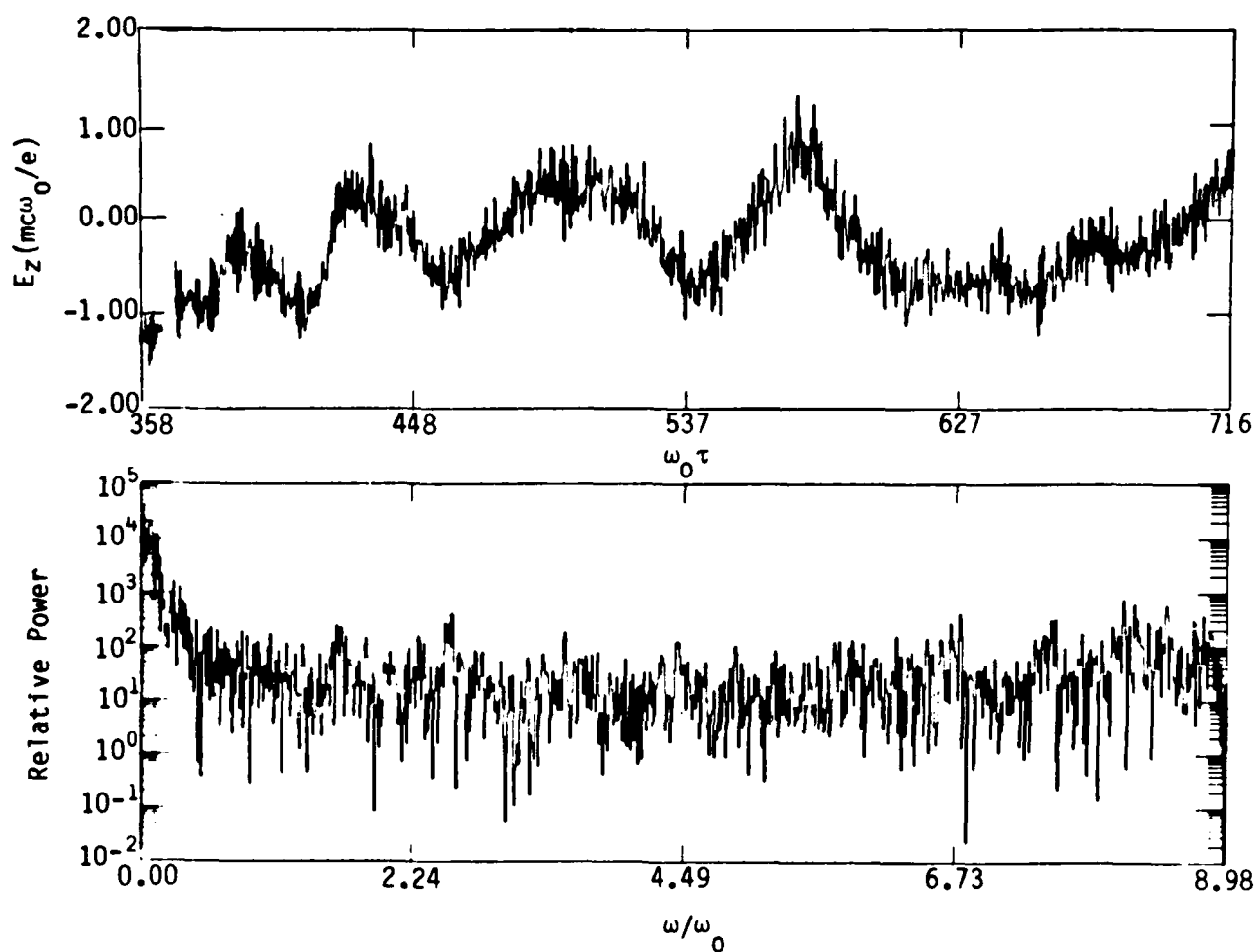


Figure 20. Probe history of the axial electric field at $r = 0.6$ cm; $Z = 20$ cm from 12 ns to 24 ns and its Fourier transform. Largest amplitude frequency $f = 250$ MHz.

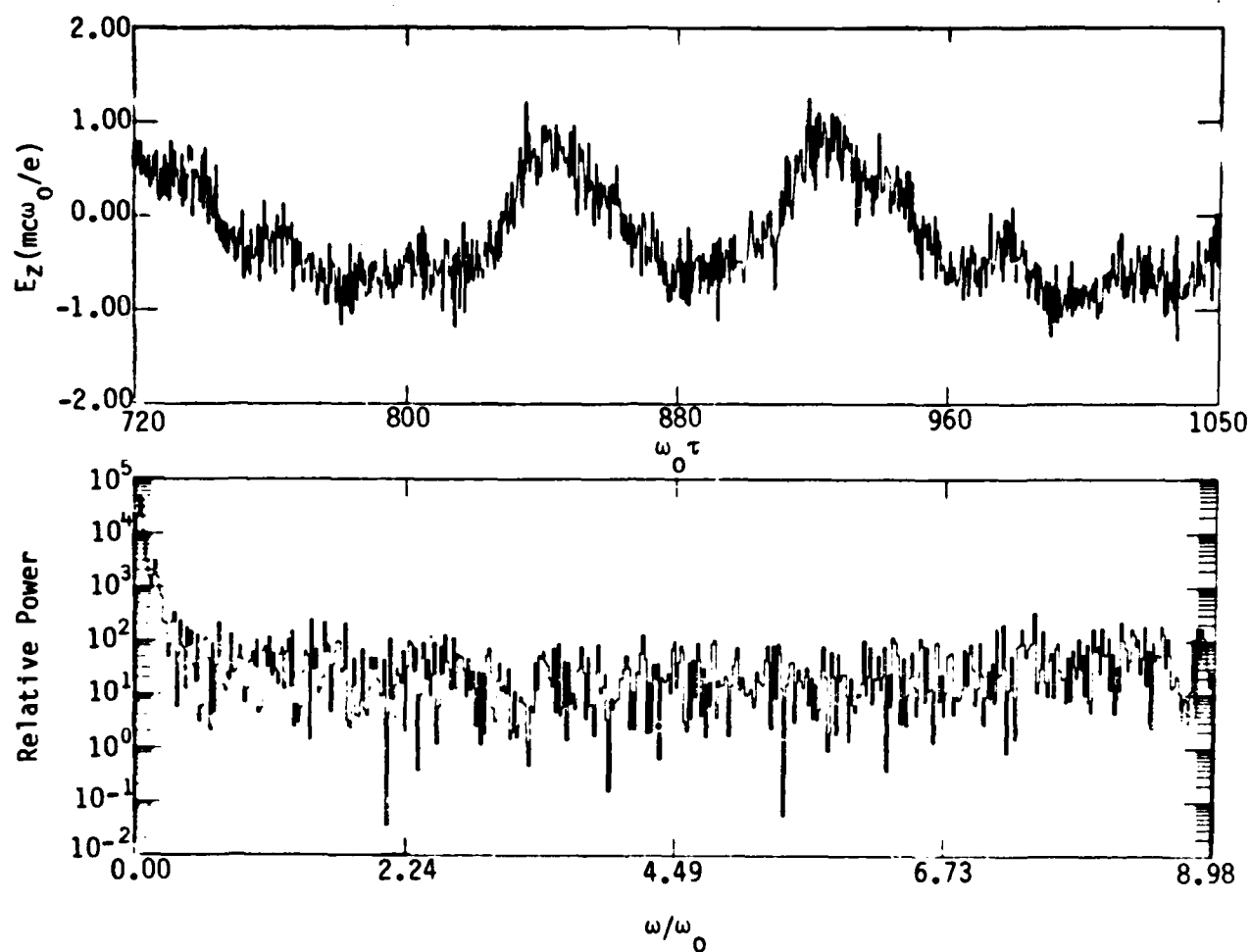
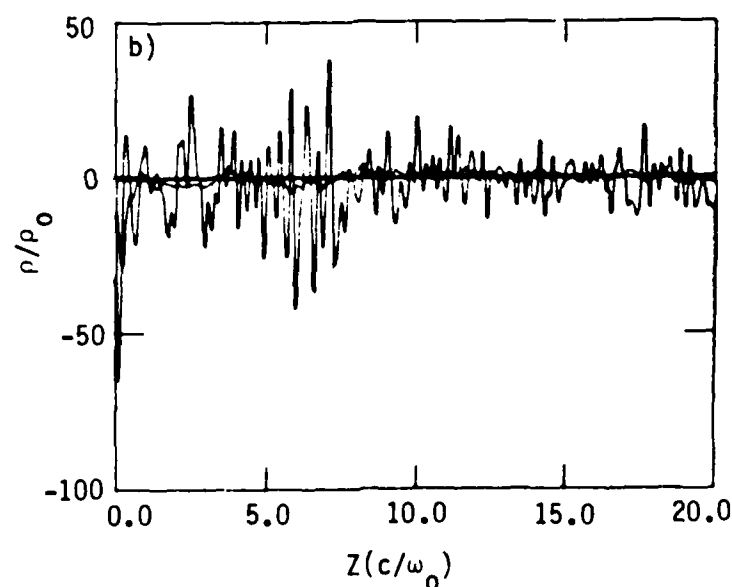
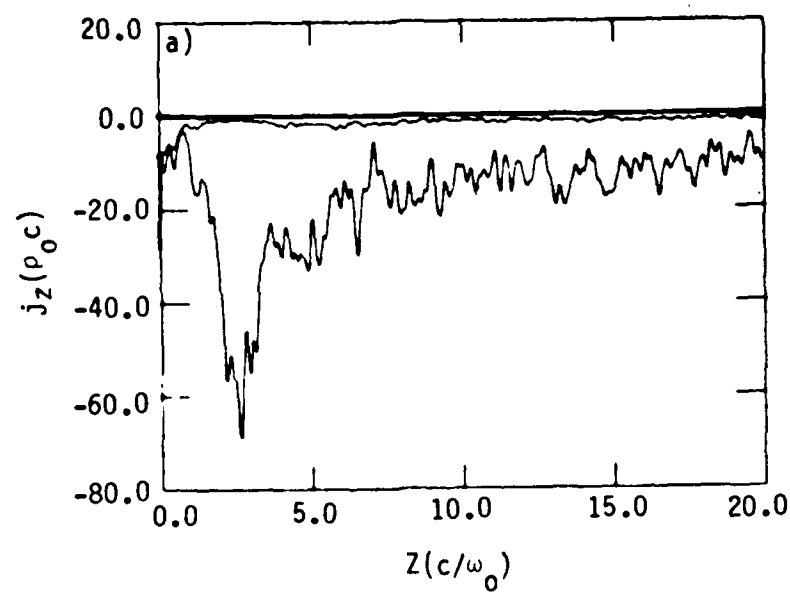
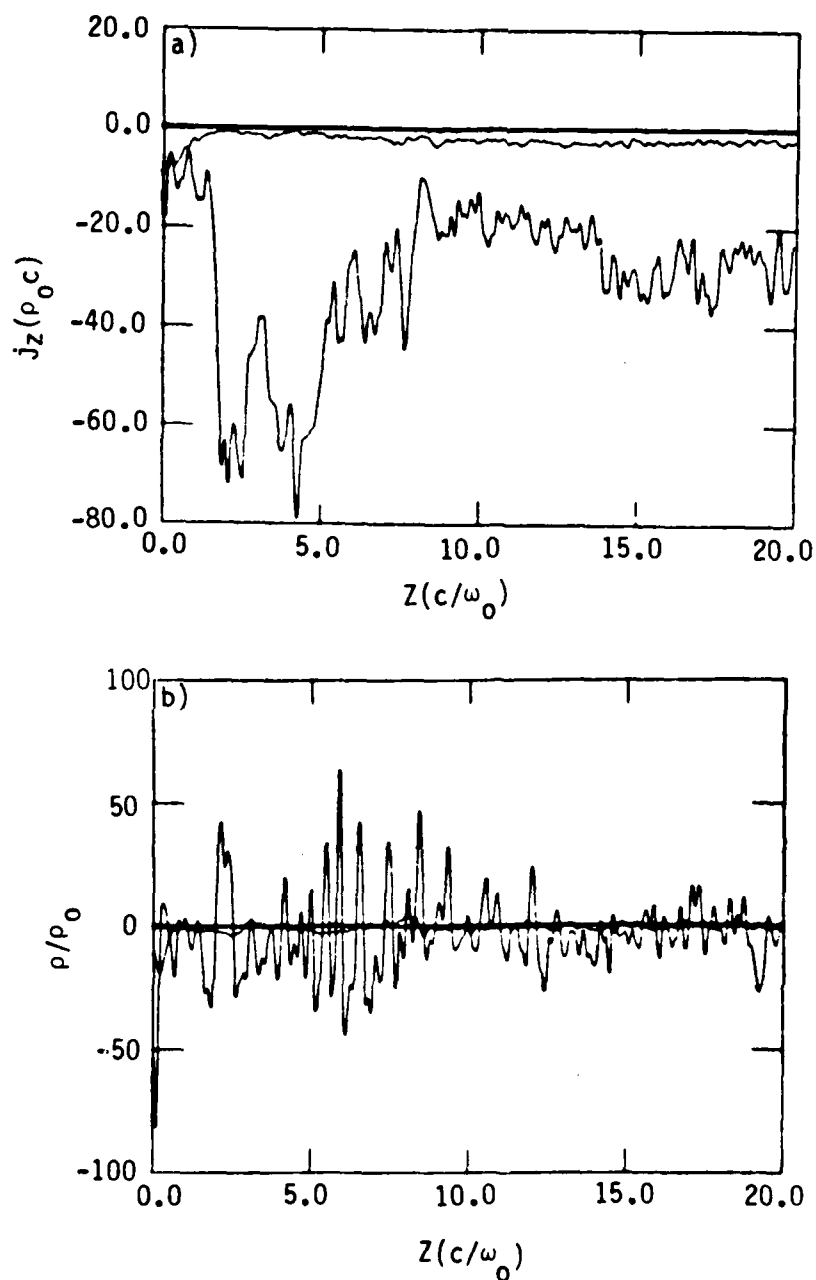


Figure 21. Probe history of the axial electric field at $r = 0.6$ cm; $Z = 20$ cm from 24 ns to 35 ns and its Fourier transform. Largest amplitude frequency $f = 250$ MHz.



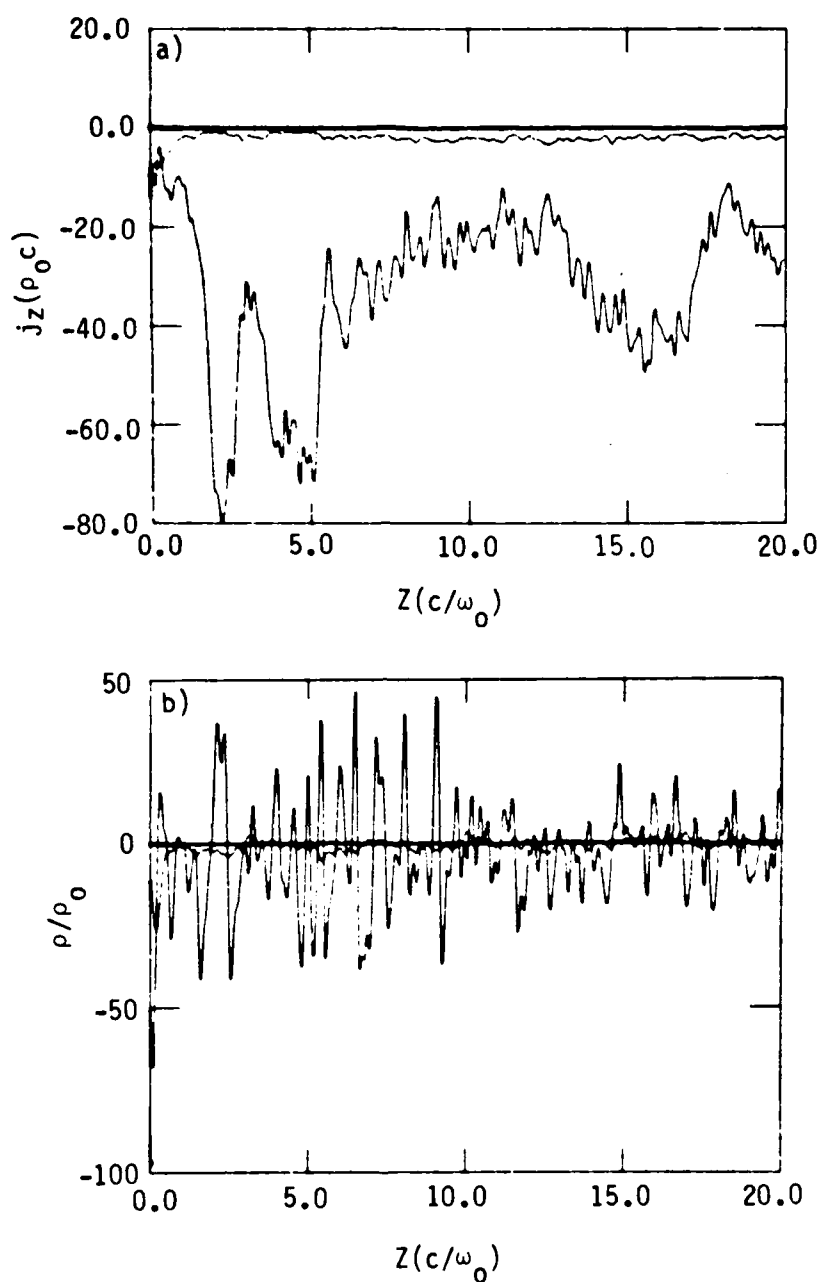
Time = 360.0000

Figure 22. Axial slices at different radii of a) axial current density and b) charge density as a function of Z at $t = 12.0$ ns. The large amplitude slice is at $r = 0$ indicating the beam pinch point is near 2.5 cm.



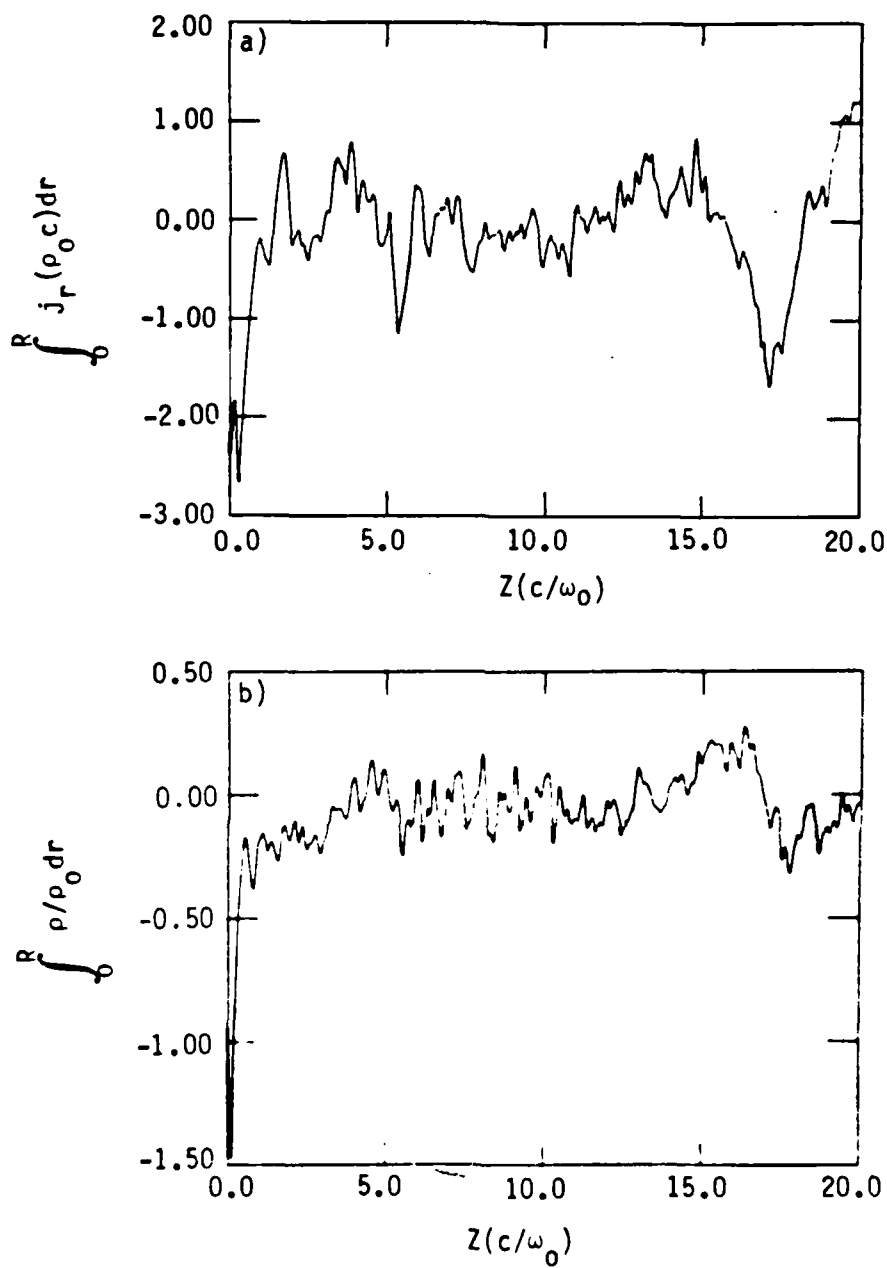
Time = 700.0000

Figure 23. Axial slices at different radii of a) axial current density and b) charge density as a function of Z at $t = 23.3$ ns. The large amplitude slice is at $r = 0$ indicating the beam pinch point is near 2.5 cm.



Time = 1040.0000

Figure 24. Axial slices at different radii of a) axial current density and b) charge density as a function of Z at $t = 34.7$ ns. The large amplitude slice is at $r = 0$ indicating the beam pinch point is near 2.5 cm.

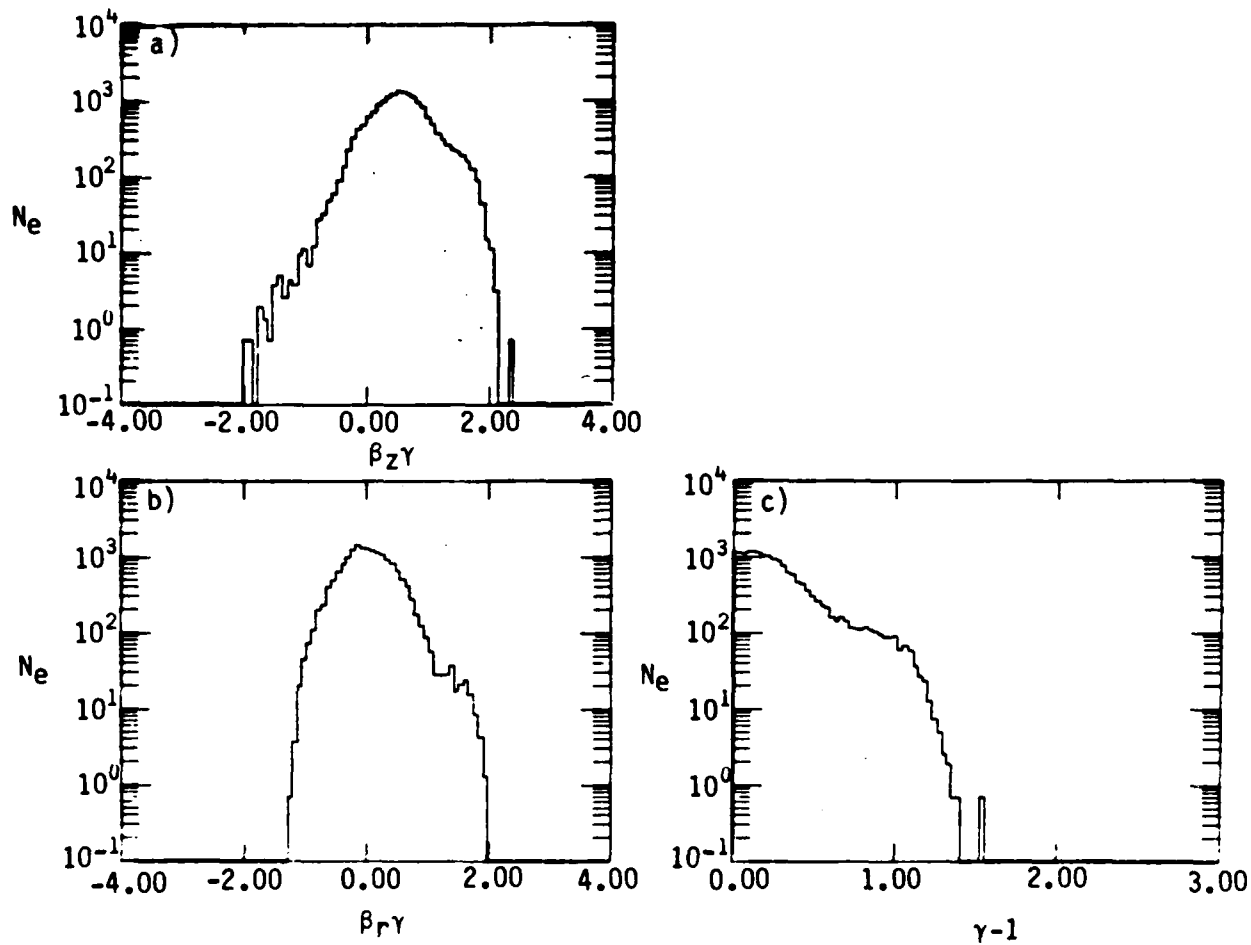


Time = 1040.0000

Figure 25. Plots of the radial integrals of a) the radial current density and b) the charge density as a function of Z at $t = 34.7$ ns.

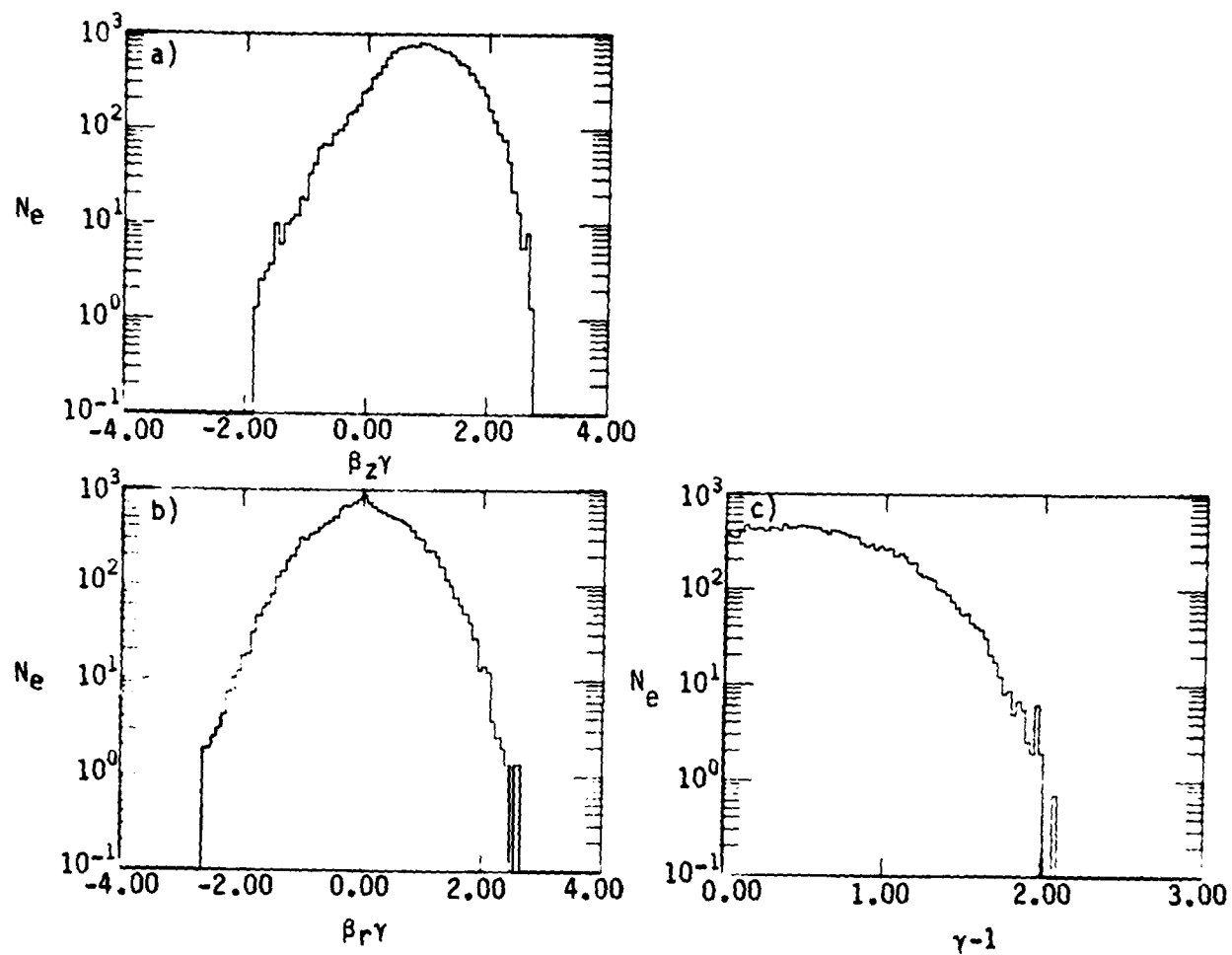
Finally, Figures 26-31 present the electron and ion (axial momentum, radial momentum, and kinetic energy) distribution functions at $t = 12, 23.3$ and 34.7 ns. First consider the electron distribution. The initial value of 600 keV yields a $(\gamma_0 - 1)$ for the electron beam of 1.17 . A vestige of this is evident in Figure 26c. Note that even at this early time the axial momentum distribution resembles a drifting Maxwellian (Fig. 26a). By $t = 23.3$ ns the distribution function is no longer Maxwellian (Fig. 27c). Rather it must be described as a Bennett distribution. This is not surprising, because the beam is being modified by an extremely strong pinch. Examining Figure 28c reveals a high energy tail. This is a direct result of the large amplitude, long wavelength instability. As the wave exits the right hand boundary, this feature disappears and the distribution again resembles that of Figure 27.

The ion distributions are also informative., Even at $t = 12$ ns (Fig. 29) the beam is relatively cold compared to the electron beam. Heating increases (Fig. 30) until the ion beam itself is best described as a drifting Maxwellian. Although the beam temperatures are not spatially resolved as they should be, nevertheless, the ratio of the electron temperature T_e to the ion temperature T_i is sufficiently different at these times to shed light on the nature of the two streaming instabilities.



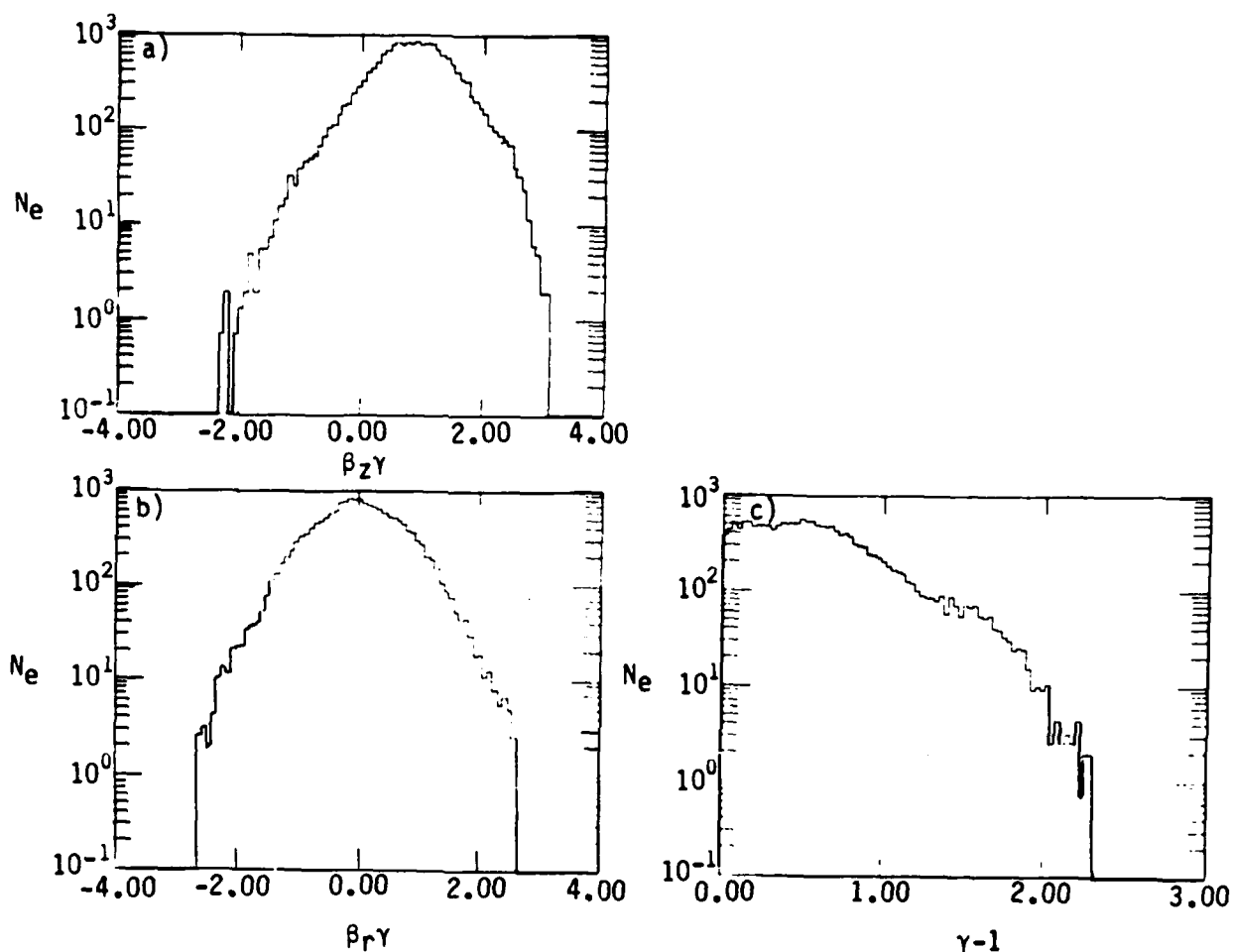
Time = 360.0750

Figure 26. Histograms of the electron beam distribution functions for a) axial momentum, b) radial momentum and c) kinetic energy at $t = 12$ ns. See Figure 4 for scaling.



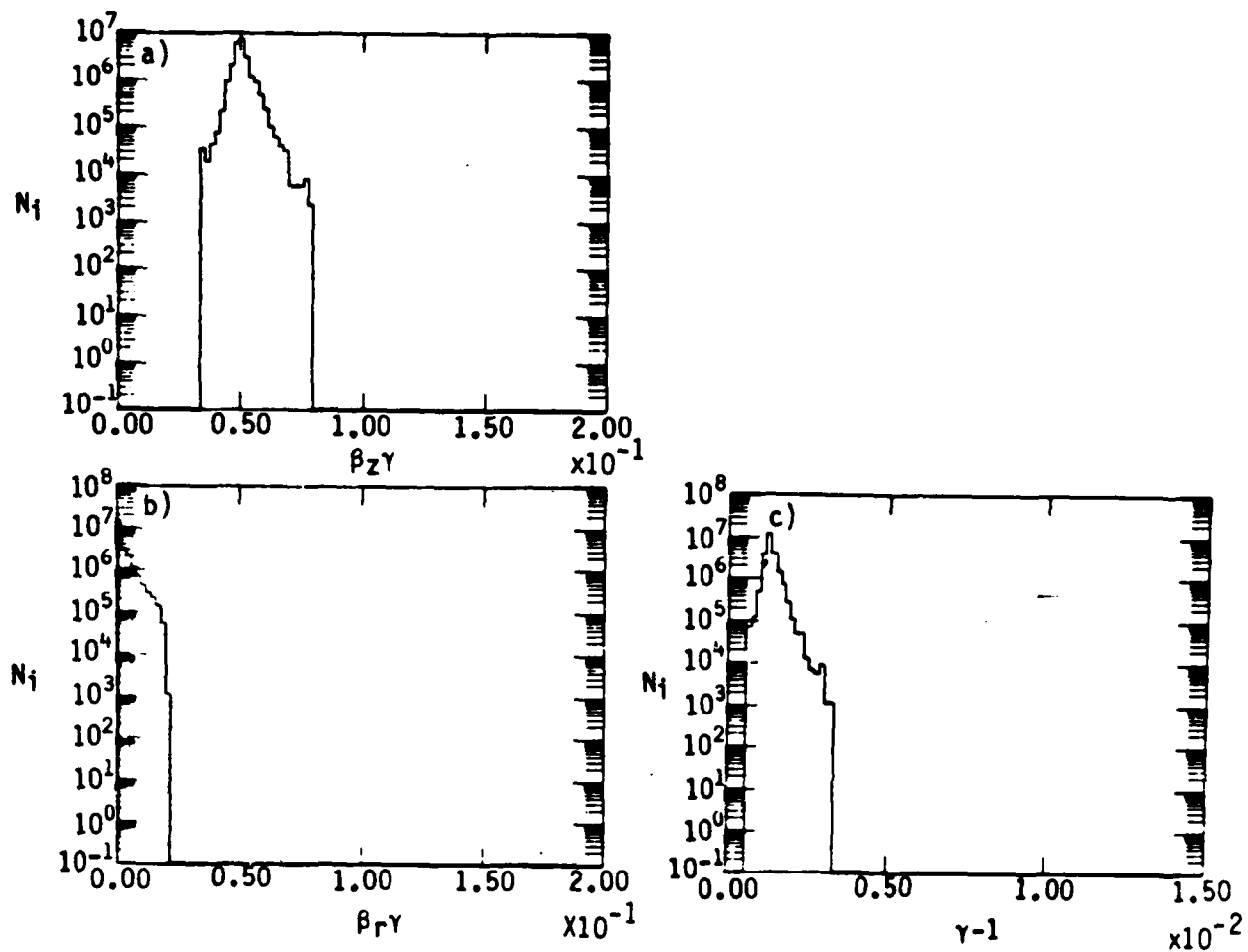
Time = 700.0750

Figure 27. Histograms of the electron beam distribution functions for a) axial momentum, b) radial momentum and c) kinetic energy at $t = 23.3$ ns. See Figure 4 for scaling.



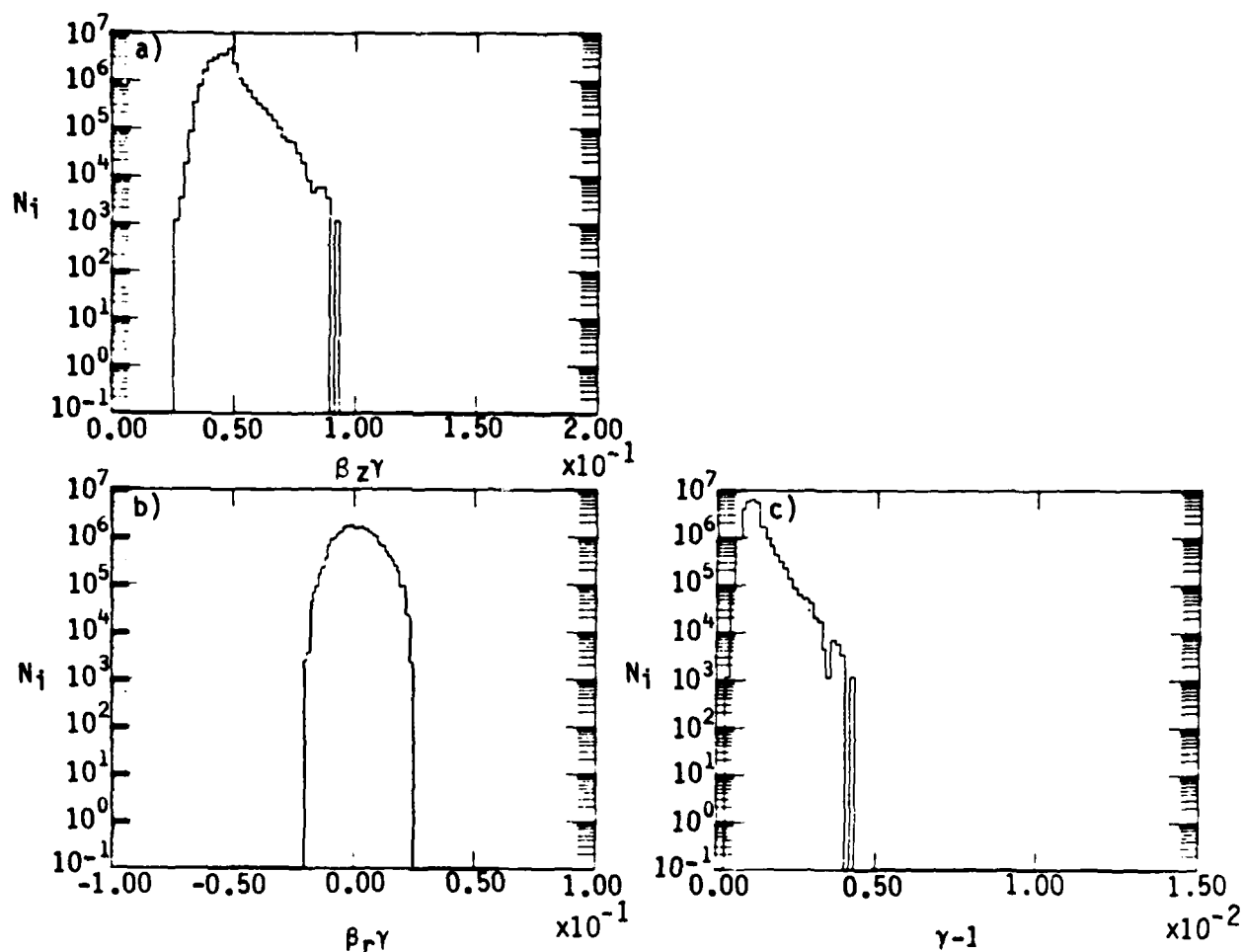
Time = 1040.0750

Figure 28. Histograms of the electron beam distribution functions for a) axial momentum, b) radial momentum and c) kinetic energy at $t = 34.7$ ns. See Figure 4 for scaling.



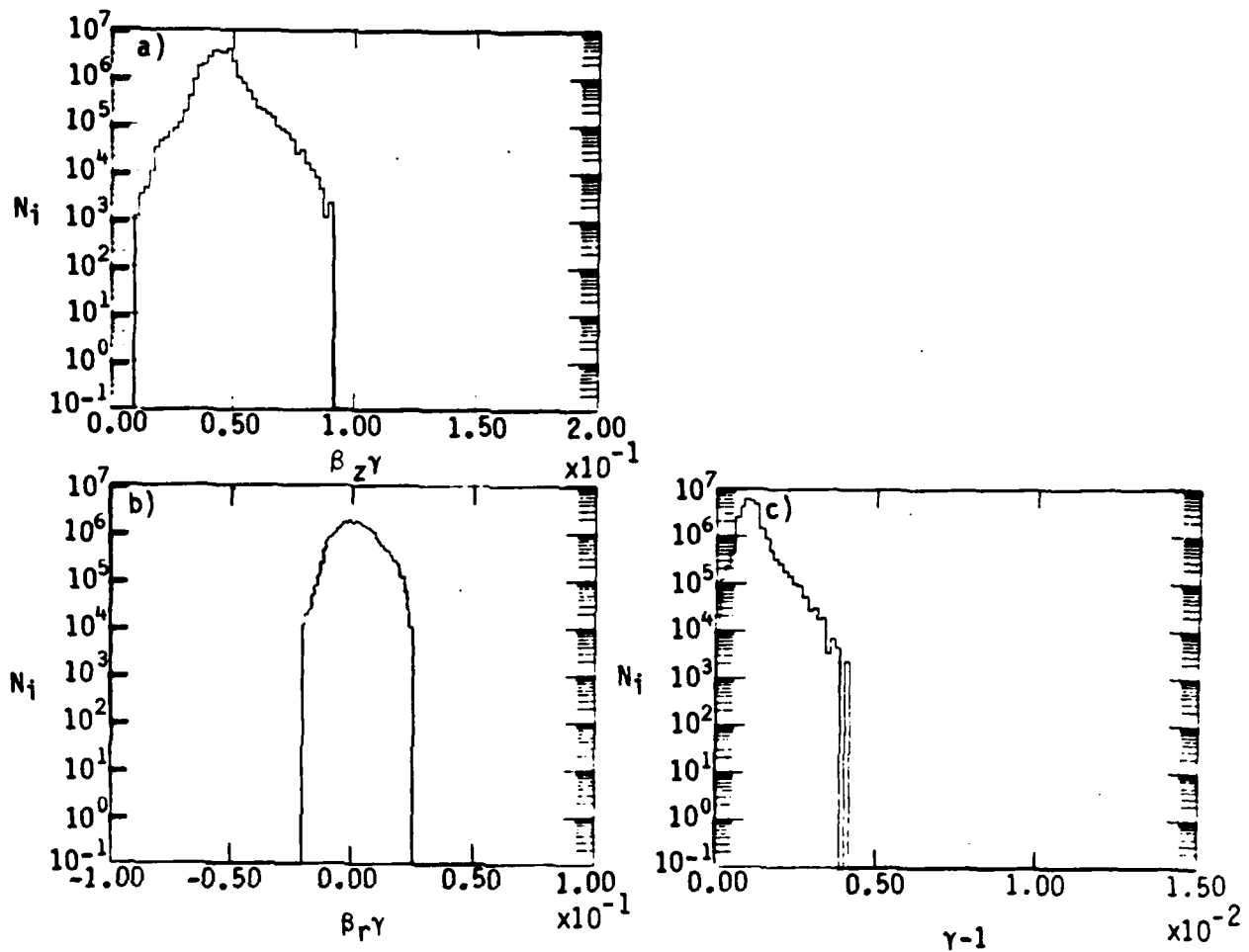
Time = 360.0750

Figure 29. Histograms of the ion beam distribution functions for a) axial momentum, b) radial momentum and c) kinetic energy at $t = 12$ ns. See Figure 4 for scaling; $m_i/m_e = 1836$.



Time = 700.0750

Figure 30. Histograms of the ion beam distribution functions for a) axial momentum, b) radial momentum and c) kinetic energy at $t = 23.3$ ns. See Figure 4 for scalings; $m_i/m_e = 1836$.



Time = 1040.0750

Figure 31. Histograms of the ion beam distribution functions for a) axial momentum, b) radial momentum and c) kinetic energy at $t = 34.7$ ns. See Figure 4 for scaling; $m_i/m_e = 1836$.

SECTION VI

THEORY OF ION ACCELERATION AND COMPARISON TO EXPERIMENT AND SIMULATION

One of the main impediments to development of an accurate, comprehensive theory of collective ion acceleration is the large number of varied experimental configurations which supposedly optimize the process. These include grooves in the cathode tip (Ref. 3), electrostatic lenses (Refs. 3, 5), and helical conductors (Ref. 10), among others. One must, therefore, concentrate only on those aspects which are common to most experiments. These include the use of a tapered cathode, an axial magnetic field which is smaller than some critical value, the formation of a virtual cathode, and energy scaling with v/γ of the injected beam. The theory described below elucidates the role and importance of these characteristics.

The schematic presented in Figure 1 is an idealized version of an electron beam, injected in the Luce diode geometry, late in its pulse. The beam envelope is depicted by the solid black line, and the dashed lines are meant to show typical high energy ion trajectories. Roughly 80% of these ions are lost to the wall by the time the acceleration mechanism saturates (Ref. 6). This mechanism has three distinct stages separated spatially, as shown in the diagram. Each of these will now be discussed in detail.

Region I, which includes the diode, is the most critical. An electromagnetic wave is launched down the cathode shank, which produces a cold plasma. When the radius of the cathode is sufficiently small, as the wave moves down the tapered section, explosive field emission takes place due to electric field enhancement. If the conical portion of the dielectric anode is covered by a conductor, the E-field lines will be perpendicular to both the cathode and conductor (provided the angle θ is the

same). This will lead to electron impact of a large area of this conductor with subsequent damage, plasma formation, and gap closure. Without the conductor, however, the field lines are curved, and a parapotential (Brillouin) flow model can be invoked to determine the critical taper angle θ_{\min} for optimal current flow. By varying θ and d , the A-K spacing, for the given machine relativistic factor, γ_0 , the electrons can be made to impact only the innermost portion of the anode. This has been experimentally proven to be the optimal configuration for ion acceleration (Ref. 6). It produces a sufficient number of ions to approximate beam charge neutralization while maximizing electron flow through the anode hole and minimizing gap closure. Our simulations indicate that the optimal value of d is determined by having the pinch point of the electron beam, whose location is obvious in all of our simulations, coincide with the axial location of the anode back plane. Because the pinch point is determined by the beam voltage and current, this self-consistently sets a narrow range of impedance for good acceleration as seen experimentally.

In the absence of an axial magnetic field, the electron beam pinches. One of the main characteristics of such a diode is the beam temperature. It is given by

$$\frac{T_e}{(\gamma_0 - 1)mc^2} \approx \left(\frac{\beta_{\perp}}{\beta_{\parallel}} \right)^2 = \frac{I_0}{I_A} \approx \frac{v_0}{\gamma_0} \quad (3)$$

where T_e , β_{\perp} and β_{\parallel} are the beam electron temperature and the perpendicular and parallel electron velocities normalized to the speed of light, respectively. I_0 and I_A are the injected beam and Alfvén currents. v_0 is the dimensionless injected current in units of mc^3/e . It should be noted that the temperature is due to the pinch which occurs in the diode at the anode back plane. The taper on the cathode creates an E-field which is not perpendicular to the axis of the drift tube and enhances the strength of the pinch.

As noted earlier, maximizing v_0/γ_0 increases ion acceleration. The reason is that it maximizes the injected current as a fraction of Alfvén current. This has a two-fold effect. First, it increases the momentum transfer of the electrons to ions (see Appendix C). Second, it increases the temperature of the electron beam. If a large axial magnetic field is placed on the diode, where the electron beam plasma frequency is on the order of the cyclotron frequency, the electrons will follow field lines. Since the electrons will not self pinch on the cathode tip, a cold beam will result.

As the hot beam enters the drift region, it forms a virtual cathode, since $v_0 > v_\lambda$ where v_λ is the dimensionless space-charge limiting current. The virtual cathode is drawn in Figure 1 as a lens shaped region. The virtual cathode plays a major role in the collective ion acceleration of the Luce diode. It ensures quasi-neutrality of the plasma. Ions from the dielectric undergo space-charge limited emission and acceleration into the virtual cathode. The ion flux is determined by the potential well depth. If too many ions enter the well, the ion flux is decreased. In this way, the virtual cathode maintains its integrity and never collapses or detaches from the anode. Because the virtual cathode remains in place during the entire beam pulse, the charge neutralization fraction is given by

$$f_e = \frac{n_i}{n_b} \leq 1 - \frac{v_\lambda}{v_0} \quad (4)$$

where n_i and n_b are the ion and electron beam number densities. The virtual cathode with its extremely high frequency oscillation also tends to heat up the electron beam.

We have outlined the significance of the common aspects of Luce diode designs. The energy scaling with v/γ of the injected beam, tapered cathode and lack of a strong axial magnetic field all contribute to creating a hot electron beam resulting from a pinched diode. The importance of the virtual cathode is in maintaining a quasi-neutral plasma for an extended period, as well as, also contributing to the beam temperature.

The plasma transmitted by the virtual cathode in Region I is characterized by a hot electron beam and a cold ion beam as seen in Figure 11. Although this is not the condition for a classic Buneman instability, it does lend itself to an ion-electron two-stream instability where $v_D > v_{Te}$ and $v_D > (m_i/m)^{1/3} v_{Ti}$. Here v_D is the electron beam drift velocity, m_i is the ion mass and v_{Te} and v_{Ti} are the electron and ion thermal velocities, respectively. This can best be seen in Figure 32 which depicts the stable and unstable regimes of ion-electron streaming instabilities for a drifting Maxwellian distribution. The critical axes are the ratios of v_{Te}/v_D and T_e/T_i with T_i being the ion beam temperature. The boundary between stable and unstable is denoted by a critical value of v_D/v_{Te} .

In Region I because $v_D > v_{Te}$ and $T_e \gg T_i$, the instability initially lies in the upper right corner of Figure 32. The instability growth rate is quite large here, although it is less than the Buneman growth rate for the most unstable mode.

The crucial role of the warm electron beam to the ion acceleration process in Region I has two aspects. The first is the reduction in the phase velocity of the most unstable mode generated by the instability. This is shown in Figure 33, which is derived from a numerical model developed to incorporate the effect of beam temperature. This result is based on 500 keV electron and ion beams and 1/4 proton mass ions. It predicts phase velocities as low as 0.09 c for a v_{Te} of greater than

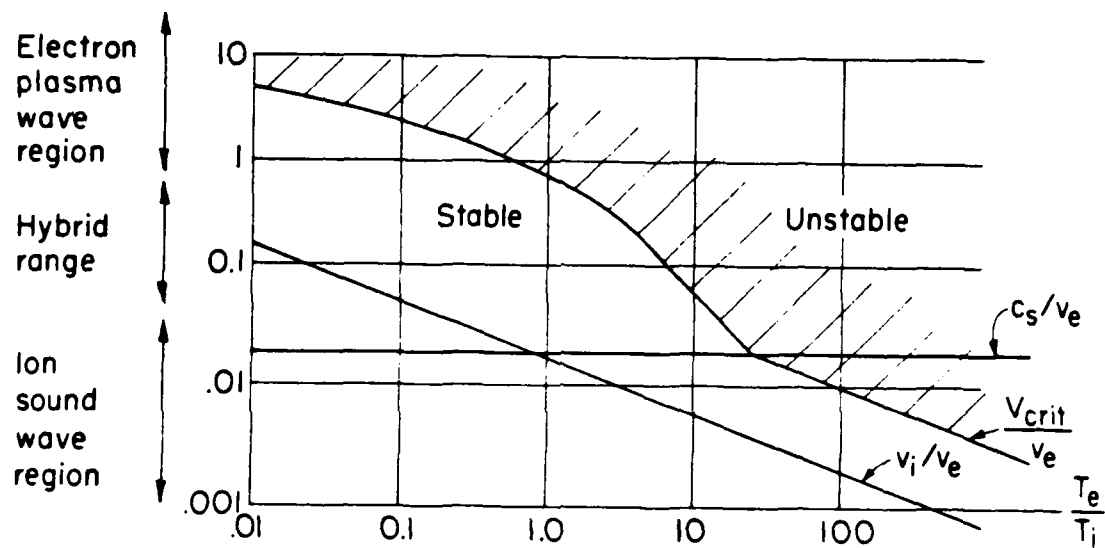


Figure 32. Plot of critical drift velocity as a function of T_e/T_i for the onset of electrostatic instability in an electron-ion plasma.

0.5 c. Recall that the phase velocity observed in the simulation was 0.044 c consistent with the full proton mass used in the CCUBE run. It is clear that for a cold electron beam the observed ion trapping and acceleration would not occur ($v_{ph} \sim 0.17$ c) due to the high phase velocity of the wave generated.

The second aspect also relates to the lowered phase velocity of the wave. Not only does the electric field required to trap ions of a constant energy equivalent to the electron beam energy decrease, but also the electric field required to trap electrons increases. Because the heating of trapped electrons in a nonlinear wave-particle interaction is the usual saturation mechanism for the streaming instability, the electric field of the wave can grow larger before experiencing damping. This leads to higher acceleration gradients, as well as, larger final ion energies. For our simulation the maximum ion energy resulting from this stage of acceleration is 2.4 MeV or four times the electron beam energy and $v_{i\max} = 0.072$ c.

Of course, saturation does eventually occur as electrons are trapped in the wave. Region I extends into the drift tube until $v_D \sim v_{Te}$. This occurs where wave growth due to the costreaming of the ion and electron beams is balanced out by the damping of the wave due to the high electron beam temperature. In Region II $T_e \gg T_i$ still holds. The velocity relationships now, however, are given by

$$v_{Te} \equiv \sqrt{\frac{KT_e}{m}} > v_D > \sqrt{\frac{KT_e}{m_i}} \equiv C_s \quad (5)$$

where C_s is the ion-acoustic speed. Referring to Figure 32 the instability has migrated from the electron plasma wave region into the hybrid range. The instability is not a classic ion-acoustic interaction until $v_{Te} \gg v_D$, which does not occur during our 20 cm simulation

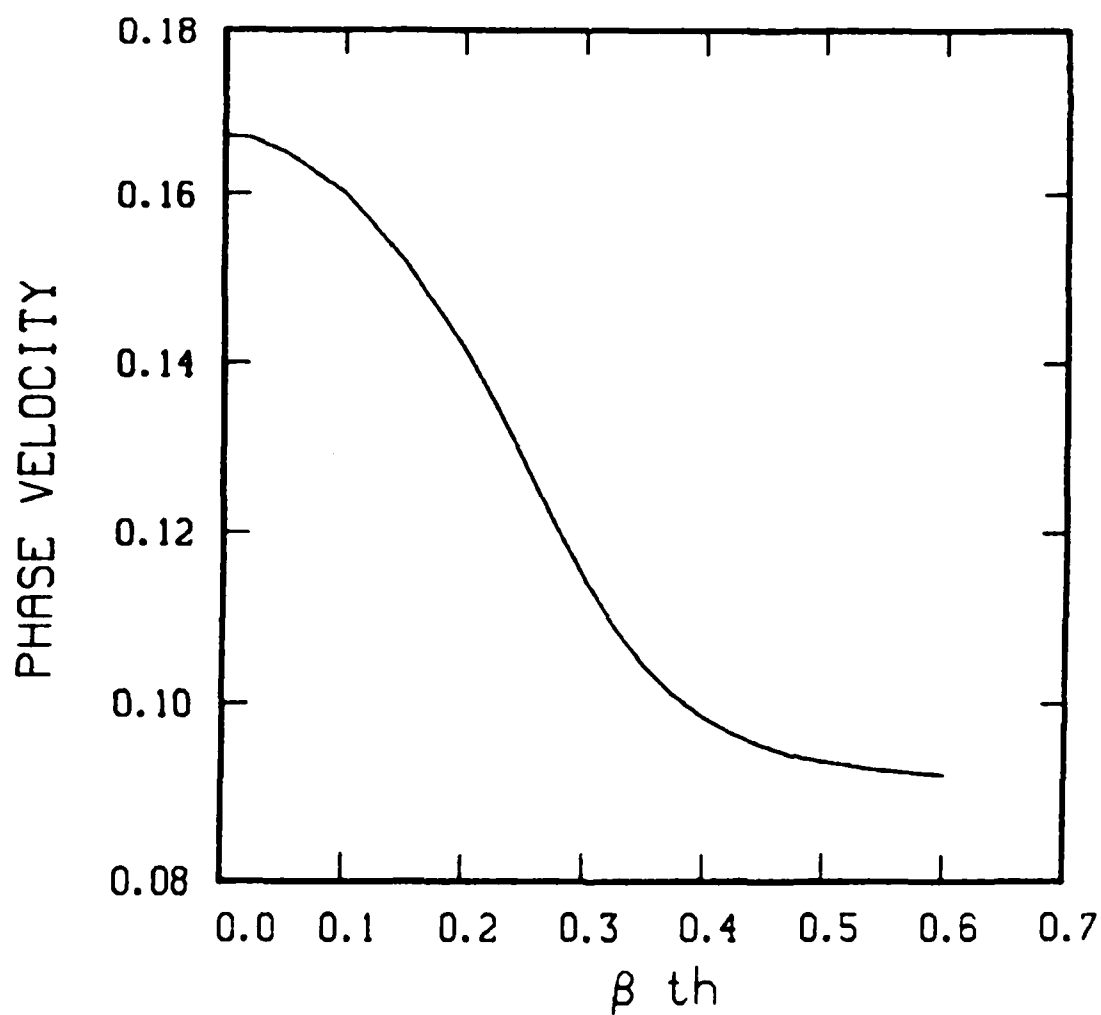


Figure 33. Scattering (temperature) reduces phase velocity of the most unstable mode. This example is for 500 keV electron and ion beams, and quarter mass protons.

with the current beam parameters. Nevertheless, the hybrid appears to be very much an ion wave. A normal mode analysis shows that ion waves are only weakly damped when $T_e \gg T_i$ by the Maxwellian component of the electron distribution. This allows an unstable mode to grow with a rather small electron drift.

The linear dispersion relation for the standard ion acoustic instability is given by

$$1 + \frac{k D_e^2}{k^2} \left(1 - \frac{2 v_D^2}{v_{Te}^2} \right) - \frac{\omega_{pi}^2}{\omega_k^2} = 0 \quad (6)$$

where $k D_e$ is the electron Debye wave number, ω_{pi} is the ion plasma frequency, and ω_k and k are the ion-acoustic frequency and wave number, respectively. Initially, the fastest growing mode is given by $2k D_e^2 = k D_e$. This tends to be a long wavelength. By imposing a strong axial magnetic field, wave growth at substantial angles to the field lines is precluded.

By choosing $v_D \sim v_{Te}$ at the entrance to Region II and noting that the density in this region is down by a factor of three (see Figure 24b), the ion-acoustic frequency would be 297 MHz for a $3 \times 10^{12} \text{ cm}^{-3}$ density beam interacting with protons. This is in good agreement with experiments and simulations (Ref. 6).

The quasi-linear rate of the instability is (Ref. 29)

$$\gamma_k = \sum_{s=i,e} \gamma_s = \frac{\pi}{2 \omega_{pi}^2 / \omega_k} \sum_s \frac{n_{ps}^2}{k^2} \int dv k \frac{\partial f_s}{\partial v} \delta(\omega_k - k v) \quad (7a)$$

where

$$f_{e0} = \left(\frac{m_e}{2 T_{e0}} \right)^{\frac{1}{2}} \exp \left[\frac{-m_e (v - v_D)^2}{2 T_{e0}} \right] \quad (7b)$$

$$f_{i0} = \left(\frac{m_i}{2\pi T_{i0}} \right)^{\frac{1}{2}} \exp \left[\frac{-m_i v^2}{2T_{i0}} \right] \quad (7c)$$

and the subscript 0 denotes the value at $t = 0$. Numerical solution (Ref. 29) of Equations 6 and 7 along with the quasi-linear equation for $\partial f_e / \partial t$ shows that a portion of the ion spectrum can be approximated by $T_{i\text{hot}} \sim T_e$ in a time of $60 \omega_{pi}^{-1}$. Because ω_{pi}^{-1} is 0.44 ns for a proton plasma of $3 \times 10^{12} \text{ cm}^{-3}$ density, this implies a 26.5 ns period. During this process ion-acoustic solitons form and collapse spatially leading to stochastic ion acceleration up to 3-4 times the beam kinetic energy (Ref. 29). It is proffered as the reason the highest energy ions are not seen until late in typical beam pulses (Ref. 6).

Because the peak energy ions are already moving at 0.07 c as is the ion wave, we could expect saturation of the wave to result in a three to four times increase in their energy. This would imply a total energy increase of 12-16 times the electron beam kinetic energy. Unfortunately, because our net current and impedance in Region II of the simulation are a factor of 3 less than experimentally observed, our scale lengths are longer, and acceleration has not saturated by $Z = 20 \text{ cm}$. We only see a factor of two increase in the peak ion energy by the end of the drift region for a total energy increase of eight times the initial electron beam kinetic energy in the two stage process.

It is interesting to note the time sequence of the ion acceleration from simulation and theory and compare it to the experiment. First, there is a 6-10 nanosecond time required to set up bipolar flow in the diode prior to plasma motion into the drift tube is observed. This is not modelled in the simulations with no diode. Next the simulations show that it takes a total of 12 ns for the quasi-neutral plasma to propagate out far

enough for the ion-electron streaming instability to grow and then for the instability to saturate. Finally, it takes 28 ns from the start of the run for large ion waves to grow and propagate to the right hand boundary of the simulation. However, they are not saturated at that time. If we substitute the quasi-linear result for saturation time of $60 \omega_{pi}^{-1}$, we obtain the 26.5 ns figure. Adding the timing of all three stages together (bipolar flow, plasma propagation and plasma wave saturation, and ion wave saturation), we obtain a total time to saturation of the ion acceleration process and peak ion energy production of 44.5-48.5 nano-seconds. This explains the late time observation of peak ion energies in the Cornell University experiment.

Region III is denoted by ion wave saturation and loss of a large fraction of the high energy ions to the wall due to lack of confinement. As already discussed ion wave saturation is due to ion tail formation in a quasi-linear process. Lack of ion confinement results when

$$\beta_i B_\theta < E_r \quad (8)$$

where β_i is the ion velocity normalized to c , B_θ is the azimuthal magnetic field and E_r is the radial electric field. This can be written to show that lack of confinement occurs when

$$\beta_i > \frac{v_d}{\beta_e v_0} \quad (9)$$

This places a severe constraint on the maximum ion acceleration and shows that high energy ions are preferentially lost to the drift tube walls.

Finally, the source of microwave radiation, which was witnessed during Luce diode experiments (Refs. 6,7) and in gas puff experiments only when comparable acceleration was obtained (Ref. 31), can be readily explained. The mechanism for microwave generation is based on three wave mixing (Refs. 36,37). Microwaves will be created when the plasma wave scatters off of ion acoustic turbulence in an inverse parametric decay. Conservation of energy and momentum require that the electromagnetic frequency and wavenumber be equal to the sum or difference of the two electrostatic waves' frequency and wavenumber. As the ion acoustic wave has a low frequency, the microwave frequency is an excellent approximation to the plasma wave frequency. The experimentally observed frequencies of 1.7 - 2.8 GHz are in excellent agreement with the frequencies of the plasma waves noted in simulations. This process is pictured graphically in Figure 34. Because the interacting electrostatic waves in three dimensions have a large phase space over which they can attempt to meet the condition of conservation of momentum, the k vector of the output wave is fairly arbitrary and the radiation pattern will tend to be broad.

In summary, the most successful collective ion acceleration to date has been observed when a relativistic electron beam has been discharged in the Luce diode (dielectric anode) geometry. In these experiments, the ratio of peak proton energy to beam kinetic energy has been as high as 30. The ion source is a plasma formed on the anode surface by electron impact ionization of the dielectric material. The diode physics, which couples the electron beam generation to the number of ions extracted from the plasma, is an essential feature of the acceleration mechanism in the Luce configuration. Simulations where the electron beam is injected through a preformed dense plasma are significantly different from those where the electron beam self-consistently determines the ion plasma density and dynamics in the diode. The main difference is in unstable wave growth. In the Luce diode the instability is predominant.

INVERSE PARAMETRIC DECAY

$$\omega_o = \omega_p + \omega_i \approx \omega_p$$

$$\mathbf{k}_o = \mathbf{k}_p - \mathbf{k}_i$$

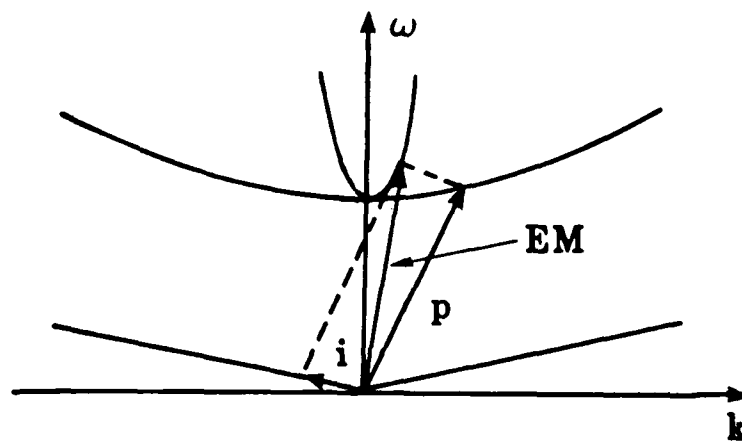


Figure 34. The plasma wave scatters off of the ion acoustic wave to create the electromagnetic wave.

In other localized plasma source collective ion accelerators the main acceleration takes place due to a hydrodynamic plasma free expansion. However, both Luce diodes and other plasma source accelerators can display both mechanisms to some extent.

Two-dimensional electromagnetic particle-in-cell simulations which are based on the Cornell University Luce diode experiments have been carried out. The simulations include an exact model of the electron beam generator's diode and the drift space where the collective ion acceleration takes place. Ions with peak energies eight times the electron beam kinetic energy are observed. Ion acceleration is clearly due to trapping in a train of traveling waves. The source of the waves is two-fold. First occurring spatially, as well as, temporally is an ion-electron two-stream instability. This is not a classical Buneman instability because of the high temperature of the electron beam. The relativistic warm beam instability results in a significantly lower wave phase velocity. This is important for two reasons. It allows for the trapping of low velocity ions exiting the diode. It also results in a significantly longer growth distance before trapping of electrons in the instability generated plasma wave leads to nonlinear saturation. The second wave growth mechanism is a result of the saturation of the first. As the electron beam continues to heat due to electron trapping, the electron and ion distributions become unstable to an ion acoustic instability leading to large amplitude wave generation and further ion acceleration. The presence of two electrostatic waves of different frequencies allows for microwave production through an inverse parametric instability. The instability growth rates, saturation length and microwave production are consistent with experimental results.

SECTION VII

TECHNICAL REQUIREMENTS AND TASKS

HOW THE STATEMENT OF WORK HAS BEEN SATISFIED

In this section we review the tasks encompassed by the statement of work and detail how these technical requirements have been satisfied. We also include a list of publications and talks given on this subject and professional personnel associated with this research effort.

Statement of Work (0001AA)

Task a. Identify the source of electrostatic waves responsible for the high energy ion acceleration witnessed in Luce diode experiments.

Two distinctly different electrostatic wave acceleration mechanisms have been identified which work in tandem to create the extremely high peak ion energies observed in the Luce diode. The first is an ion-electron two stream instability. It is not a classical Buneman instability, because it results from a warm electron beam and cold ion beam. The presence of a broad electron velocity distribution function results in the generation of a lower phase velocity plasma wave than otherwise expected. This has two consequences. First, low energy ions are readily trapped in the plasma wave. Second, electron trapping is more difficult resulting in larger amplitude waves. Ions are accelerated up to 4 times the initial electron beam energy. For an electron-proton plasma with maximum densities on the order of 10^{13} cm^{-3} the plasma wave has a frequency, wavelength, phase velocity and maximum electric field of 3.3 GHz, 0.4 cm, 0.044 c, and 2 MV/cm, respectively. The wave saturates within 5 cm of the electron beam pinch point, and is damped significantly by the time it is 10 cm past the pinch point. By this time the protons have attained maximum velocities of 0.072 c.

The second wave acceleration process results from the saturation of the first. An ion acoustic wave begins to grow when the electron beam drift velocity becomes less than or comparable to the electron beam thermal velocity. While the electron plasma wave is severely damped by this condition the ion acoustic wave is only weakly damped. Thus, the electron drift energy, which is still large, strongly drives the ion wave growth. For the same plasma noted above the ion wave parameters are 250 MHz, 8.5 cm, 0.07 c and greater than 1 MV/cm. This is the source of the experimentally observed low frequency bunching of the highest energy ions. Ions, which have been accelerated in the electron plasma wave of the first stage, are easily trapped and receive an additional acceleration from the ion wave. The simulations only show an additional factor of two in peak ion energy. This results from a net current density which is too low to observe the entire acceleration process to ion wave saturation in the 20 cm modelled. It is expected that acceleration of ions in the ion wave should produce a factor of four increase in peak ion energy. The total two stage process would create a 16 fold increase in ion energy in good agreement with the Cornell University Luce diode experiment.

Task b. Establish the role of the virtual cathode in producing low frequency ion bunching and the effect this bunching has on acceleration.

The virtual cathode oscillation frequency is not affected by the presence of the ions. It is still on the order of the electron beam plasma frequency. This is much too high for protons to respond to. As noted in the previous task result, it is the ion acoustic wave which creates the low frequency ion bunching.

Task c. Determine the wave saturation mechanism. The saturation mechanisms for both waves are those naturally expected to occur.

The saturation of the ion-electron two stream instability occurs due to electron trapping in the electron plasma wave. This results in a

nonlinear particle-wave interaction which modifies the electron velocity distribution until the electron thermal velocity is on the order of the electron drift velocity. Once this happens the wave growth due to particle streaming is exactly balanced by the wave damping due to particle heating. As the particles heat further the wave is damped.

The saturation of the ion acoustic wave results from a quasi-linear mechanism. As the ions are trapped and heat, an ion tail forms in their velocity distribution. This results in wave damping. During this process the ion tail is created by the repeated formation and collapse spatially of ion acoustic solitons. Stochastic ion acceleration up to 3-4 times the initial ion energy can result.

Task d. Define the role of a large axial magnetic field in suppressing ion acceleration.

A large axial magnetic field prevents the electron beam from pinching. This allows a relatively cold electron beam to propagate. The consequence is an ion-electron two stream instability whose plasma wave has too high a phase velocity to trap and accelerate ions.

Task e. Delineate key experimental parameters which optimize the coherence of the acceleration process and maximize ion energy.

The ion acceleration process is dependent on the interaction of a hot electron beam and cold ion beam. This is best accomplished by using a pinched electron beam diode to maximize electron beam temperature. The optimal characteristics for this are a tapered cathode, high v/γ beam, injected electron currents at the Alfvén current limit (17 $\beta\gamma$ kA), and formation of a virtual cathode. The latter is determined by the injected current, beam energy and ratio of drift tube wall radius to beam radius. An axial magnetic field would impede the beam pinch.

The instabilities which create the circumstances for ion acceleration have maximum growth when the ion and electron densities are equal. The major role of the virtual cathode is in maintaining quasi-neutrality in the plasma for an extended period. The larger the ratio of injected current to space-charge limited current the closer the plasma approaches neutrality. The ion source should be localized upstream of the virtual cathode and should be space-charge limited. The use of gas puffs or other extended ion sources leads to ill defined neutrality and possible ion depletion before maximum ion acceleration can occur. This raises another important beam characteristic. It must have a long enough pulse length for both instabilities to saturate.

A final consideration for the amount of ion acceleration comes from simple momentum considerations advanced by R. Adler. Momentum transfer to the ions is maximized when the beam current approaches the Alfvén limit, and the beam is injected into a large drift tube.

Because the stages of acceleration, which rely on saturation for maximum ion acceleration, are stochastic, attaining a coherent monoenergetic ion beam is unrealistic. However, the problem of peak energy ions being lost radially may be alleviated by placing an axial magnetic field downstream of the diode pinch point.

Bibliography of Talks and Publications

Archival Scientific Publications

"Theory of Collective Ion Acceleration in the Luce Diode", in Beams '83, 5th International Conference on High Power Beams edited by R. Briggs and A. Toepfer (Lawrence Livermore National Laboratory, Livermore, Ca., 1983) p. 501 (D. J. Sullivan and R. J. Faehl).

"The Collective Acceleration of Ions in Luce Diode Geometries", to be submitted to Physical Review Letters (D. J. Sullivan and R. J. Faehl).

"Theory of Collective Ion Acceleration in Two Different Regimes", to be submitted to Particle Accelerators (R. J. Faehl, W. K. Peter and D. J. Sullivan).

Talks and Meetings

Fifth International Conference on High Power Beams - San Francisco, California (Sep., 1983).

"Theory of Collective Ion Acceleration in the Luce Diode".

American Physical Society Division of Plasma Physics - Los Angeles, California (Nov., 1983).

"Theory of Collective Ion Acceleration in the Luce Diode".

American Physical Society Division of Plasma Physics - Boston, Massachusetts (Nov., 1984).

"Numerical Simulation and Comparison Between Two Experimentally Demonstrated Modes of Collective Ion Acceleration".

Professional Personnel (Alphabetical Order)

Mark M. Campbell
Rickey J. Faehl
William K. Peter
Donald J. Sullivan

REFERENCES

1. N. Rostoker and M. Reiser (ed.) Collective Methods of Acceleration, (Harwood Academic Publishers, New York, 1979).
2. J. S. Luce, H. L. Sahlin and T. R. Crites, IEEE Trans. Nuc. Sci. NS-20, 336 (1973).
3. J. S. Luce, W. Bostick, and V. Nardi, in Collective Methods of Acceleration, edited by N. Rostoker and M. Reiser (Harwood Academic Publishers, New York, 1979), p. 493.
4. J. Adamski, idem, p. 341.
5. R. Adler, G. Gammel, J. A. Nation, G. Providakes and R. Williams, idem, p. 249.
6. R. Adler, Collective Acceleration of Ions in Vacuum, Ph.D. Thesis, Cornell (1980).
7. R. Adler, J. Nation and V. Serlin, Phys. Fluids 24, 347 (1981).
8. R. F. Hoeberling, in Collective Methods of Acceleration, edited by N. Rostoker and M. Reiser (Harwood Academic Publishers, New York, 1979), p. 463.
9. O. Zucker, J. Wyatt, H. Sahlin, J. S. Luce, B. Freeman and R. Gullickson, idem, p.475.
10. W. W. Destler, H. Kim, T. Zorn and R. F. Hoeberling, idem, p. 509.
11. J. Adamski, P. S. P. Wei, R. L. Copeland, J. R. Beymer, R. L. Guay, and R. C. Kennedy, FX-75 Experiments, Boeing Report D180-24767-1, (1978).
12. D. J. Sullivan, Bull. Am. Phys. Soc. 24, 1013 (1979).
13. R. J. Faehl and D. J. Sullivan, Bull. Am. Phys. Soc. 26, 1037 (1981).
14. D. J. Sullivan, AMRC-N-165, Mission Research Corporation (1981).
15. R. J. Faehl, and D. Sullivan, in 1982 Conference Record - IEEE Intl. Conf. on Plas. Sci., p. 28 (1982).
16. D. J. Sullivan, M. Arman, and R. J. Faehl, Bull. Am. Phys. Soc. 28, 1212 (1983).
17. D. J. Sullivan and R. J. Faehl, in Beams '83, edited by R. Briggs and A. Toepfer (Lawrence Livermore National Laboratory, Livermore, CA., 1983) p. 501.

REFERENCES (Continued)

18. R. J. Faehl, W. K. Peter and D. J. Sullivan, Bull. Am. Phys. Soc. 29, 1329 (1984).
19. A. Greenwald and R. Little, in Collective Methods of Acceleration, edited by N. Rostoker and M. Reiser (Harwood Academic Publishers, New York, 1979), p. 371.
20. J. A. Pasour, R. K. Parker, R. L. Gullickson, W. O. Doggett and D. Pershing, idem, p. 383.
21. R. A. Mahaffey, J. A. Pasour, J. Golden and C. A. Kapetanacos, idem, p. 521.
22. C. L. Olson, Bull. Am. Phys. Soc. 18, 1356 (1973).
23. C. L. Olson, Phys. Fluids 18, 585 (1975).
24. C. L. Olson, Phys. Rev. A 11, 288 (1975).
25. C. L. Olson and U. Schumacher, Springer Tracts in Modern Physics: Collective Ion Acceleration, edited by G. Hohler (Springer, New York, 1979), Vol. 84.
26. B. B. Godfrey and L. E. Thode, IEEE Trans. Plas. Sci. PS-3, 201 (1975).
27. O. Ishihara and A. Hirose, Phys. Rev. Lett. 46, 771 (1981).
28. O. Ishihara, A. Hirose and A. B. Langdon, Phys. Rev. Lett. 44, 1404 (1980).
29. O. Ishihara, A. Hirose and A. B. Langdon, Phys. Fluids 24, 452 (1981).
30. D. J. Sullivan, in Proc. of the 3rd Int'l Topical Conference on High Power Electron and Ion Beam Research and Technology (INP, Novosibirsk, USSR, 1979), p. 769.
31. R. Mako, A. Fisher, C. Roberson, N. Rostoker and D. Tzach in Collective Methods of Acceleration, edited by N. Rostoker and M. Reiser (Harwood Academic Publishers, New York, 1979), p. 317.
32. W. W. Destler, L. E. Floyd and M. Reiser, Phys. Rev. Lett. 44, 70 (1980).

REFERENCES (Continued)

33. W. W. Destler, H. S. Uhm, H. Kim and M. Reiser, J. Appl. Phys. 50, 3015 (1979).
34. D. D. Ryutov and G. V. Stupakov, Fiz. Plazmy 2, 566 (1976) [Sov. J. Plasma Phys. 2, 309 (1976)].
35. D. D. Ryutov and G. V. Stupakov, Fiz. Plazmy 2, 767 (1976) [Sov. J. Plasma Phys. 2, 427 (1976)].
36. G. Benford, D. Tzack, K. Kato and D. F. Smith, Phys. Rev. Lett. 45, 1182 (1980).
37. D. A. Whelan and R. L. Stengel, Phys. Rev. Lett. 47, 95 (1981).

APPENDIX A

THEORY OF COLLECTIVE ION ACCELERATION IN THE LUCE DIODE

D. J. Sullivan
Mission Research Corporation
1720 Randolph Rd., SE
Albuquerque, New Mexico 87106

and

R. J. Faehl
Los Alamos National Laboratories
P.O. Box 1663
Los Alamos, New Mexico 87545

Abstract

The most successful collective ion acceleration to date has been observed when a relativistic electron beam has been discharged in the Luce diode (dielectric anode) geometry. In these experiments, the ratio of peak ion energy to beam kinetic energy has been as high as 30. The ion source is a plasma formed on the anode surface by electron impact ionization of the dielectric material. The diode physics, which couples the electron beam generation to the number of ions extracted from the plasma, is an essential feature of the acceleration mechanism in the Luce diode.

Two dimensional electromagnetic particle-in-cell simulations which are based on the Cornell University Luce diode experiments have been carried out. The simulations include an exact model of the electron beam generator's diode and the drift space where the collective ion acceleration takes place. Ion acceleration is clearly due to trapping in a train of traveling waves. The source of the waves appears to be an ion-electron two stream instability. The instability growth rate, saturation length and coincident microwave production are consistent with experimental results.

Introduction

Although experiments and theory have been carried out over the last ten years to explain collective ion acceleration in the Luce diode, it remains both the most successful and least understood of all collective ion acceleration schemes [1-6]. The ratio of peak proton energy to beam kinetic energy has been as high as 30 [2]. In its simplest form the Luce diode consists of a tapered cathode and a dielectric anode. This is depicted in Fig. 1. The center of the anode has a hole concentric with and of a size approximately equal to the cathode shank diameter. The electron beam is generated by explosive field emission. The electrons are emitted from the tapered section of the cathode, which experiences the highest electric fields and is not magnetically insulated as is the cathode shank.

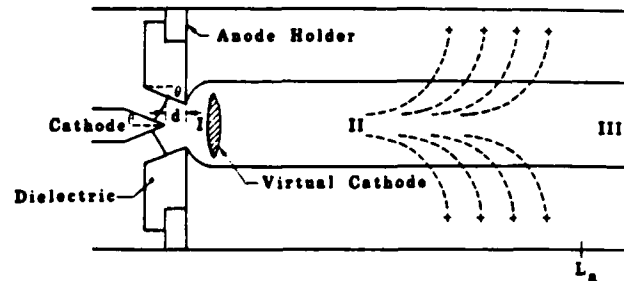


Figure 1. Idealized configuration for a Luce diode. The half angles θ are equal. d is the A-K gap spacing. L_a is the saturation acceleration length. The region enclosed by the solid line contains a large fraction of the beam. The electrons actually fill the entire drift region. Dashed lines are typical high energy ion trajectories.

Since the dielectric anode acts initially as an insulator, the potential difference the electrons experience is due to the voltage rise between the cathode and outer conducting wall of the drift tube. Thus, in the absence of a strong, externally imposed, axial magnetic field, the electrons move radially outward from the cathode tip. These electrons bombard the dielectric. After a sufficient amount of energy is deposited, a plasma is formed on the anode surface, which acts to ground the anode to the drift tube wall. This process is accomplished in the first several nanoseconds of the beam pulse. Ions from the anode plasma are drawn toward the cathode to establish a bipolar flow across the anode-cathode (A-K) gap. Once a sufficient number of ions are present to provide neutralization, the electron and ion plasma begins to propagate into the drift tube region where collective ion acceleration takes place.

Many variations on the Luce diode have been tried experimentally with different degrees of success. These include dielectric channels [7] reflex tetrodes [8] and addition of "lenses" [2] or a helical slow wave structure [5] to the basic dielectric anode design. There exist almost as many theories to explain the collective acceleration as there are

experiments. They range from vortex filaments [2] to cavity resonators [9] to a deep stationary well/moving potential well [3,5,7,8]. Until recently, this latter explanation has been used most frequently to describe the acceleration process. It is based on the same theory used to depict collective ion acceleration in a low density gas [10].

Recent experiments [6] on the Luce diode at Cornell University, however, shed doubt on these schemes. We have chosen to model these studies in our work, because they contain the most detailed diagnostics available. Also, the experiments were conducted on the fundamental dielectric anode design, so that the results are not ambiguously tied to elaborate configurations.

The most crucial results of the experiments were the following:

The maximum ratio of ion energy to beam kinetic energy was 22.0. This is the highest acceleration factor witnessed in a basic Luce diode. The highest energy ions did not occur until late in the beam pulse ($t > 55$ nanoseconds) and were correlated in time with moderate frequency microwaves (1.7 GHz - 2.8 GHz). The highest energy ions appeared in bunches corresponding to a frequency of 200 - 300 MHz. The propagating beam front had a measured velocity of from 0.04 to 0.05 c, corresponding to an ion energy approximately twice the electron beam kinetic energy. No electrons with an energy greater than 1.2 times the electron beam energy were observed early in the pulse. The net beam current increased monotonically in time and axial length over the beam pulse. The maximum was approximately equal to the Alfvén current of the beam. The maximum ion energies were measured within 13 cm of the anode back plane indicating a short saturation length for the acceleration mechanism.

The deep stationary potential well/moving potential well has grave difficulty in explaining several of these observations. Indeed, in light of these results any beam front mechanism is called into question. The Cornell researchers have speculated, based on the microwave frequency observed, that electrostatic waves generated by an ion-electron two-stream instability are responsible for the highest energy ions. The linear theory of the instability is in fair agreement with the experimental results. The possibility that this instability is responsible for the ion acceleration was first proposed by Godfrey and Thode [11].

Theory

A more encompassing theory has been drawn up to explain other details of the observed acceleration [12,13]. The acceleration is viewed as occurring in three stages corresponding to regions I, II, and III of Fig. 1. Because of the brevity of this note only an outline will be presented here.

Region I is the diode. In the absence of an axial magnetic field, the electron beam is hot. Its temperature normalized to the diode voltage is approximately v_0/γ_0 where v_0 is the dimensionless diode current in units of mc^3/e and γ_0 is the beam relativistic factor. In the diode region the characteristic that the thermal velocity be greater than the electron drift velocity is easily met. On the other hand, the ion temperature has been measured experimentally to be 2-5 eV. These conditions lead to a classic ion acoustic instability. The linear dispersion relation is:

$$1 + \frac{k_D^2}{k^2} \left(1 - \frac{2v_i^2}{v_{Te}^2} \right) - \frac{\omega_{pi}^2}{\omega^2} = 0 \quad (1)$$

where k_D is the electron Debye wave number, ω_{pi} is the ion plasma frequency, and ω and k are the ion-acoustic frequency and wave number, respectively. Initially, the fastest growing mode is given by $2v_i^2 = k_D^2$. The turbulence experienced by the electrons in the diode due to emission and reflexing from the virtual cathode can be approximated by

$$\left(\frac{v_{Te}}{v_i} \right)^2 = \frac{(\gamma_0 - \gamma_0^{1/3})}{(\gamma_0^{1/3} - 1)} \quad (2)$$

For a 500 kV beam this ratio is -3. The ion-acoustic frequency, therefore, would be 160 (510) MHz for a 10^{12} (10^{13}) cm^{-3} density beam interacting with protons. The instability growth rate can be obtained by numerical solution of the quasilinear equations [14]. They show that a portion of the ion spectrum can be approximated by $T_{i, \text{hot}} \sim T_e$ in a time of $60 \frac{\omega_{pi}^{-1} - \omega_{pi}^{-1}}{\omega_{pi}^{-1} - \omega_{pi}^{-1}}$ is .76 (.24) ns for a proton plasma of 10^{12} (10^{13}) cm^{-3} density. During this process ion-acoustic solitons form and collapse spatially leading to stochastic ion acceleration up to 3-4 times the beam kinetic energy [14]. More importantly, the turbulent heating results in a broad ion velocity spectrum. As shown above, this will occur on the time scale of tens of ion plasma periods.

The presence of an ion-acoustic instability, therefore, explains several features of the Cornell experiments. It describes the bunching of ions at several hundred Megahertz. The high energy ion tail provides an ion spectrum suitable for trapping by electrostatic waves of higher phase velocity than the ion sound speed. Its long growth time tends to correlate with the production of high energy ions late in the beam pulse. Finally, note that if a large axial magnetic field is placed on the diode, the electrons will follow field lines rather than pinch leading to a cold beam. A cold beam would not excite the ion-acoustic instability.

The virtual cathode, which is drawn in Fig. 1 as a lens shape, forms the boundary between regions I and II. It performs several roles in addition to reflecting electrons into the diode. The first is to produce a quasineutral plasma. Ions from the dielectric undergo space-charge limited emission and acceleration into the virtual cathode. The ion flux is determined by the potential well depth. If too many ions enter the well, the ion flux is decreased. In this way, the virtual cathode maintains its integrity and never collapses or detaches from the anode. The plasma exiting the diode is neutral to within a factor of $(1 - v_x/v_0)$.

Second, an extremely hot beam in the foilless diode region becomes cooler on the downstream side of the virtual cathode. The potential well is in effect a filter which keeps hot electrons confined, since only those electrons with the highest axial momenta are transmitted. Therefore, the plasma entering region II consists of a warm ion beam and costreaming warm electron beam. Although this is not the condition for the classic Buneman instability, it does lend itself to an electron-ion two-stream instability. The most unstable mode for the Buneman instability has a frequency of 290 (920) MHz for a 10^{12} (10^{13}) cm^{-3} density plasma interacting with protons. A linear two-dimensional analysis of the warm relativistic beam case shows that not only does the instability take place but the phase velocity is lower than expected for the cold beam case.

Also a nonlinear dispersion relation for the ion-electron two-stream exists [15,16]. It is much too detailed to consider in this note. Suffice it to point out that harmonics of the Buneman instability frequency are important in saturation of the instability by electron trapping. This leads to a

frequency up shift in time. In addition, ω_{pe} is increasing, since ion flow and charge neutralization can lead to increased current up to or slightly greater than the Alfvén limit. Note that the presence of both ion bunches and plasma waves leads to the possibility of a three-wave interaction (inverse parametric decay) resulting in microwaves whose frequency is the sum or difference of the two electrostatic wave frequencies. Not only does microwave production correlate with the detection of bunched high energy ions, but also increasing RF frequency as a function of time has been noted experimentally [6].

The development of this instability, and its frequency variation in conjunction with the large spread in ion velocity developed in region I, produce the accelerated high energy ion tail. Large amplitude electrostatic waves select out, trap, and accelerate those ions which are close to its phase velocity. This elongates the ion energy spectrum. The process continues as frequency and, therefore, phase velocity increase over time. The predicted result is that ion energy grows monotonically in time. This is precisely the result seen experimentally [6]. As the phase velocity of the waves increases, fewer and fewer ions have the initial velocity necessary to be trapped and accelerated. This leads to the exponential ion energy spectrum.

Ion acceleration saturates over a distance L_0 - 10 cm in most collective ion acceleration experiments [6,9]. While the electrons experience a pinch effect because of the current induced azimuthal magnetic field, B_0 , the ions are expelled by the oppositely directed $v_z \times B_0$ force. The highest energy ions are preferentially driven to the drift tube walls [6]. At the same time, the electrons are heated by trapping until their temperature is sufficient to saturate the instability. This is shown in Fig. 1 as region III. The saturation length due to nonlinear electron trapping is expected to be several wavelengths in agreement with the experimental observation.

Simulations

Because of earlier simulations and the Cornell experiments, it has become clear that accurate inclusion of the diode physics is an important aspect of studying the Luce diode. In the simulation presented here a 500 kV TEM wave is launched down the coaxial transmission line and onto the cathode. When the electric field on a cathode cell exceeds a

threshold value, electrons are emitted from the cell. Electrons bombarding the anode trigger ion emission from anode cells in the tapered section of the dielectric. Ion emission takes place on an ion time scale and electron emission occurs every time step. The reference value of ω_p in these simulations is taken to be $3 \times 10^{10} \text{ sec}^{-1}$ so that $c/\omega_p = 1.0 \text{ cm}$ and $\omega_p^{-1} = .033 \text{ nanoseconds}$. Note that a very short pulse risetime and a mass ratio of $m_i/m_e = 459$ are used to save computer time.

The instability of interest is clearly evident in Fig. 2 of the ion momentum space 11.0 nanoseconds into the simulation. It shows that the high energy ion acceleration is occurring in a wave train. The wavelength, frequency and phase velocity of the instability are 3.7 cm, 1.1 GHz and .135 c, respectively. Although the frequency spectrum of the plasma is turbulent, there is a definite frequency component at 410 MHz. Correcting for the fictitious mass ratio the frequencies for a proton plasma would be 690 MHz and 210 MHz respectively. These are in agreement with linear theory for the ion-electron two-stream and the ion-acoustic instabilities. The latter is in excellent agreement with experiment. The peak ion energy is six times the beam kinetic energy. Peak proton energies would be 23 times the beam energy for the same maximum ion velocity ($v_i^{\text{max}} = 0.155 c$). The streamers accelerating out of the main ion beam phase space coincide with high density ion bunches. Finally, the trapping of electrons, which is the non-linear saturation mechanism for the instability, takes place 10 cm downstream of the anode in good agreement with the saturation length of ion acceleration seen experimentally.

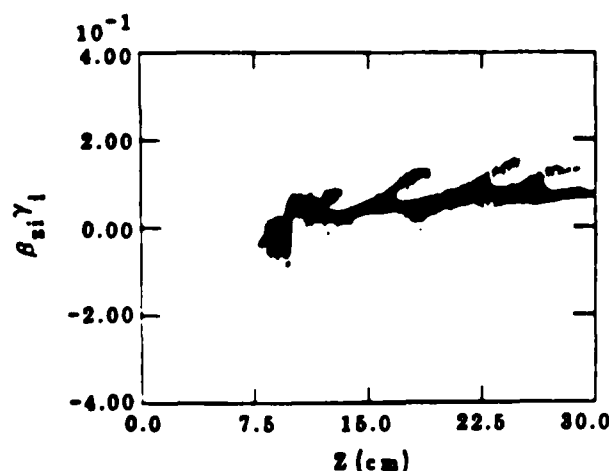


Figure 2. Ion momentum space at 11.0 nanoseconds. m_i/m_e is 459.

Acknowledgment

This work was supported by the Air Force Office of Scientific Research and the Department of Energy.

References

1. J. S. Luce, H. L. Sahlin and T. R. Crites, IEEE Trans. Nuc. Sci. **NS-20**, 336 (1973).
2. J. S. Luce, W. Bostick, and V. Nardi, in Collective Methods of Acceleration, edited by N. Rostoker and M. Reiser (Harwood Academic Publishers, New York, 1979), p. 493.
3. J. Adamski, *idem*, p. 341.
4. R. Adler, G. Gammel, J. A. Nation, G. Providakes and R. Williams, *idem*, p. 249.
5. W. W. Destler, H. Kim, T. Zorn and R. F. Hoeberling, *idem*, p. 509.
6. R. Adler, J. Nation and V. Serlin, Phys. Fluids **24**, 347 (1981).
7. A. Greenwald and R. Little, in Collective Methods of Acceleration, edited by N. Rostoker and M. Reiser (Harwood Academic Publishers, New York, 1979), p. 371.
8. R. A. Mahaffey, J. A. Pasour, J. Golden and C. A. Kapetanakis, *idem*, p. 521.
9. O. Zucker, J. Wyatt, H. Sahlin, J. S. Luce, S. Freeman and R. Gullickson, *idem*, p. 475.
10. C. L. Olson and U. Schumacher, Springer Tracts in Modern Physics: Collective Ion Acceleration, edited by G. Hohler (Springer, New York, 1979), Vol. 84.
11. B. B. Godfrey and L. E. Thode, IEEE Trans. Plas. Sci. **PS-3**, 201 (1975).
12. D. J. Sullivan, AMRC-N-165, Mission Research Corporation (1981).
13. R. J. Faehl and D. J. Sullivan, Bull. Am. Phys. Soc. **26**, 1037 (1981).
14. O. Ishihara and A. Hirose, Phys. Rev. Lett. **46**, 771 (1981).
15. O. Ishihara, A. Hirose and A. B. Langdon, Phys. Rev. Lett. **44**, 1404 (1980).
16. O. Ishihara, A. Hirose and A. B. Langdon, Phys. Fluids **24**, 452 (1981).

1983 APS Bull. Am. Phys. Soc. 28, 1212.

72 10 THEORY OF COLLECTIVE ION ACCELERATION IN THE LUCE DIODE.* D. J. Sullivan and M. Arman, Mission Research Corporation, Albuquerque, New Mexico 87106, and R. J. Faehl, Los Alamos National Laboratories, Los Alamos, New Mexico 87545.--Two dimensional electromagnetic particle-in-cell simulations which are based on the Cornell University Luce diode experiments have been carried out. The ion source is a plasma formed on the anode surface by electron impact ionization of the dielectric material. The diode physics, which couples the electron beam generation to the number of ions extracted from the plasma, is an essential feature of the acceleration mechanism in the Luce diode. The simulations include an exact model of the electron beam generator's diode and the drift space where the collective ion acceleration takes place. Ion acceleration is clearly due to trapping in a train of traveling waves. The source of the waves appears to be an ion-electron two stream instability. The instability growth rate, saturation length and coincident microwave production are consistent with experimental results.

*Work supported by the Air Force Office of Scientific Research.

7E6 Numerical Simulation and Comparison Between Two Experimentally Demonstrated Modes of Collective Ion Acceleration,* R. J. FAEHL, W. K. PETER, Los Alamos National Laboratory, and D. J. SULLIVAN, Mission Research Corporation.--Many scenarios have been advanced to harness the power of intense relativistic electron beams to accelerate ions. Two have demonstrated best results to date, virtual cathode acceleration and the Luce diode. Both share the characteristic that intense, hot expanding electron beams are correlated with the ion acceleration. Detailed numerical simulations have shown qualitative differences however. The virtual cathode mechanism bears many similarities to an ambipolar plasma expansion. The shock-like structure of the electron beam in the vicinity of the virtual cathode introduces a unique localized feature into the ion flow. The Luce diode behaves like a true ion diode, although with strong similarities to the pinch reflex diode. This produces an ion beam with energy comparable only to the diode voltage. Under certain circumstances we have observed the downstream flow to be unstable due to a relativistically hot electron-ion streaming instability. The characteristics of the pinched electron flow are responsible for lowering the unstable wave phase velocity to the point where it can interact resonantly with the ions.

APPENDIX B
SPACE-CHARGE DRIVEN COLLECTIVE ION ACCELERATION

SPACE-CHARGE DRIVEN COLLECTIVE ION ACCELERATION*

R. J. FAEHL
Intense Particle Beam Theory Group
Los Alamos National Laboratory

D. J. SULLIVAN
Mission Research Corporation

Two-dimensional electromagnetic PIC simulations have been employed in the study of collective ion acceleration due to injection of intense relativistic electron beams into vacuum drift tubes. Observations of large numbers of ions at energies up to several times the beam energy have been made in many experiments. Experimental differences seem to yield qualitatively different results. The Cornell collective ion acceleration experiment¹ was simulated with actual dimensions and realistic time scales. Field fluctuations were analyzed on the ion time scale. Potential wells significantly in excess of the beam kinetic energy are not found to be associated with the bulk acceleration process. More highly energetic ion tails are correlated with late time system dynamics. Temperature in the hot propagating electron beam may play an important role in that phase.

1. R. Adler, J. Nation, and V. Serlin, Phys. Fluids 24, 347 (1981).
- *Work supported by the U.S. Department of Energy and the Air Force Office of Scientific Research.

Los Alamos

Los Alamos National Laboratory
Los Alamos, New Mexico 87545

Conclusions

- ① Luce diode simulation results show inter-connected ion/electron dynamics
- ② Beam injection into plasma can yield ion acceleration to $\underbrace{\epsilon_b = 2-3 mc^2(\gamma_0-1)}_{\epsilon_b}$, without "deep" potentials
i.e. $|e\phi| \lesssim mc^2(\gamma_0-1)$.
- ③ Virtual cathode + reflexing leads to hot electron cloud: Qualitative agreement with Ryutov, et al.

LUCE GEOMETRY DIODE* HAD YIELDED BEST COLLECTIVE ION ACCELERATION RESULTS, BUT STILL REQUIRES MUCH THEORY.

WE HAVE STUDIED VARIOUS ASPECTS OF
THE SELF-CONSISTENT ACCELERATION
PROCESS TO DETERMINE THE MECHANISMS.

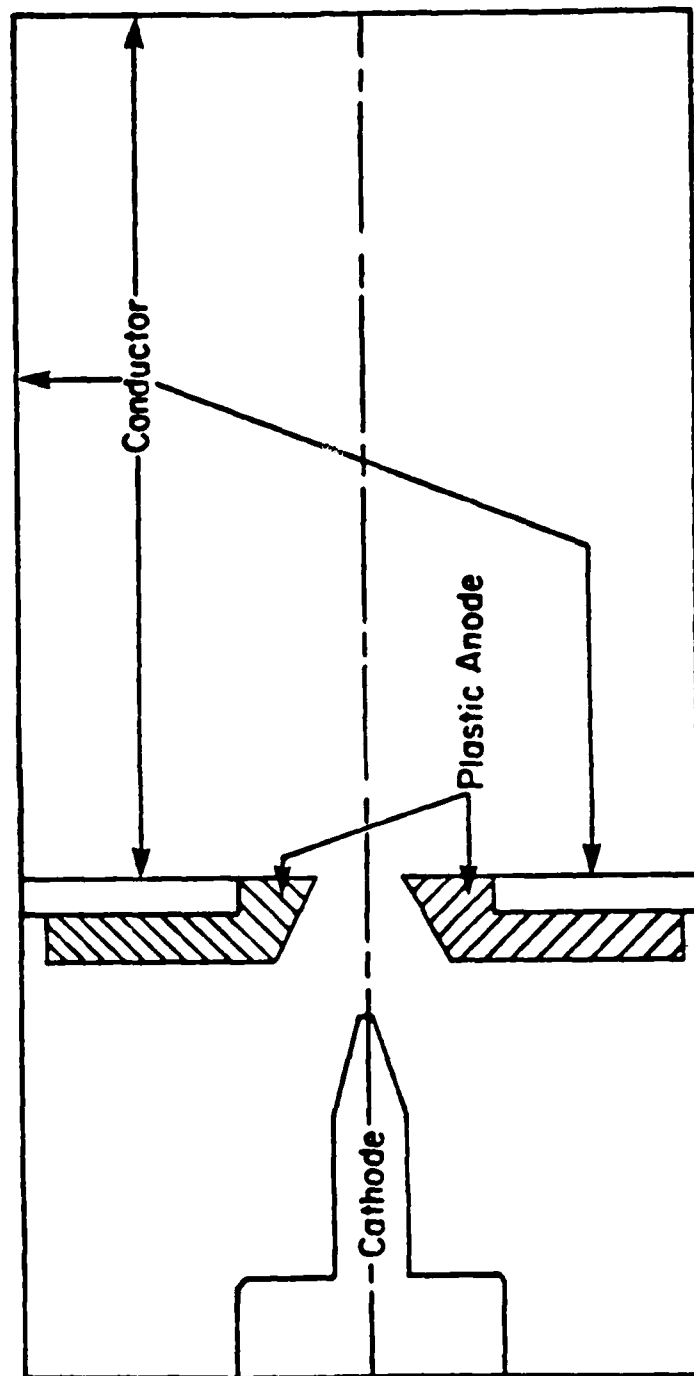
• INSULATED. APERTURED ANODE

A BRIEF (AND INCOMPLETE) SUMMARY OF
EXPERIMENTS IN THE LUCE GEOMETRY

Experiment	E_b (MeV)	I_b (kA)	E_i (protons) (MeV)	E_i/E_b
Luce	2.5	65	>15	6
Hoerberling, Miller	2.2	23	5.8 ± 2	1.7-3.6
Hoerberling	6.0	190	50	8.0-8.5
Adamski	3.5	70	30-40	8.5-11.5
Bistrisky, Didenko	0.85	40	5	6-8
Nation, Adler	0.55	50	12	22.0

THE CORNELL EXPERIMENTAL CONFIGURATION WAS THE MODEL FOR PIC SIMULATIONS.

DIODE WAS OPERATED AT $9-11 \Omega$



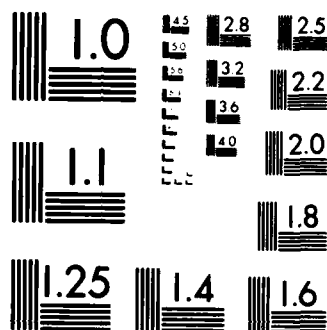
THEORETICAL STUDY OF COLLECTIVE ION ACCELERATION IN THE
LUCE DIODE(U) MISSION RESEARCH CORP ALBUQUERQUE NM
D J SULLIVAN ET AL. NOV 84 AMRC-R-663 AFOSR-TR-84-1224
E49620-82-C-0087 E/G 20/9

NL

F49620-82-C-0087

F/G 20/9

ENI

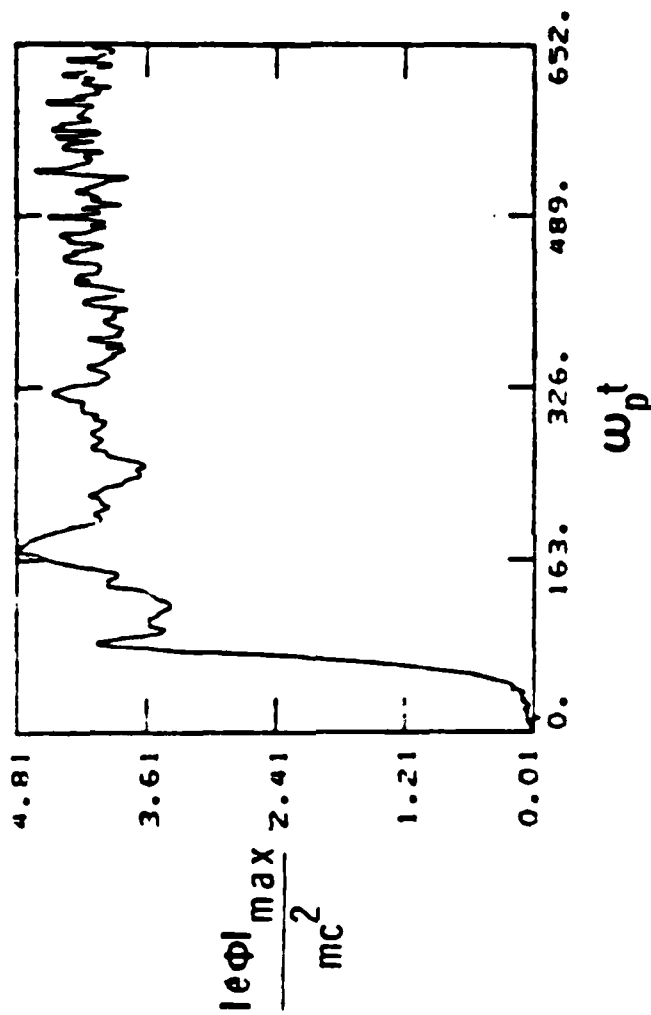


MICROCOPY RESOLUTION TEST CHART
NATIONAL BUREAU OF STANDARDS-1963-A

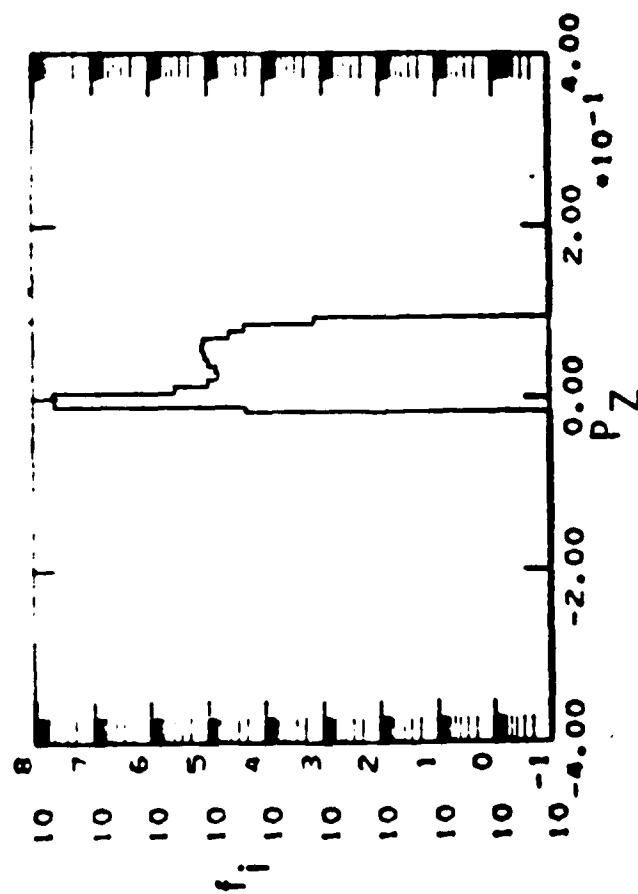
INITIAL SIMULATIONS USED BEAM INJECTION INTO DENSE PRE-FORMED PLASMAS.

1. CONFIGURATION SIMILAR TO UNIV. OF MARYLAND GAS PUFF EXPERIMENTS (DESTLER, ET AL).
2. PARAMETERS: $\gamma_0 = 5(2.0 \text{ MeV})$, $I_b = 48 \text{ kA}$, $n_p/n_b = 35$.
3. SEPARATION OF ACCELERATION FROM DIODE DYNAMICS SIMPLIFIES PROBLEM BUT...
MAY NOT BE GERMAINE TO LUCE DIODE.

POTENTIAL NEVER EXCEEDED BEAM KINETIC ENERGY ($\gamma_0 - 1 = 4.0$) BY MORE THAN 20%.

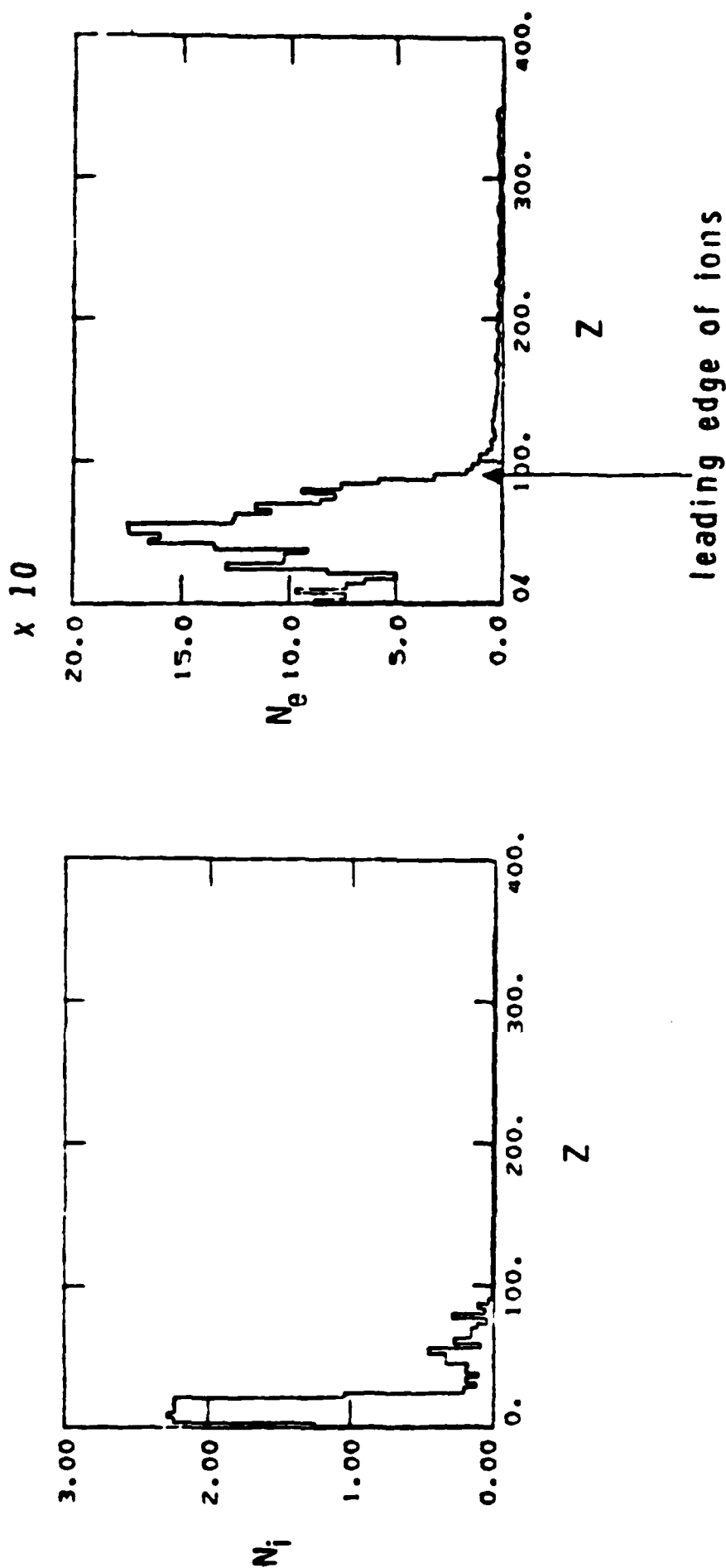


IONS HAD REACHED VELOCITIES OF $\beta=0.1$ AFTER 15 CM PROPAGATION'

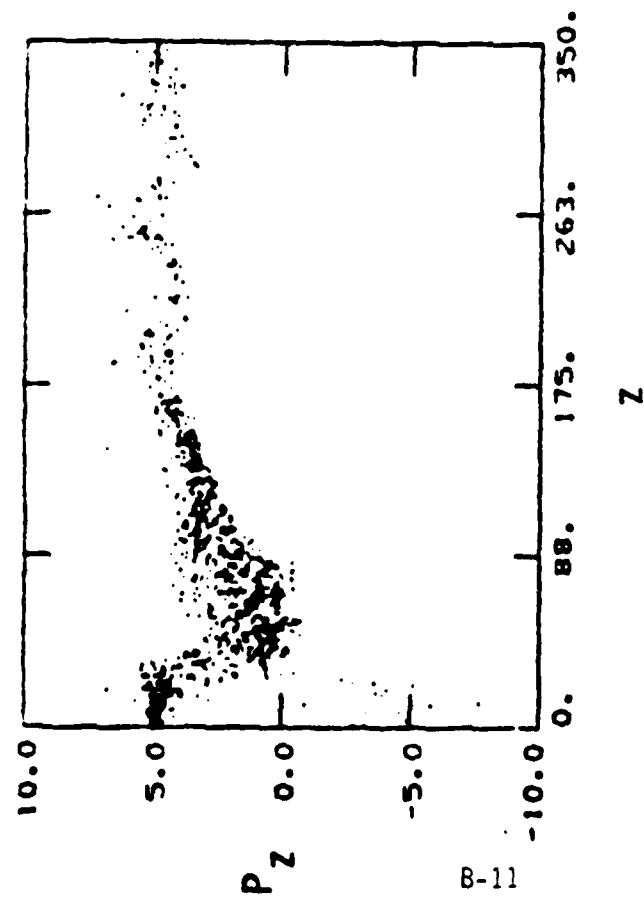


IONS ALSO ALLOW FURTHER ELECTRON PROPAGATION.

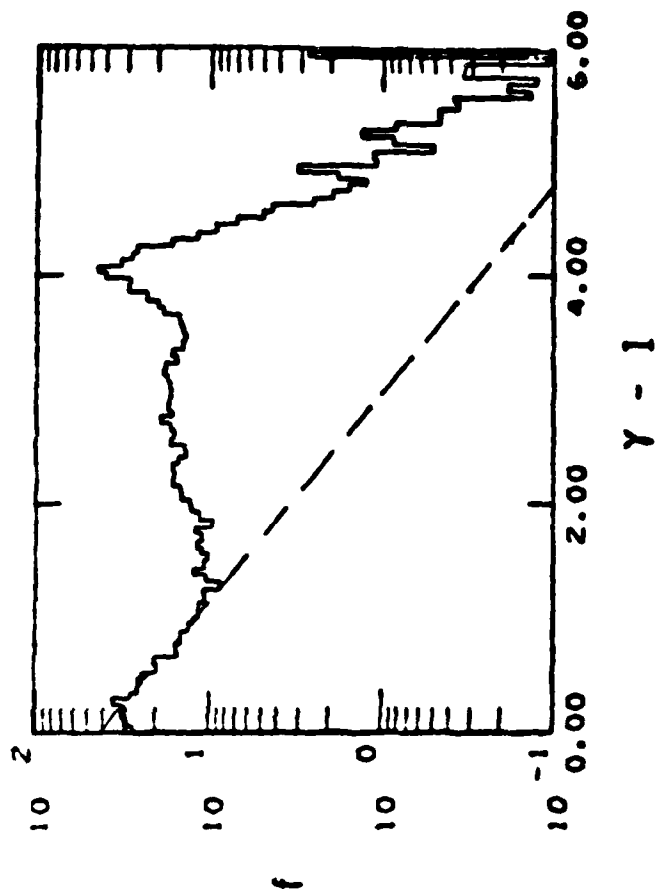
TYPICAL DENSITY PROFILES ($N_i = \int n_i dr$)



PHASE SPACE SHOWS HOT ELECTRON CLOUD WHERE ELECTRON DRIFTING ARE CO-PROPAGATING.

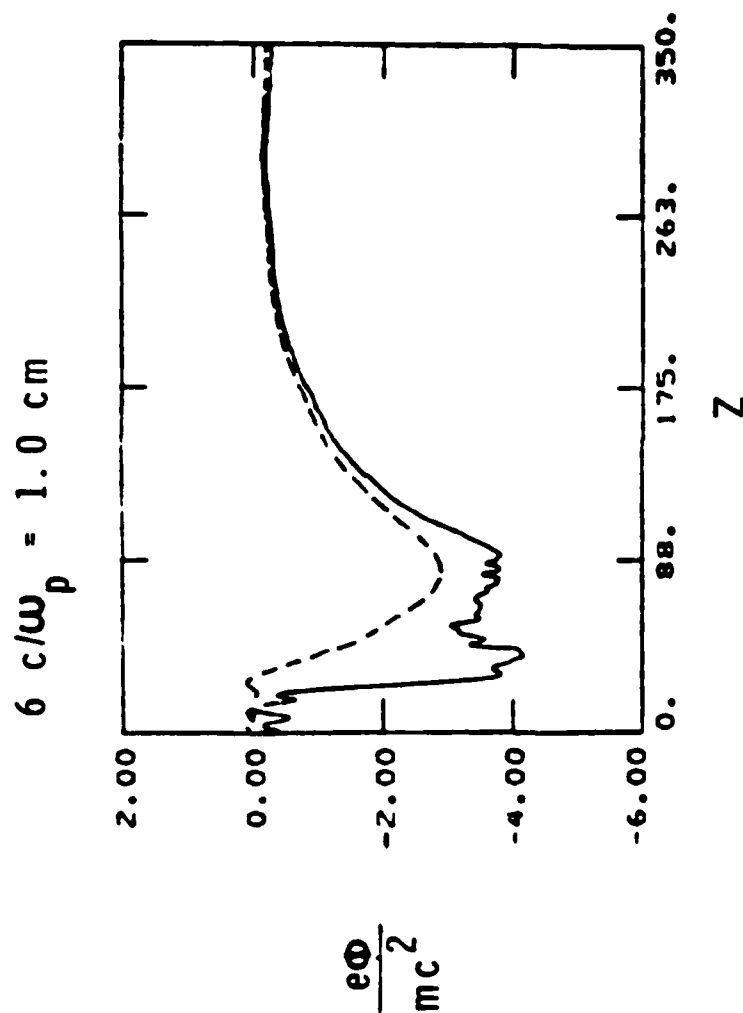


note greatly reduced drift velocity



dashed line gives $kT_e = 400 \text{ keV}$

THE ON-AXIS POTENTIAL REMAINED NEAR $\gamma_0 - 1$ OVER ENTIRE REGION.



—: $r = 0$ (on axis)

- - -: $r = 2.4$ (half-way to wall)

Los Alamos
Los Alamos National Laboratory
Los Alamos, New Mexico 87545

RYUTOV AND STUPAKOV TREATED ELECTRON CLOUD FORMATION ON ANODE PLASMA DUE TO REFLEXING ELECTRONS.

FROM 1-D ANALYSIS, THEY CONCLUDED:

- (1) CLOUD DENSITY COULD GREATLY EXCEED n_0 BEAM DENSITY.
- (2) ELECTRON PRESSURE WOULD DRIVE PLASMA EXPANSION.
- (3) EXPANSION WOULD TRANSFER CLOUD ENERGY TO IONS.
- (4) SOLUTION OF PLASMA EXPANSION, ASSUMING QUASI-NEUTRALITY, YIELDS

$$E_{ion} = 2(\gamma_0 - 1)mc^2 \quad \gamma_0 \geq 1$$

$$E_{ion} = 5(\gamma_0 - 1)mc^2 \quad \gamma_0 \gg 1$$

WE HAVE SIMULATED SUCH A CONFIGURATION USING PARAMETERS APPROPRIATE TO CORNELL LUCE DIODE EXPERIMENTS.

$$\gamma_0 = 2.1 (0.55 \text{ MeV})$$

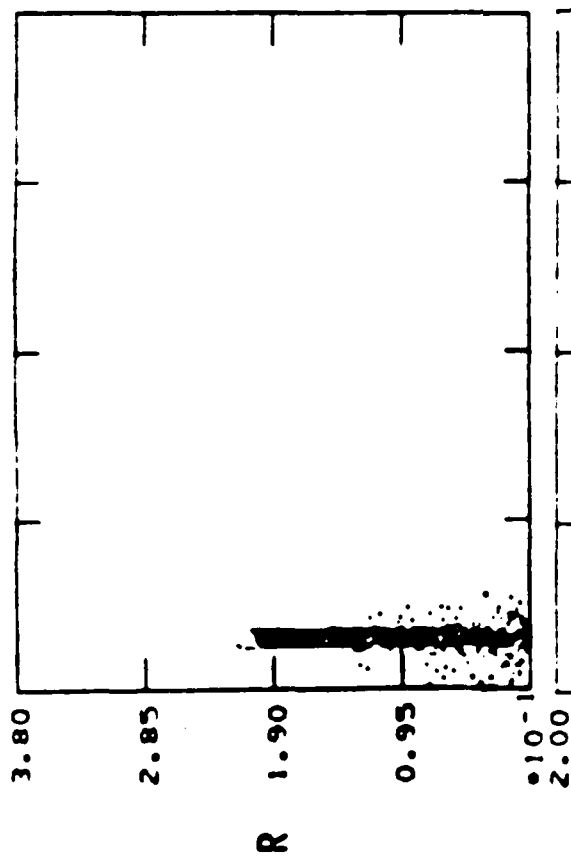
$$I_b = 50 \text{ kA}$$

CONCLUSIONS:

- (1) ELECTRONS DENSITY AROUND ANODE HAD REACHED MANY TIMES BEAM DENSITY BY END OF BEAM RISETIME.
- (2) EVEN WITHOUT ANODE SCATTER, VIRTUAL CATHODE SCATTER MAKES SYSTEM HOT, RATHER THAN BEAM-LIKE.
- (3) PEAK PROTON ENERGIES REACHED 2.0-2.5 MeV.

ELECTRONS EXCEED INITIAL DENSITY BY LARGE FACTOR AS THEY REFLEX AROUND DENSE PLASMA.

Ions



Beam Electrons



P

Z

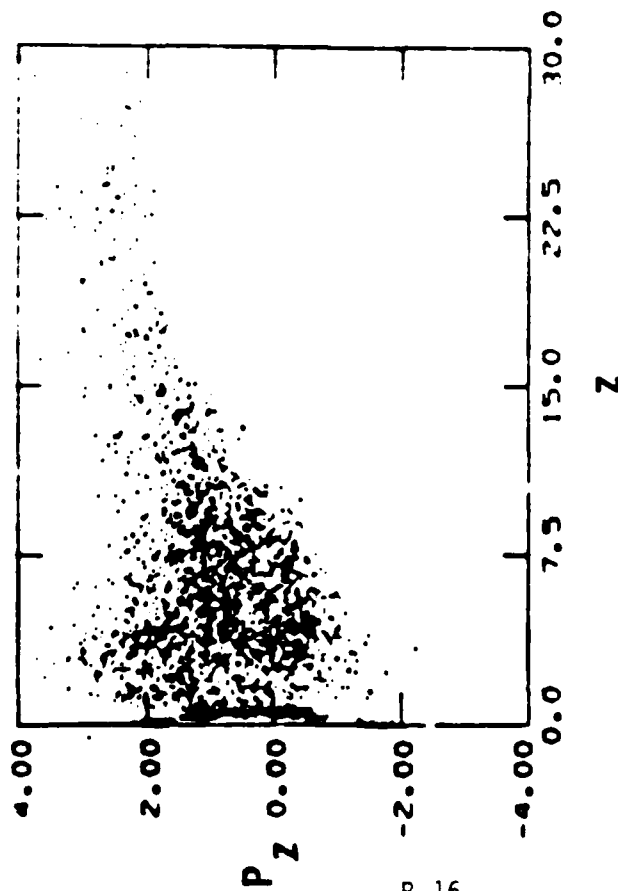
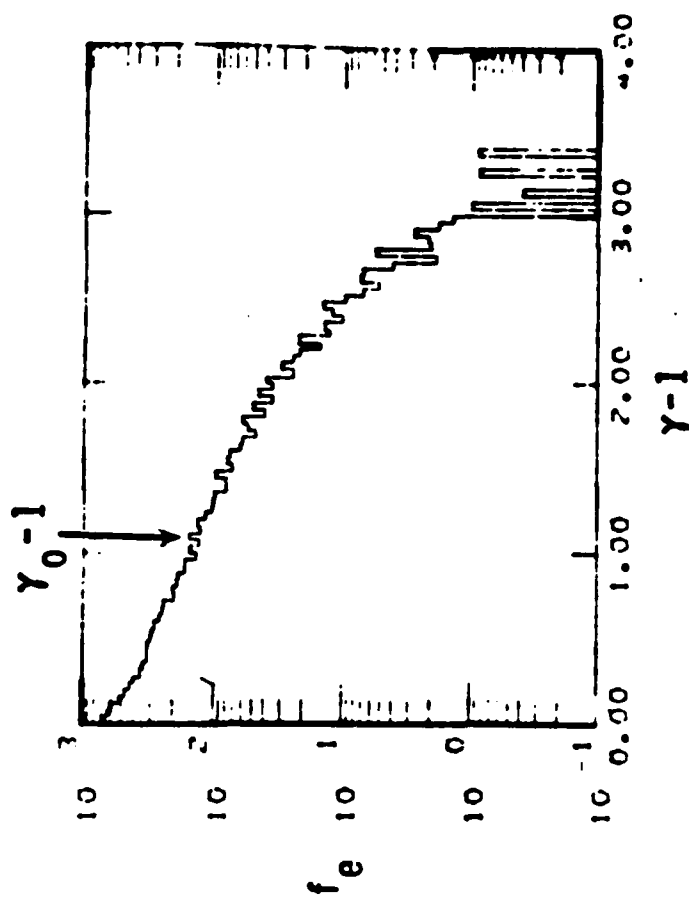


Z

Z

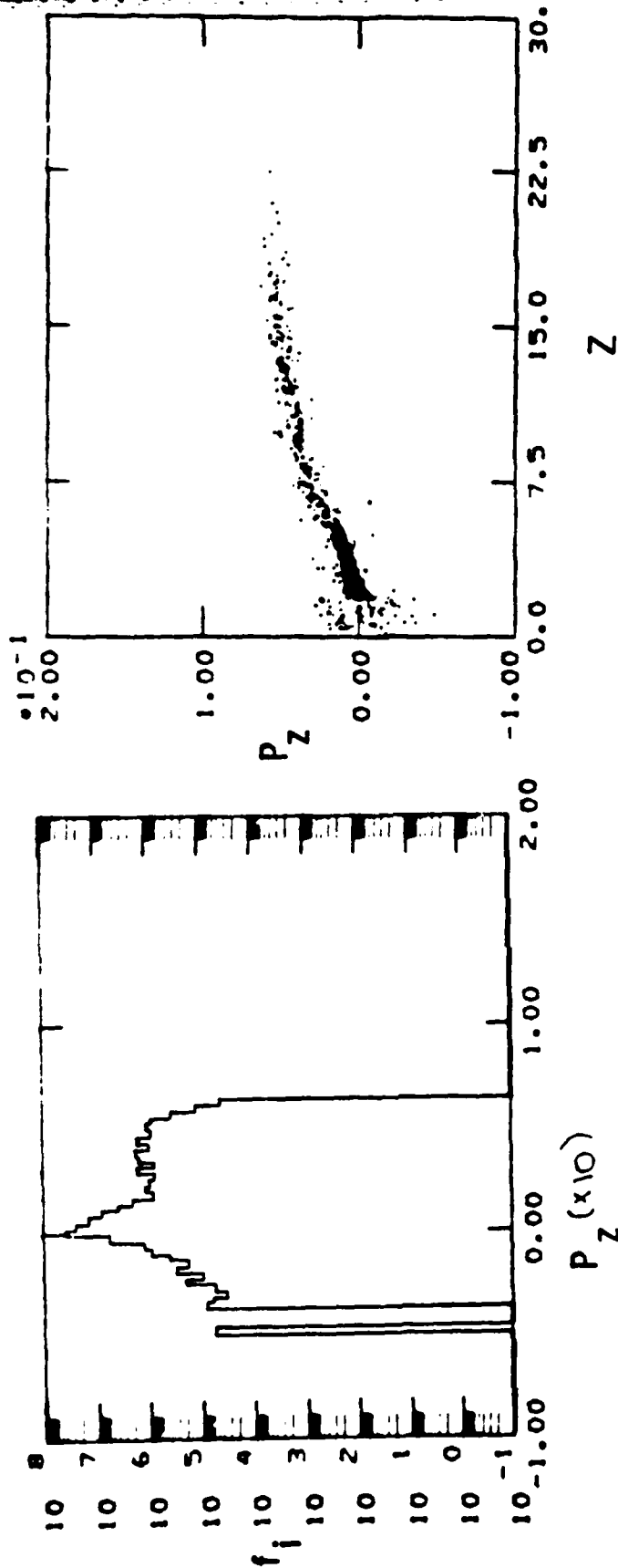
Los Alamos

THE EXPANDING ELECTRON CLOUD IS HOT, RATHER THAN BEAM-LIKE
(FAST ELECTRONS ARE NOT WELL CONFINED).

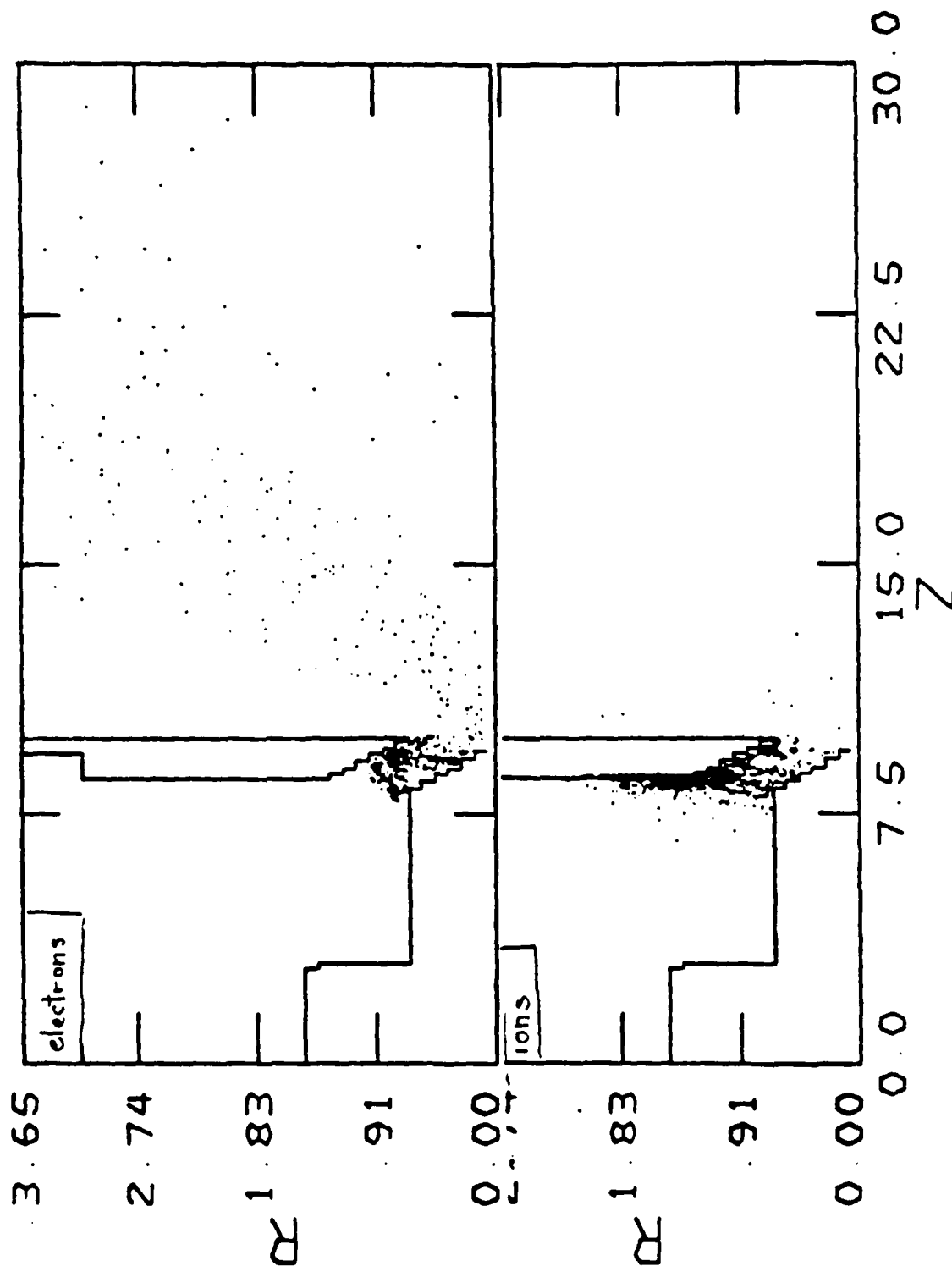


B-16

ION ENERGIES OF 2.0-2.5 MeV ($4-5 E_b$) WERE REACHED IN 15 CM.



ACTUAL LUCE DIODE REQUIRES SELF-CONSISTENT ELECTRON AND ION
FLOWS TO ESTABLISH ACCELERATION PHASE.



APPENDIX C

APPENDIX C

AMRC-N-164

LOCALIZED PLASMA SOURCE COLLECTIVE
ACCELERATOR: PHYSICS AND APPLICATIONS

R. Adler

Supported by: Air Force Weapons Laboratory
Kirtland Air Force Base
New Mexico 87117

Under Contract: F29601-79-C-0043
and MRC Internal Funds

Presented at: DOE Collective Acceleration Meeting
19-20 February 1981

Prepared by: MISSION RESEARCH CORPORATION
1400 San Mateo Boulevard, S.E.
Suite A
Albuquerque, New Mexico 87108

LOCALIZED PLASMA SOURCE COLLECTIVE
ACCELERATORS: PHYSICS AND APPLICATIONS

RICHARD ADLER
MISSION RESEARCH CORPORATION

EXPERIMENTS WITH COMMON CHARACTERISTICS

1. DIELECTRIC ANODE: CORNELL
MARYLAND
LIVERMORE
BOEING
AFWL
2. FOIL SOURCE: CORNELL
NORTH CAROLINA STATE
GENERAL ATOMIC
3. GAS PUFF: MARYLAND
4. PLASMA PUFF;
(FLASH-BOARD) CORNELL
(LASER) MARYLAND

EXPERIMENTAL PARAMETERS
(LUCE DIODE)

(EXPERIMENT IN COLLABORATION WITH J. NATION, V. SERLIN)

E-BEAM	VOLTAGE	.5-.7 MEV
	CURRENT	40-60 KA
	PULSE DURATION	100 NSEC

ION BEAM	NUMBER	$3-8 \times 10^{14}$
	PEAK ENERGY	15 MEV
	AVERAGE ENERGY	1 MEV

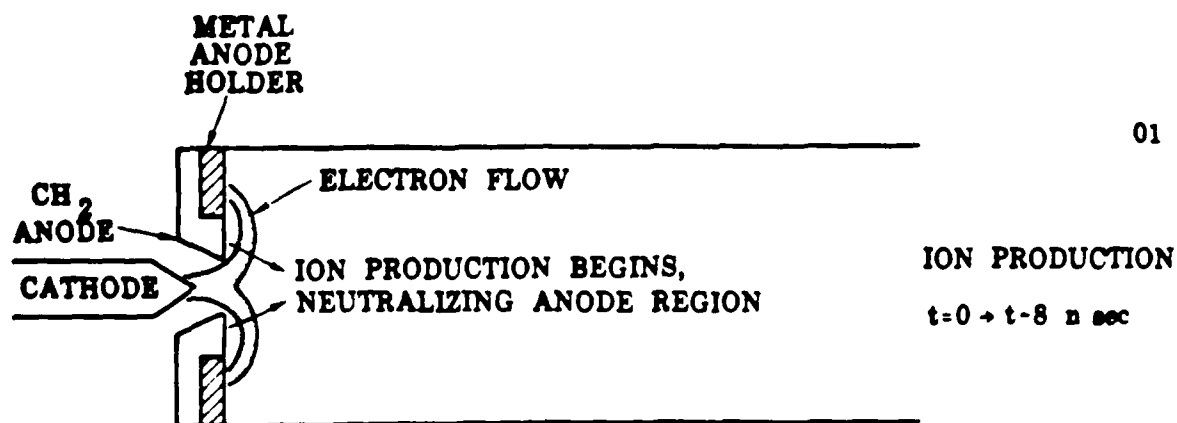
NEUTRONS	FOR PROTONS ON AN LIF TARGET	$>10^9$
----------	---------------------------------	---------

DRIFT TUBE RADIUS	3.6 CM
BEAM RADIUS	.6 CM
ACCELERATION LENGTH	13 CM
EFFICIENCY	2-4%

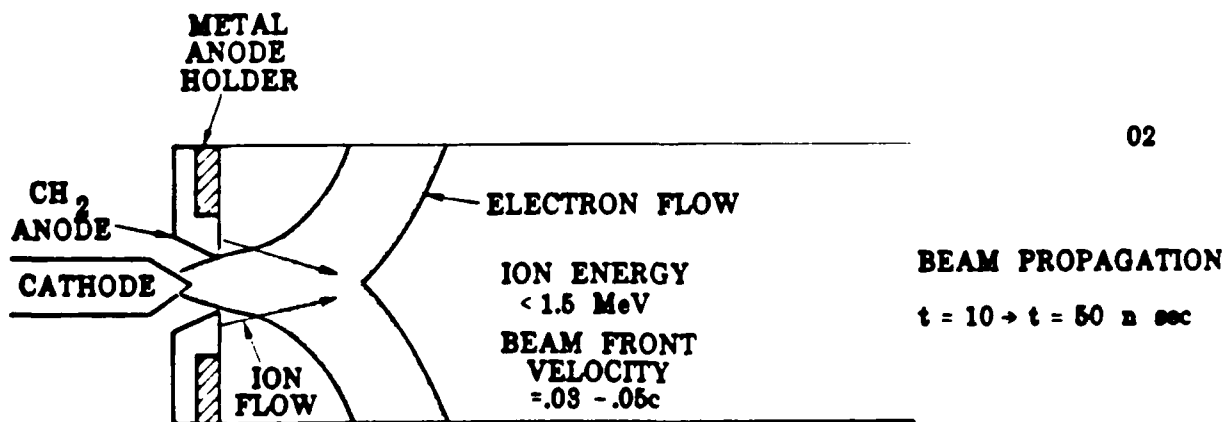
COMMON PROPERTIES OF LOCALIZED PLASMA
SOURCE CONFIGURATIONS

1. EXPONENTIAL (APPROXIMATELY) ENERGY SPECTRUM
2. ION SOURCE AS CLOSE AS POSSIBLE TO CATHODE
3. ION ACCELERATION ONLY ABOVE THE SPACE CHARGE LIMIT
4. ACCELERATION SCALES WITH POWER
5. IN GENERAL, ACCELERATION IS BEST WITH LARGE DRIFT
TUBES (SEE POINT 3)
6. AVERAGE ION VELOCITY IS IN REASONABLE AGREEMENT WITH
MOMENTUM TRANSFER CONSIDERATIONS

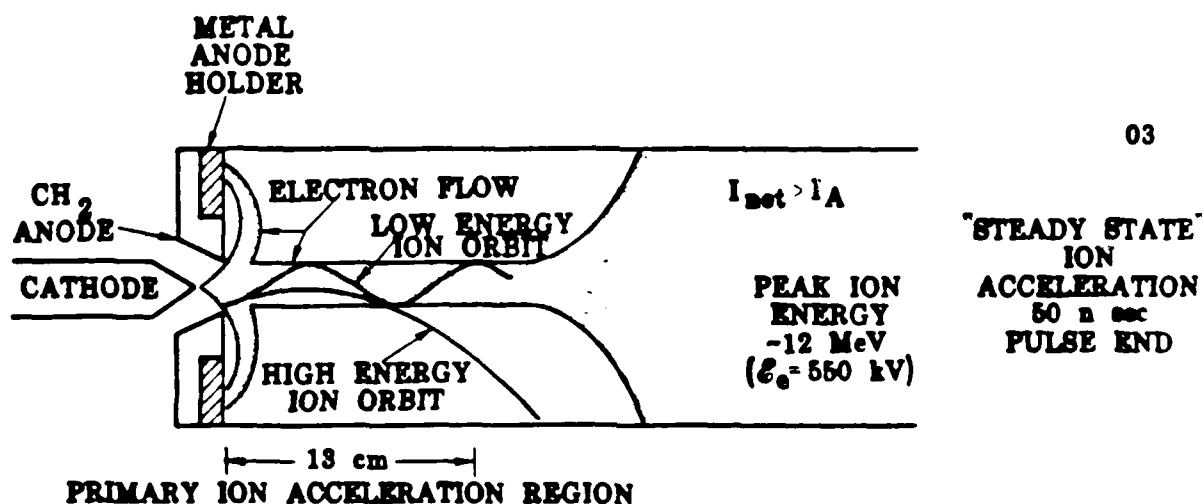
1. ION PRODUCTION BEGINS NEAR THE BEGINNING OF THE CURRENT PULSE, RESULTING IN BEAM FRONT MOTION IN 6-10 NANoseconds.



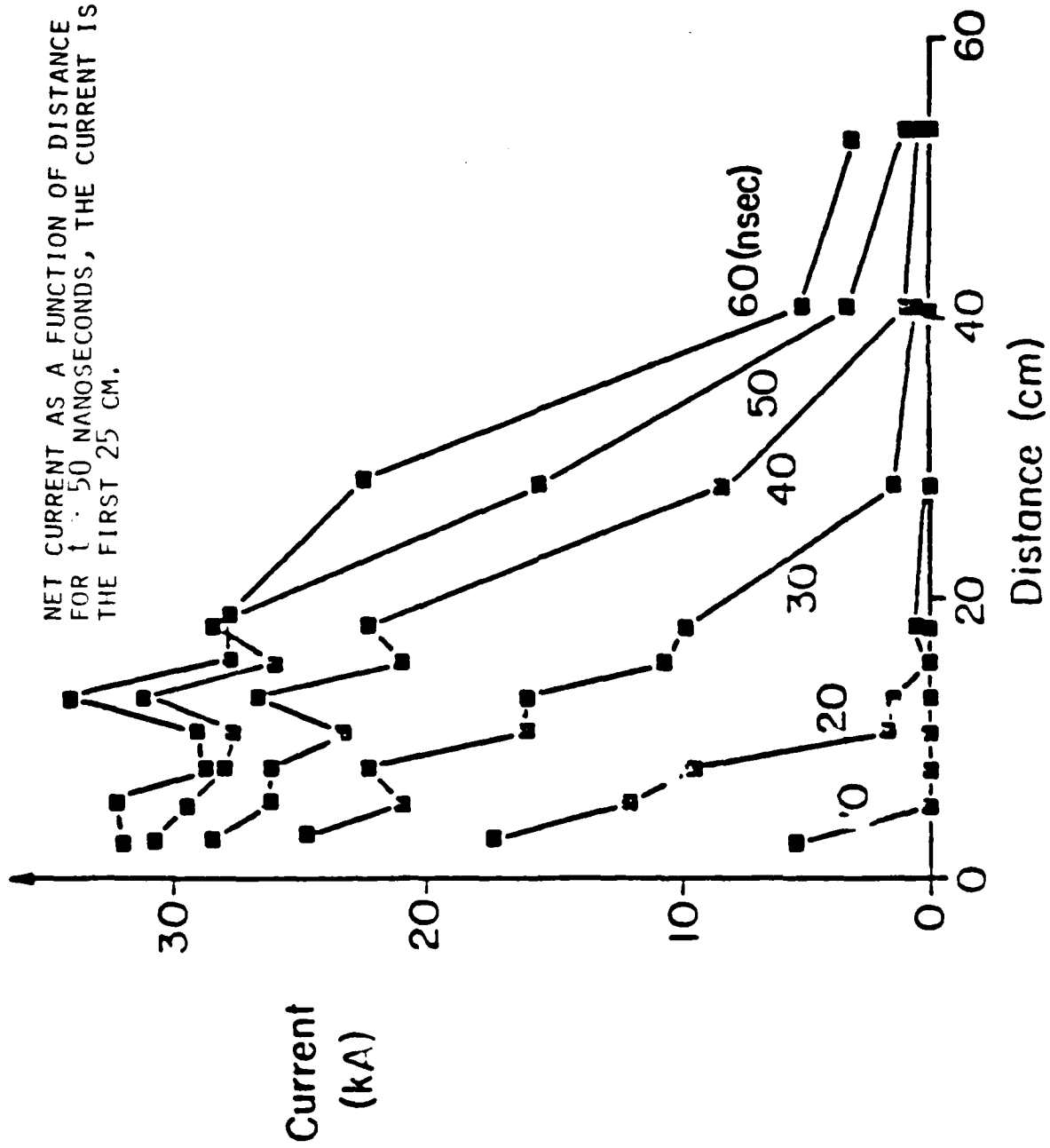
2. THE BEAM BEGINS TO PROPAGATE IN A QUASI-NEUTRAL MODE BY ACCELERATING IONS. THE BEAM FRONT VELOCITY IS $.03-.05 c$, AND THE LENGTH OF THE NEUTRALIZED COLUMN INCREASES WITH TIME.

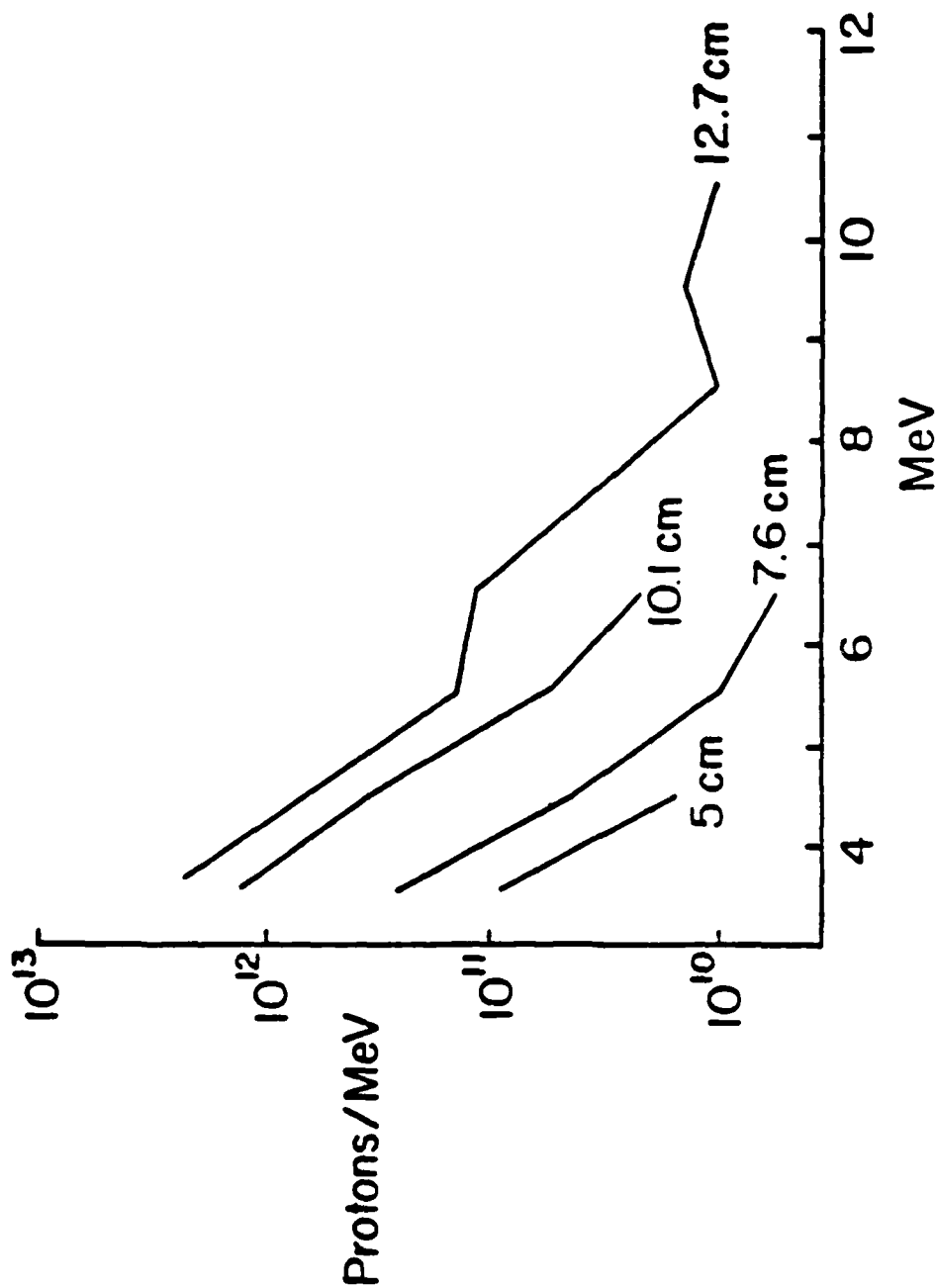


3. AT ~50 NANoseconds, BEAM PROPAGATION SATURATES AT THE FINAL CURRENT PROFILE WHICH IS UNIFORM OVER THE FIRST ~25 CM OF DRIFT TUBE. ACCELERATION OF PROTONS TO >10 TIMES THE BEAM ENERGY BEGINS, COINCIDENT WITH MICROWAVES AT 1.5-3 GHz.

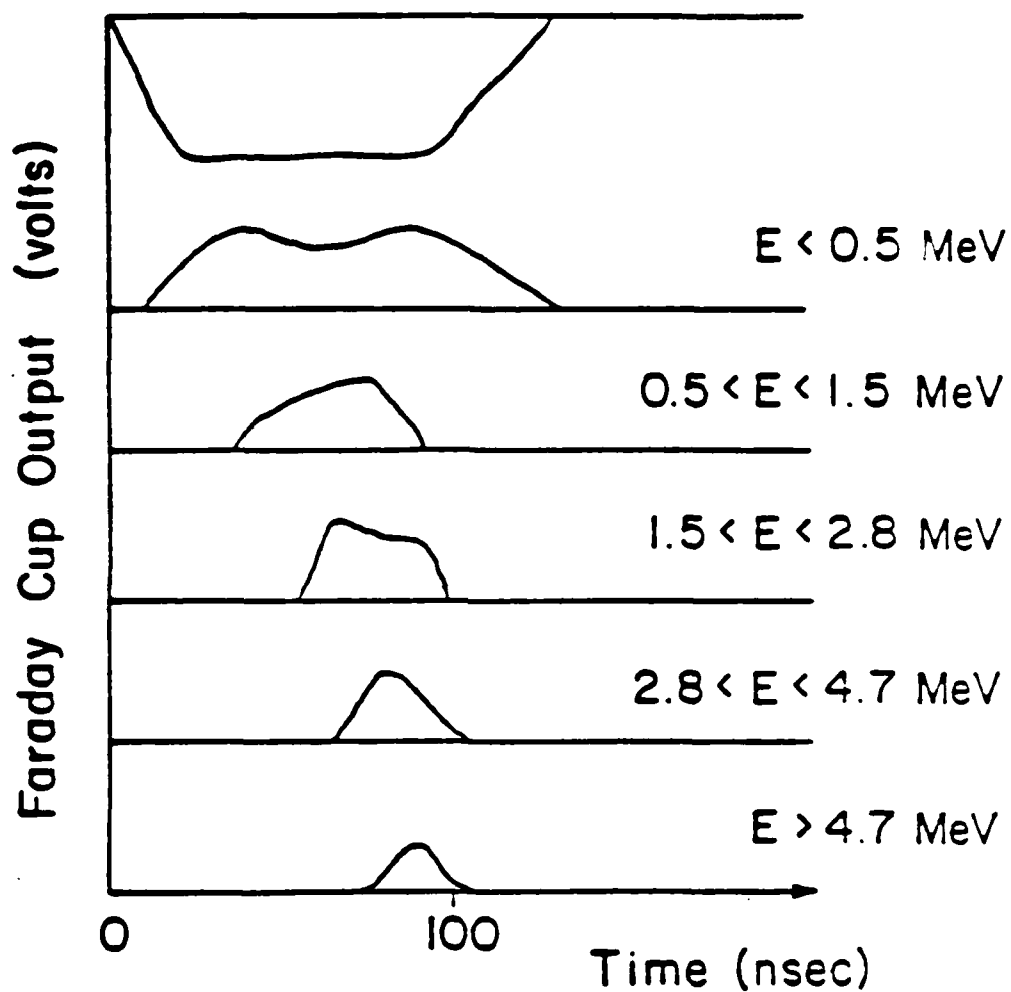


NET CURRENT AS A FUNCTION OF DISTANCE FOR THE TIMES INDICATED.
 FOR $t = 50$ NANoseconds, THE CURRENT IS VIRTUALLY UNIFORM OVER
 THE FIRST 25 CM.





TIME AVERAGED PROTON ENERGY SPECTRA FOR THE AXIAL POSITION (IN CM) INDICATED. THE ENERGY SPECTRUM IS EXPONENTIAL FOR ALL POSITIONS. MEASUREMENTS WERE MADE BY A NEUTRON TIME OF FLIGHT TECHNIQUE.



RELATIVE TIMING OF STACKED FOIL FARADAY CUP DATA. SIGNALS ARE EXTRAPOLATED INTO THE ACCELERATING REGION FROM THE DETECTOR POSITION (1 M). SENSITIVITIES INCREASE BY A FACTOR OF ORDER TWO FOR EACH INCREASING ENERGY 'WINDOW'.

NEUTRON DIAGNOSTICS USING A SMALL SCINTILLATOR A DISTANCE OF 8 M FROM THE TARGET

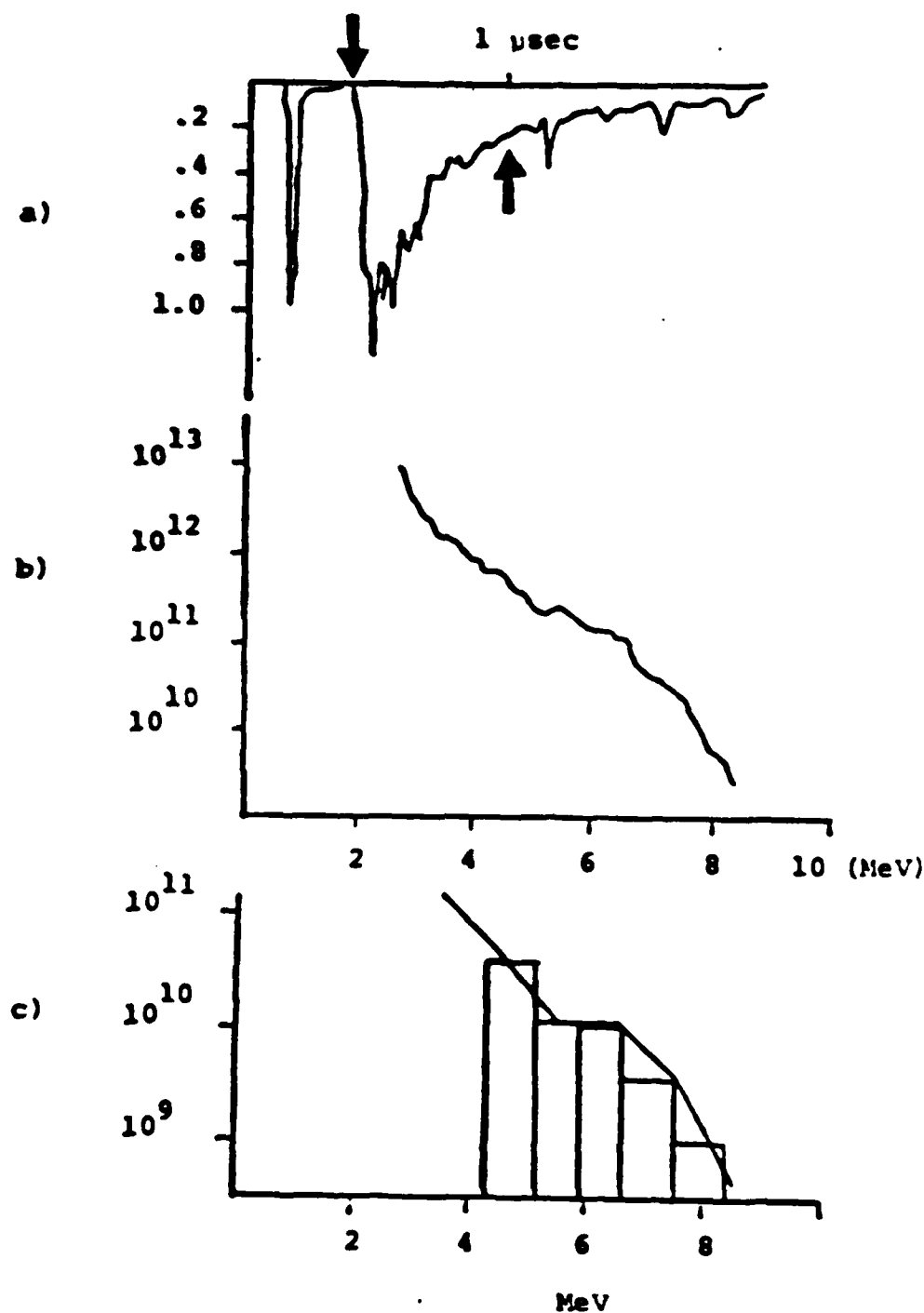
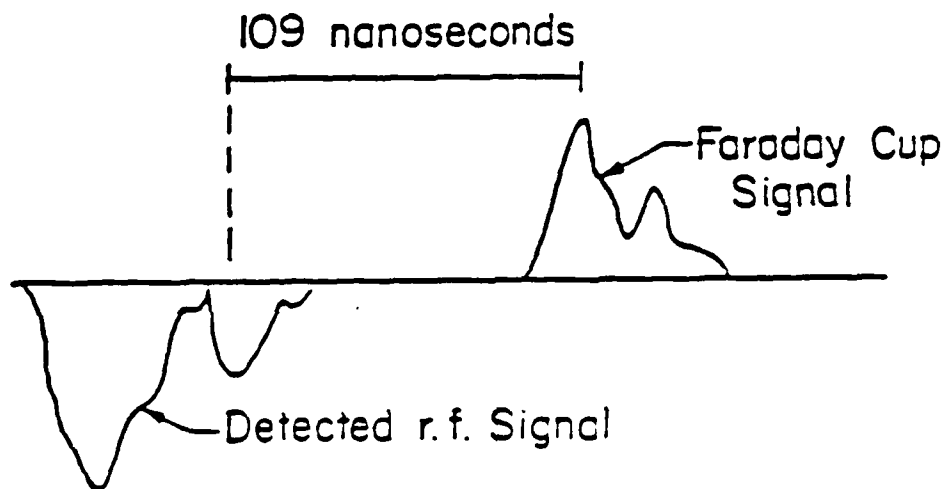


Figure 6. a) Time-of-flight signal, b) Integral spectrum, and c) Differential spectrum (line graph) and stacked Cu foil method (bar graph).



CORRELATION BETWEEN THE SECOND RF PULSE AND ION PRODUCTION. THE NEGATIVE SIGNAL IS THE DETECTED 2 GHZ MAGNETIC FIELD OF THE BEAM MEASURED AT THE DRIFT TUBE WALL. THE POSITIVE SIGNAL IS AN ABSORBER-COVERED FARADAY CUP DETECTING PROTONS OF ENERGY > 4.7 MEV AT $Z = 70$ CM. A PASSIVE DELAY LINE (90 NSEC) PLUS PROTON TIME OF FLIGHT (15-20 NSEC) RESULT IN THE TOTAL DELAY.

THE EFFICIENCY LIMIT
(VALID FOR ALL COLLECTIVE ACCELERATORS)

FROM GENERALIZED MOMENTUM CONS.
(PARTICLE + FIELD STRESS TENSORS)

$$\frac{\epsilon_{\text{ion}}}{\epsilon_{\text{electron}}} \leq \frac{\beta_i}{2} \left(\frac{\gamma_0 + 1}{\gamma_0 - 1} \right)^{1/2} \times$$

$$\times \left\{ \underbrace{1 - n}_{\text{fraction of single particle momentum transferred to ions}} + \frac{I}{4I_A} (1 + 4 \ln b/a) \right\}$$

fraction
of single
particle
momentum
transferred
to ions

$I_A = 17 \epsilon_0 \gamma_0$ kiloamps

γ_0 = Injected relativistic
factor

- ASSUMPTIONS:
- 1) CYLINDRICAL GEOMETRY
 - 2) SEMI-INFINITE DRIFT TUBE
 - 3) $\epsilon_i = \langle \epsilon_i^2 \rangle / \langle \epsilon_i \rangle$

- NOTE:
- 1) EQUALITY ABOVE ONLY HOLDS IF $E_z(z=0)=0$
 - 2) EQUALITY ABOVE ONLY HOLDS IF $I(+\infty)=0$
 - 3) $n < 0$ ONLY FOR SYSTEMS WITH NET ELECTRON REFLECTION

Experiment	Reference	Particle	V (MV)	I _e	I _L	Theory $\overline{\beta_e}$	Expt.
6		H ⁺	1.42	29.2	0	0.072	0.054
		H ⁺	1.96	38.6	0	0.083	0.063
		H ⁺	2.78	47.7	0	0.094	0.063
		H ⁺	3.24	55.4	0	0.10	0.083
9		H ⁺	1.5	30.0	0	0.74	0.041
		H _e ⁺²	1.5	30.0	0	0.052	0.028
7 (late in pulse)		H ⁺	0.55	50.0	35	0.043	0.04
(early in pulse)		H ⁺	0.4	20.0	0	0.038	0.045

Table I. A comparison of theoretical and experimental values of β_i .

The theoretical values are from Equation 21 and the peak experimental V and I have been used. For References 6 and 9, the values were found by approximating Farady cup signals as triangular, and integrating analytically. For short pulses (Refs. 6, 9, and early in the Ref. 7 pulse), the electron beam does not extend out of the accelerating region and so $I_L = 0$. For the Reference 7 data late in the pulse, $I_L = 35$ kA was measured. The theoretical values of β_i were computed on the basis of the peak values of V, I.

ION CONFINEMENT:

$$f = \frac{n_i}{n_e} \quad f > (1 - I_{SCL}/I)$$

$$I_{SCL} = \frac{17(\gamma^{2/3} - 1)^{3/2}}{1 + 2 \ln b/a} \text{ kA}$$

CONFINEMENT CONDITION

$$B_i B_\theta < E_r$$

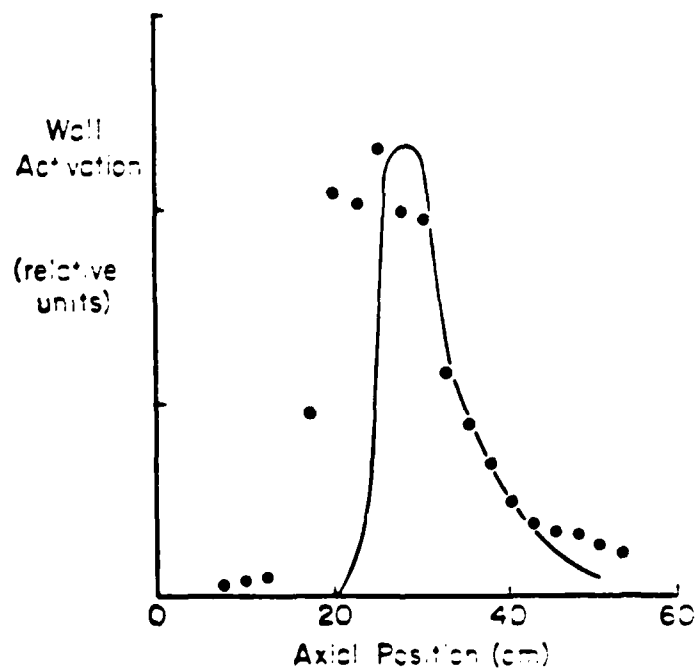
OR

$$B_i B_e < 1 - f < \frac{I_{SCL}}{I}$$

OR

$$E_i < \frac{I_{SCL}}{E_e I}$$

HIGH ENERGY IONS ARE LOST RADially AT HIGH CURRENTS.



PHYSICS CONCLUSIONS

1. THE LUCE DIODE OPERATES IN A STEADY STATE MODE -- ACCELERATION IS NOT DUE TO A BEAM FRONT PROCESS.
2. GOOD CORRELATION IS FOUND BETWEEN RF AT 1.5-3 GHZ, AND HIGH ENERGY ION PRODUCTION.
3. THE PEAK ION ENERGY INCREASES WITH TIME INTO THE PULSE, EVEN FOR $50 < T < 100$ NANOSECONDS.
4. THE ELECTRON-ION TWO-STREAM INSTABILITY IS A VIABLE CANDIDATE AS AN ACCELERATION MECHANISM.
5. ION ACCELERATION EFFICIENCY IS IN AGREEMENT WITH MOMENTUM CONSERVATION LIMITS AND SCALING.
6. THE ENERGY SPECTRUM IS A TRUNCATED EXPONENTIAL, ON AVERAGE, FOR ALL AXIAL POSITIONS, AND AT ALL TIMES.

PRIMARY APPLICATION:
COLLECTIVE ACCELERATOR NEUTRON SOURCE

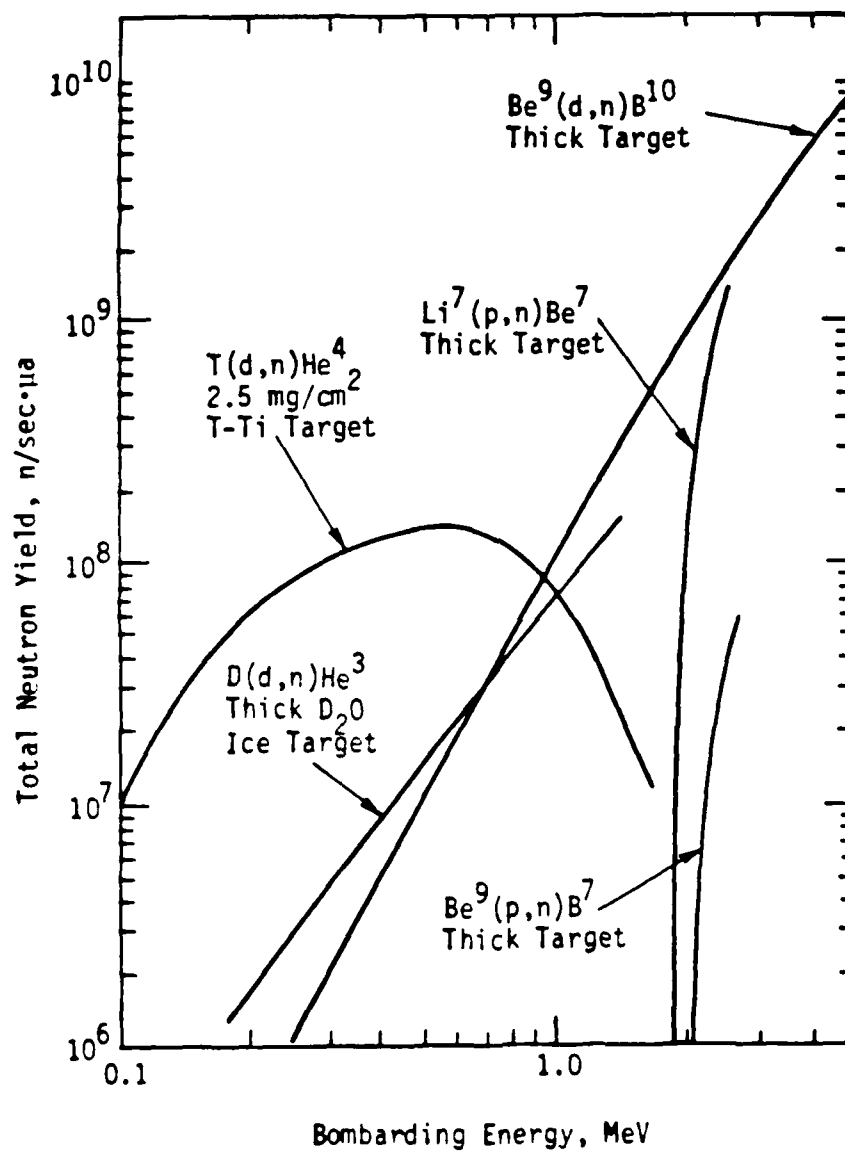
USING THE PARAMETERS OF THE EXPERIMENT, AND ASSUMING:

- 1) N_i REDUCED BY $\sqrt{2}$ (FOR DEUTERONS)
- 2) $f(E) = f_0 \exp(-E/1 \text{ MeV})$ (LOWER OR THE SAME
AVERAGE ENERGY AS FOR PROTONS)
- 3) BERYLLIUM TARGET OVER 2π SR.

A FAST NEUTRON OUTPUT OF 3×10^{10} /PULSE RESULTS.

THE NUMBER ABOVE IS AN UNDERESTIMATE BECAUSE DEUTERONS WILL
BE CONFINED $\sqrt{2}$ TIMES FARTHER (AXIALLY) THAN THE EQUIVALENT
PROTONS.

NONREACTOR NEUTRON SOURCES



NEUTRON SOURCE APPLICATIONS

1. IN-SITU REACTOR SHIELDING MEASUREMENTS

- A) EXPONENTIAL ION SPECTRUM
=> EXPONENTIAL NEUTRON SPECTRUM
- B) IF $\epsilon_e \sim .5-1$ MeV, A FISSION NEUTRON SPECTRUM CAN
BE ACCURATELY APPROXIMATED
- C) THE SHORT NEUTRON PULSE ALLOWS USE OF TIME OF
FLIGHT MEASUREMENT TECHNIQUES

2. COAL SLURRY FLOW MEASUREMENTS (COAL GASIFICATION PLANTS OR OTHER COAL PROCESSING PLANTS)

- A) FAST NEUTRON, NEUTRON-INDUCED γ MEASUREMENTS GIVE
COAL FLOW COMPOSITION
- B) PULSED NEUTRON SOURCES GIVE THE FLOW RATE IN THE
SYSTEM, EVEN FOR MULTIPHASED FLOWS

3. VERY FAST FLOW-RATE MEASUREMENTS

- A) FLOW RATES IN THE FASTEST CHEMICAL ENGINES (10 KM/SEC)
MAY BE MONITORED WITH A FAST NEUTRON PULSE ($<1 \mu\text{SEC}$)
- B) DETAILED SPATIAL FLOW ANALYSIS MAY ALSO BE POSSIBLE
- C) MAY BE APPLIED TO STUDIES OF ROCKET ENGINES,
COMBUSTION, TURBINES, ETC.

OTHER APPLICATIONS

- 1) ^3He CHARGED PARTICLE ACTIVATION ANALYSIS -- SURFACE CONCENTRATIONS IN PPM-PPB RANGE.
- 2) THE VARIETY OF LOCALIZED SOURCES AVAILABLE ACCESSES THE FULL RANGE OF ELEMENTS. THE EXTREMELY HIGH PARTICLE FLUX WOULD ELIMINATE NOISE IN BEAM FOIL SPECTROSCOPY STUDIES. (THESE HAVE BEEN USED TO DIAGNOSE TOKAMAC IMPURITIES, FOR EXAMPLE.)

ION AUTOACCELERATION

EFFICIENCY LIMIT \Rightarrow PROTON AUTOACCELERATION MAY BE AN ORDER OF MAGNITUDE MORE EFFICIENT THAN DIRECT COLLECTIVE ACCELERATION (FOR LOW VOLTAGES).

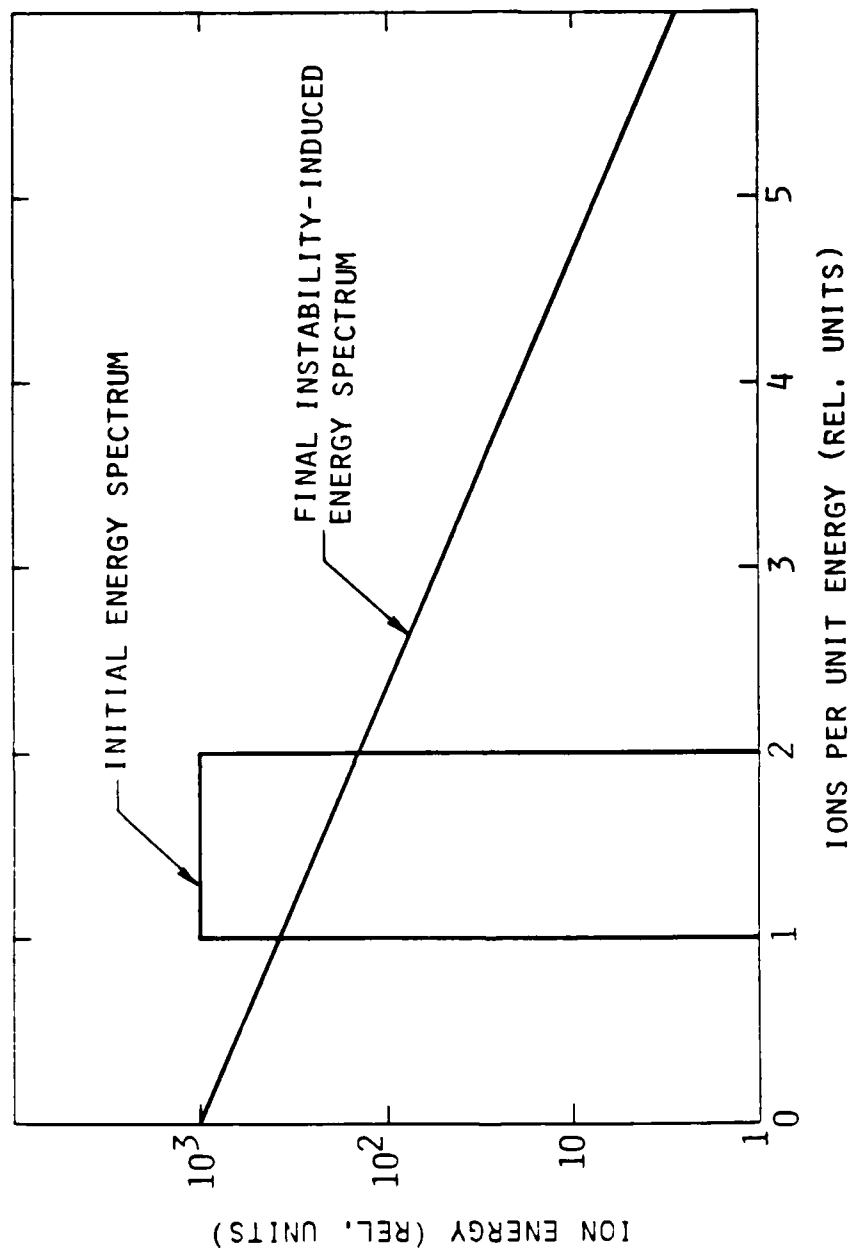
FOR NEUTRON PRODUCTION, AN EXPONENTIAL ENERGY SPECTRUM (AVE. ENERGY = E_0) IS MUCH MORE DESIRABLE THAN A DELTA FUNCTION DISTRIBUTION.

USE ELECTRONS TO CHANGE THE ION DISTRIBUTION FUNCTIONS.

EXAMPLES:

- 1) PIERCE INSTABILITY
- 2) ELECTRON-ION TWO STREAM-COINJECT FAST ELECTRONS, IONS, $n_e = n_i$; $\beta_e > \beta_i$ -- THE ELECTRON-ION INSTABILITY ACTS TO RANDOMIZE THE ION ENERGY, INCREASING NET NEUTRON PRODUCTION.

ION AUTOACCELERATION



DESIRED ION AUTOACCELERATION ENERGY SPECTRUM REDISTRIBUTES THE PARTICLES' ENERGY FOR BETTER NEUTRON PRODUCTION.

REQUIRED WORK FOR APPLICATIONS

- 1) STUDY LONGER PULSE ION PRODUCTION CHARACTERISTICS
TO DEFINE THE FINAL DISTRIBUTION FUNCTION (EXPERIMENT)
- 2) DEFINE EXTERNAL FACTORS AFFECTING THE DETAILED ION
DISTRIBUTION FUNCTION
- 3) ASSESS THE LONG PULSE APPLICABILITY OF GAS PUFF D_2
SOURCES
- 4) PERFORM 1-D SIMULATIONS TO ISOLATE A USEFUL ION
AUTOACCELERATION MECHANISM
- 5) PERFORM A DETAILED STUDY OF APPLICATIONS.

CONCLUSIONS

1. APPLICATIONS EXIST FOR LOCALIZED PLASMA SOURCE COLLECTIVE ACCELERATORS AT THE PRESENT STAGE OF DEVELOPMENT.
2. THE EXISTING PHYSICS UNDERSTANDING IS ADEQUATE FOR THE APPLICATIONS ENVISAGED. SOME QUESTIONS MUST STILL BE ANSWERED.
3. ION AUTOACCELERATION IS AN ATTRACTIVE ALTERNATIVE, AND MERITS FURTHER STUDY.

APPENDIX D

NUMERICAL SIMULATION AND COMPARISON BETWEEN
TWO KNOWN MODES OF COLLECTIVE ION ACCELERATION

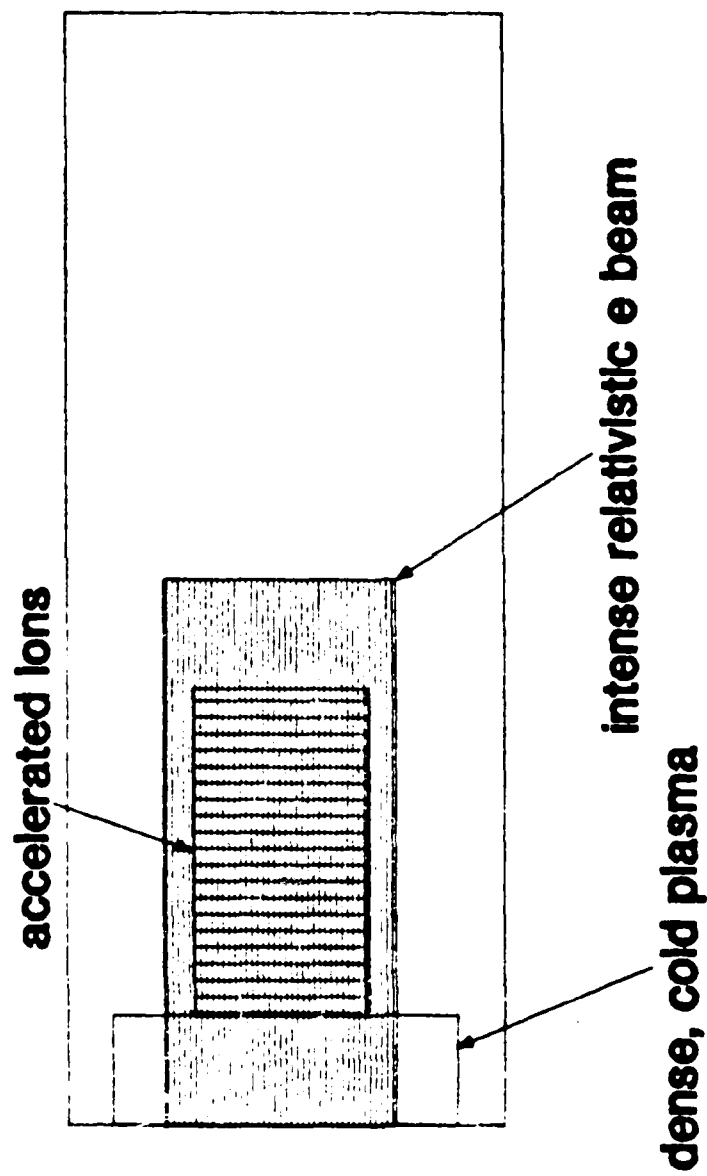
**NUMERICAL SIMULATION AND COMPARISON BETWEEN
TWO KNOWN MODES OF COLLECTIVE ION ACCELERATION**

**R. J. FAEHL, W. K. PETER
LOS ALAMOS NATIONAL LABORATORY**

**D. J. SULLIVAN
MISSION RESEARCH CORPORATION**

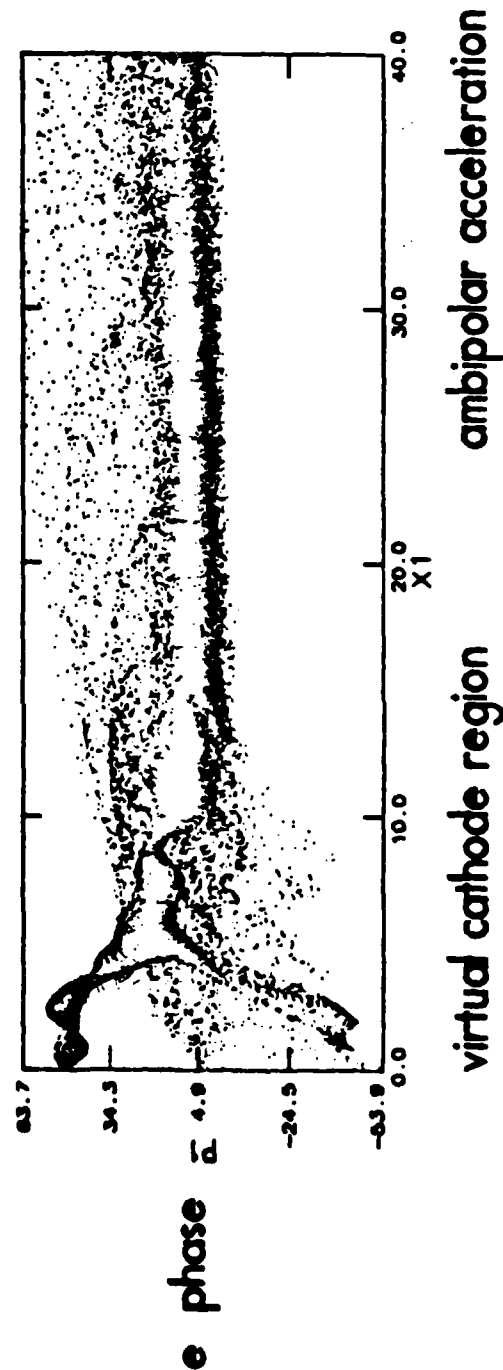
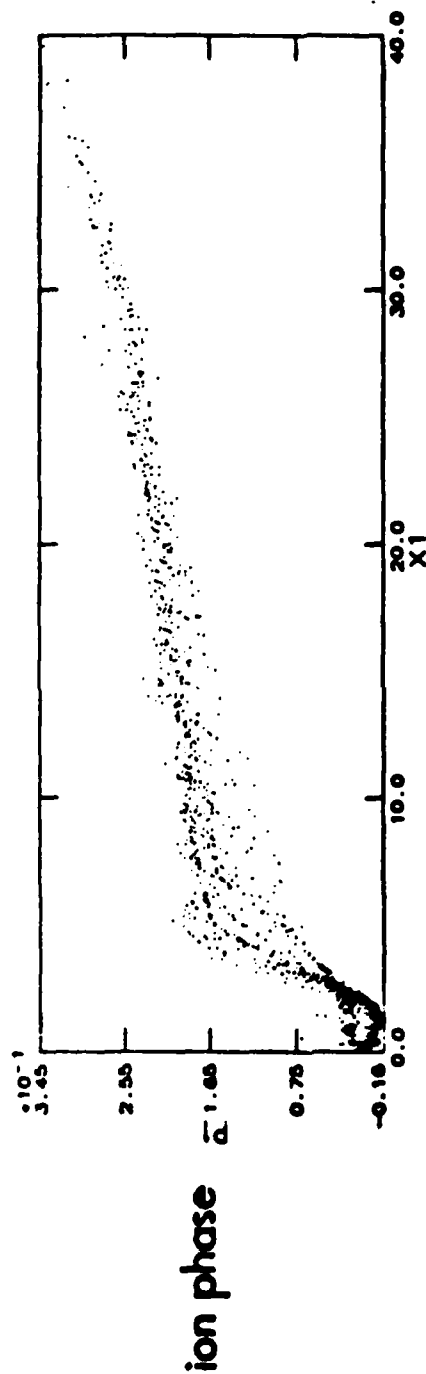
**ANNUAL MEETING OF THE PLASMA PHYSICS DIVISION
OF THE AMERICAN PHYSICAL SOCIETY
BOSTON
NOV 1 1984**

**A "HYDRODYNAMIC" MODEL CAN EXPLAIN MUCH
ABOUT ACCELERATION IN THE GAS FILL CASE**



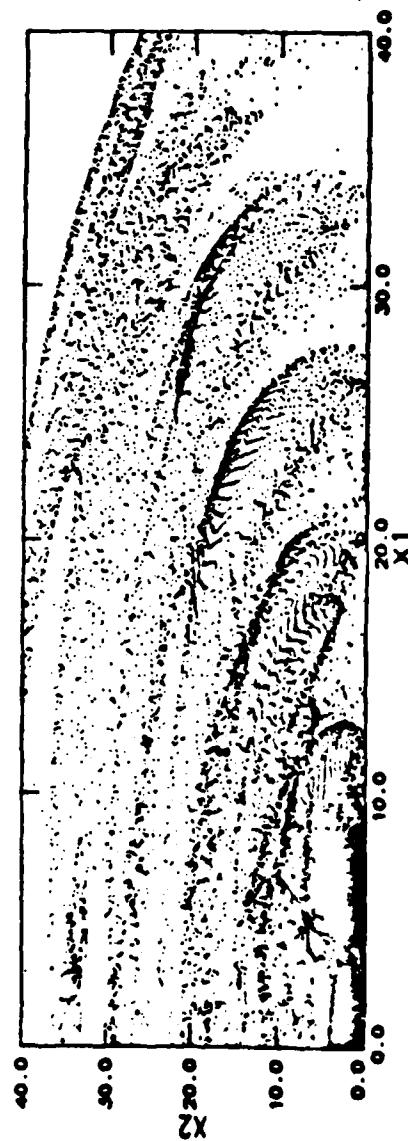
TWO MECHANISMS EXPLAIN ION ACCELERATION:

- 1) electrostatic acceleration through the virtual cathode
- 2) ambipolar plasma-expansion acceleration

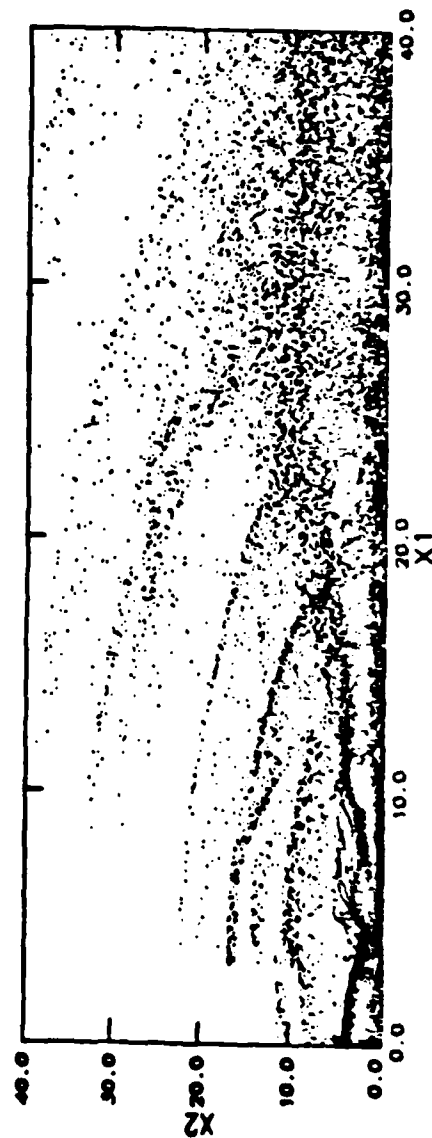


TWO DIMENSIONAL PIC SIMULATIONS SHOW AN UNEXPECTED DEGREE OF RADIAL CONFINEMENT

LITTLE CONFINEMENT BEFORE IONS PROPAGATE



SIGNIFICANT CONFINEMENT AFTER IONS PROPAGATE



**NET ELECTRON CURRENT INDUCES A PINCH FORCE:
DYNAMICS BECOME QUASI-ONE DIMENSIONAL
ELECTRON PRESSURE NEEDED TO BALANCE PINCH FORCE**

$$-e(E_r - \beta_e B_\theta) = kT \nabla \ln n_e$$

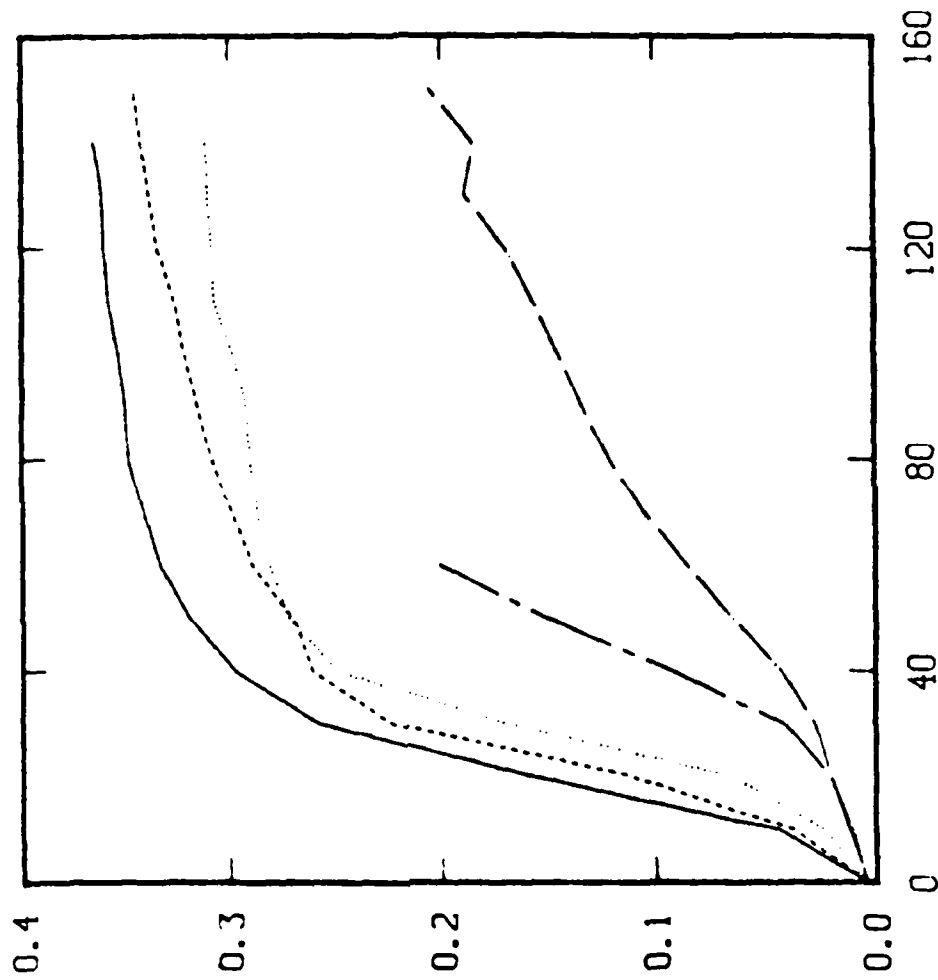
$$n_e = n_0 / \{1 + (r/a)^2\}$$

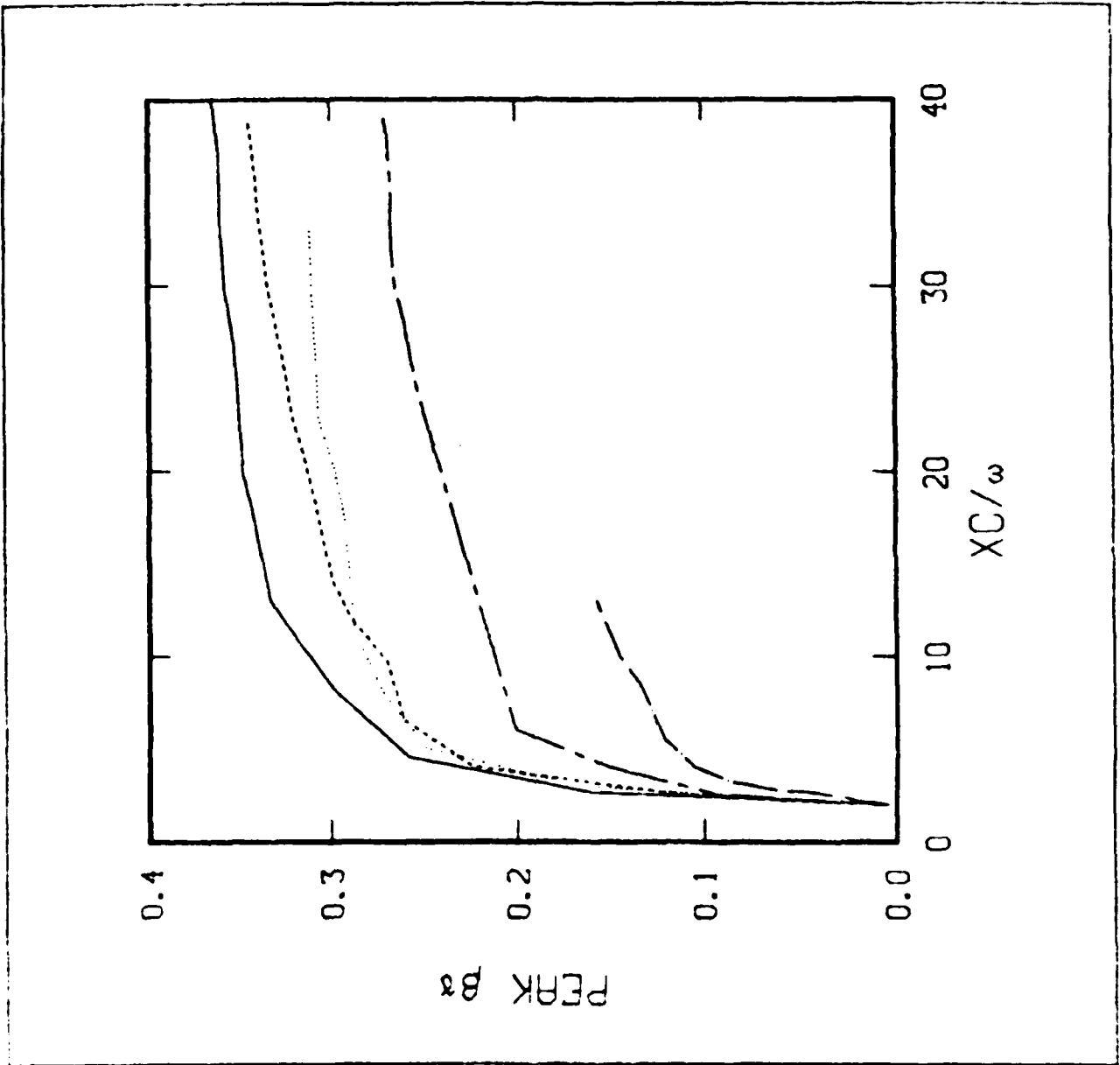
IONS CAN RADIAL FORCE BALANCE WITHOUT PRESSURE

$$E_r = \beta_i B_\theta$$

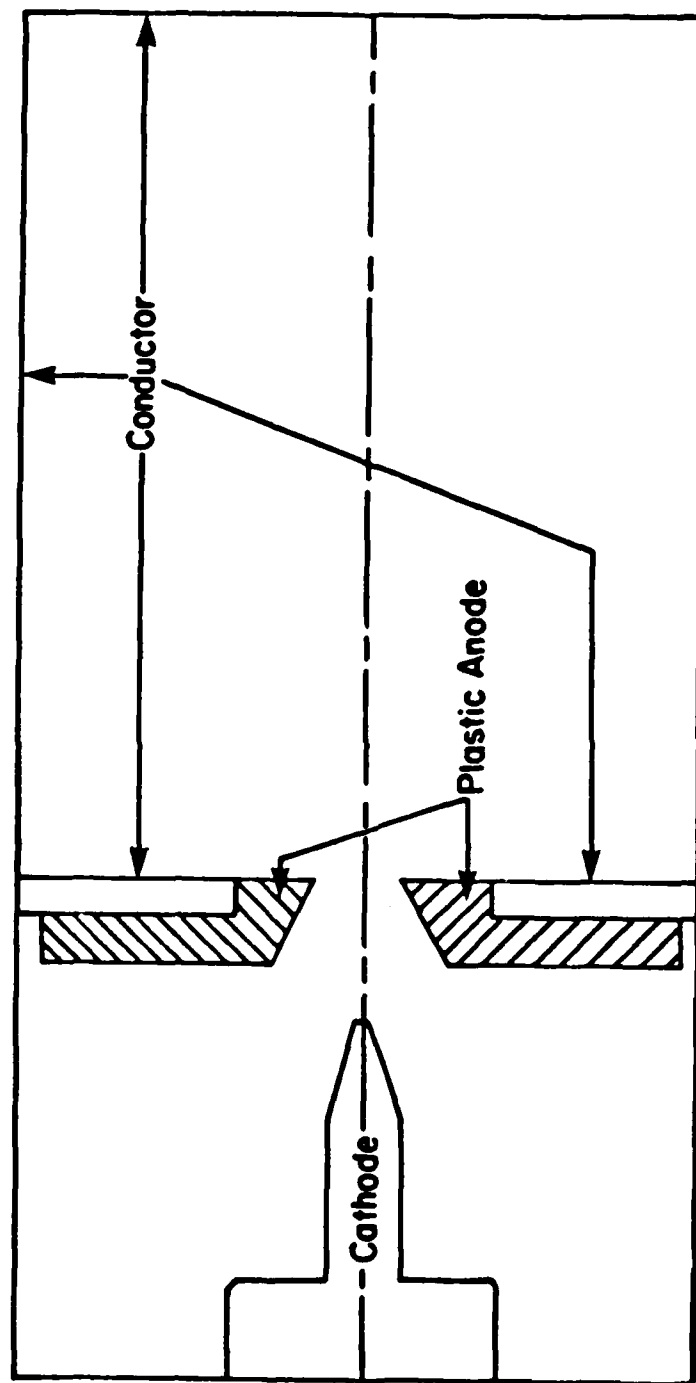
$$Z n_i = n_e (1 - \beta_i \beta_e) / (1 - \beta_i^2)$$

**PEAK ION ENERGY SCALES WEAKLY WITH CURRENT
AS LONG AS CURRENT IS ABOVE SPACE CHARGE LIMIT**



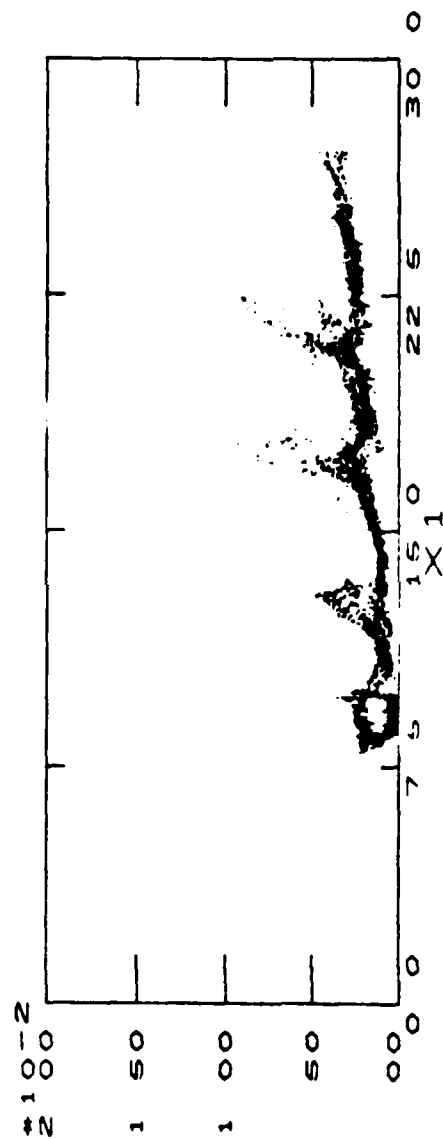


A TYPICAL LUCE DIODE CONFIGURATION SETS UP PECULIAR ELECTRON-ION FLOW PATTERN



dynamics resemble pinch reflex ion diode — set at angle

A STREAMING INSTABILITY MAY ACCOUNT FOR THE VERY HIGH ENERGY IONS IN LUCE DIODES



COLD BEAM STABILITY THEORY YIELDS PHASE VELOCITIES TOO HIGH TO TRAP IONS **INSTABILITY FIGURES OF MERIT:**

k for peak growth, $k_m = \omega_e / (v_e - v_i)$

$$\omega_m = \omega_e v_i / (v_e - v_i) + .5 \omega_i A + i .5 \sqrt{3} \omega_i A$$

where $\omega_e = \omega_{pe} / \gamma_e^{3/2}$, $\omega_i = \omega_{pi} / \gamma_i^{3/2}$

$$A = (\omega_e / 2 \omega_i)^{1/3}$$

$$\text{SO } V_{ph} = v_i + (v_e - v_i) (\omega_i / 4 \omega_e)^{2/3}$$

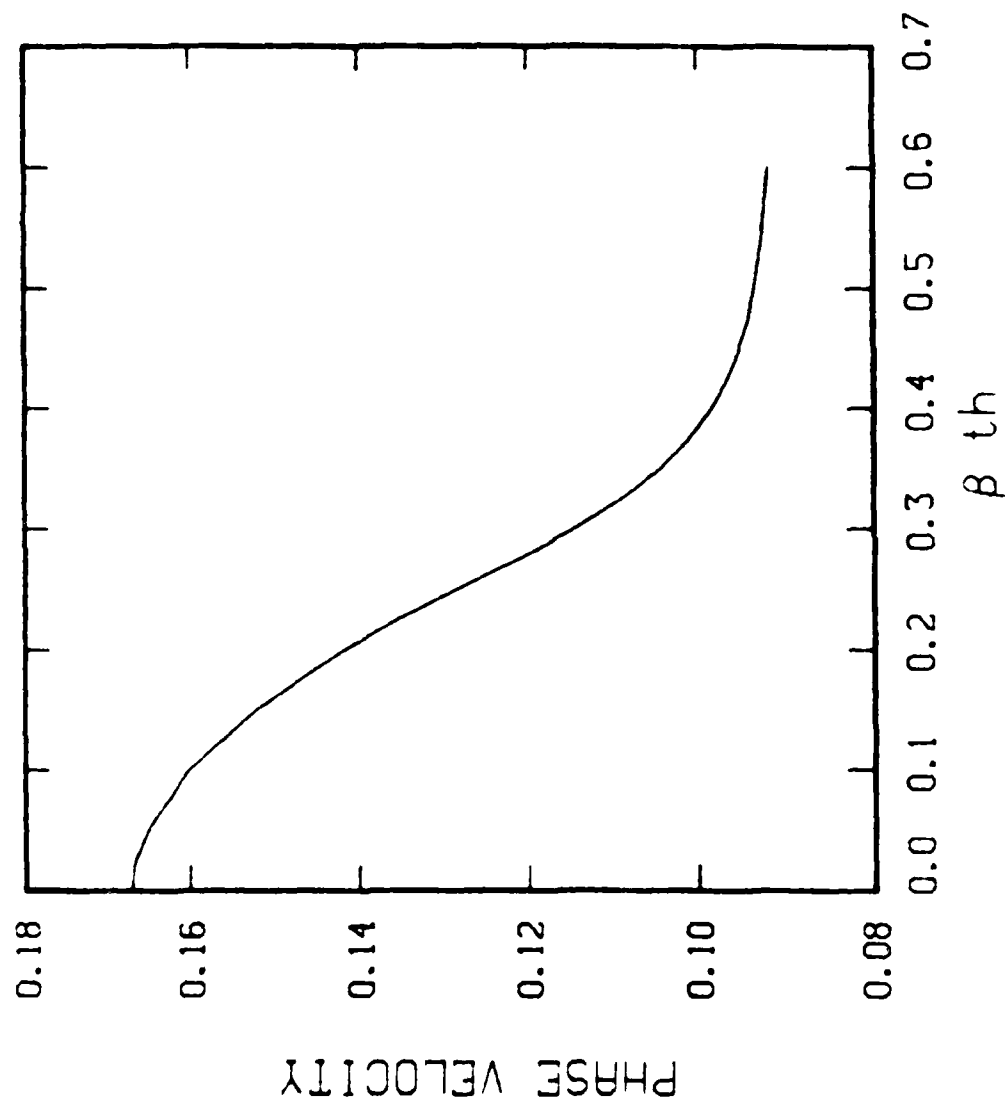
TRAPPING THRESHOLD IS HIGHER FOR IONS

$$E_{tr} = (k m c^2 / q) (\gamma \gamma_{ph} - \gamma_{ph} - 1)$$

example: $v_e = .866$, $v_i = .065$, $n_e = n_i$, $M_i / m_e = 459 \rightarrow V_{ph} = .167$

trapping for electrons, $E_{te} = .34$, for ions, $E_{ti} = 1.15$

SCATTERING (temperature) REDUCES PHASE VELOCITY OF THE MOST UNSTABLE MODE



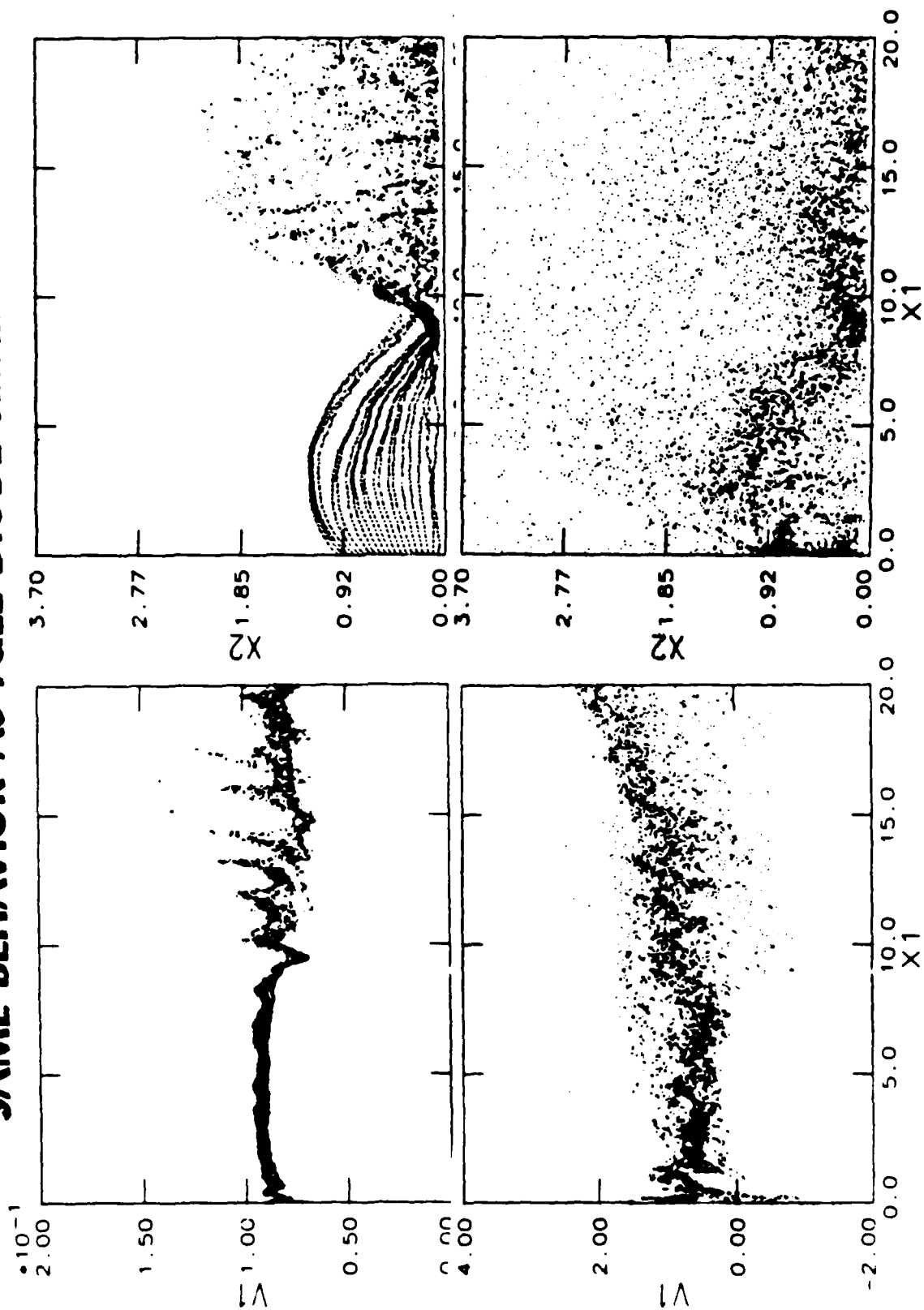
WITH REDUCED PHASE VELOCITY, IONS CAN TRAP BEFORE ELECTRONS SATURATE THE INSTABILITY

USING THE SAME PARAMETERS AS IN THE EXAMPLE:

electrons $E_{1e} = .353$

ions $E_{1i} = .197$

CO-INJECTED ION AND ELECTRON BEAMS SHOW SAME BEHAVIOR AS FULL DIODE SIMULATION



TIME = 340.0000

DOMINANT MECHANISMS IN THE TWO CLASSES ARE COMMON TO BOTH CONFIGURATIONS

Injection of an IREB above the space charge limit

Luce diode or insulated anode diode

**THERE IS A CONTINUOUS VARIATION IN DOMINANT MECHANISM
DEPENDING ON THE PARAMETER REGIME**

COLLECTIVE ION ACCELERATION HAS BEEN SHOWN IN TWO MAIN CLASSES

- **Injection of an IREB above the space charge limit**

Source of ions is gas fill, gas puff or preformed plasma

Peak ion energies up to 10x beam, usually 2-3x beam energy

Ion energy spectrum is broad

- **Luce diode or insulated anode diode**

Source of ions is proton rich hydrocarbon anode

Peak ion energies up to 22x beam

Gaussian distribution of highest energy ions

END

FILMED

3-85

DTIC